AD-A098 048 NAVAL POSTGRADUATE SCHOOL MONTEREY CA F/G 20/1
THE PROPAGATION OF A SCATTERED ACOUSTIC BOUNDARY WAVE OVER A RO--ETC(U)
DEC 80 S J HOLLIS

UNCLASSIFIED NL

1 OF 2
AD A098048

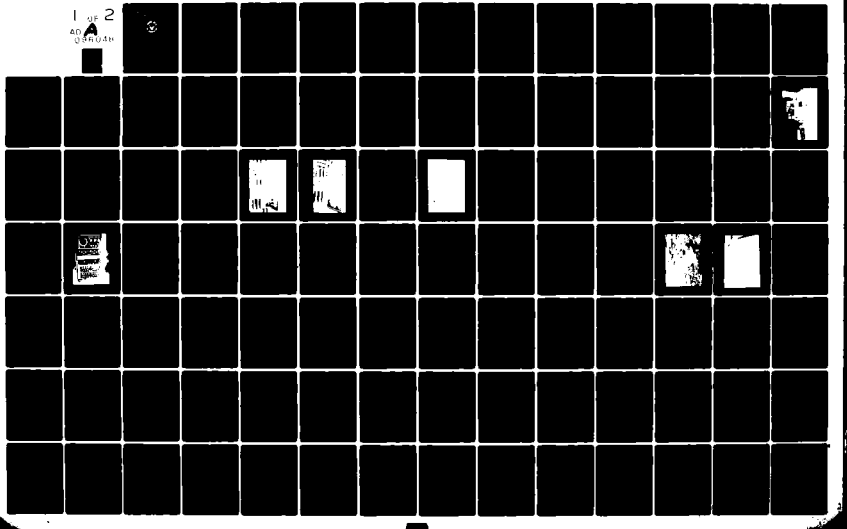

AD A098048

NAVAL POSTGRADUATE SCHOOL
Monterey, California

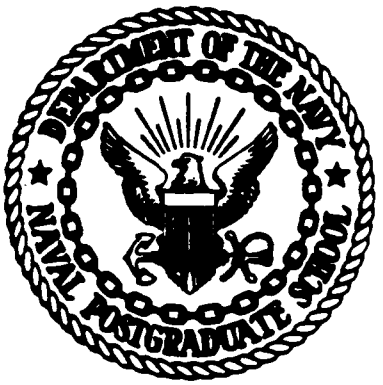

THESIS

THE PROPAGATION OF A SCATTERED ACOUSTIC BOUNDARY WAVE OVER A ROUGH WEDGE

by

Stephen Joe Hollis

December 1980

Thesis Advisor: H. Medwin

Approved for public release; distribution unlimited.

DTIC FILE COPY

UNCLASSIFIED

SECURITY CLASSIFICATION OF THIS PAGE (When Data Entered)

REPORT DOCUMENTATION PAGE	READ INSTRUCTIONS BEFORE COMPLETING FORM
1. REPORT NUMBER	2. GOVT ACCESSION NO. AD-A098 048	3. RECIPIENT'S CATALOG NUMBER
4. TITLE (and Subtitle) The Propagation of a Scattered Acoustic Boundary Wave over a Rough Wedge	5. TYPE OF REPORT & PERIOD COVERED Master's Thesis; December 1980
	6. PERFORMING ORG. REPORT NUMBER
7. AUTHOR(s) Stephen Joe Hollis	8. CONTRACT OR GRANT NUMBER(s)
9. PERFORMING ORGANIZATION NAME AND ADDRESS Naval Postgraduate School Monterey, California 93940	10. PROGRAM ELEMENT, PROJECT, TASK AREA & WORK UNIT NUMBERS
11. CONTROLLING OFFICE NAME AND ADDRESS Naval Postgraduate School Monterey, California 93940	12. REPORT DATE December 1980
	13. NUMBER OF PAGES 141
14. MONITORING AGENCY NAME & ADDRESS (if different from Controlling Office)	15. SECURITY CLASS. (of this report) Unclassified
	15a. DECLASSIFICATION/DOWNGRADING SCHEDULE

16. DISTRIBUTION STATEMENT (of this Report)

Approved for public release; distribution unlimited.

17. DISTRIBUTION STATEMENT (of the abstract entered in Block 20, if different from Report)

18. SUPPLEMENTARY NOTES

19. KEY WORDS (Continue on reverse side if necessary and identify by block number)

Acoustic Energy Diffraction
Acoustic Energy Scattering
Boundary Wave

20. ABSTRACT (Continue on reverse side if necessary and identify by block number)

The theory for the generation of a scattered acoustic boundary wave over a slightly rough planar surface has been developed by I. Tolstoy [J. Acoust. Soc. Am., 66 1135-1144 (1979)] and experimentally verified by Medwin et al., [J. Acoust. Soc. Am., 66 1131-1134 (1979)]. In the present experiment the propagation of the boundary wave over a wedge is studied. It is found that the boundary wave and the geometrically spreading volume wave

DD FORM 1 JAN 73 1473 EDITION OF 1 NOV 65 IS OBSOLETE S/N 0102-014-6601

UNCLASSIFIED

SECURITY CLASSIFICATION OF THIS PAGE (When Data Entered)

#20 - ABSTRACT - (CONTINUED)

diffract from the crest in the same manner. The amplitude ratio of the boundary wave to the diffracted volume wave, where the growth of the boundary wave from the crest is due to a phased line source at the crest caused by the diffracting volume wave, was found to have an average frequency dependence, f^2, and an average range dependence, $R^{+0.5}$. The amplitude ratio of boundary wave to diffracted volume wave due to propagation over the rough wedge gave an average frequency dependence of f^2 and an average range dependence of $R^{-0.3}$. Low wave number grazing propagation over a wedge produces a boundary wave whose amplitude can be many times that of a diffracted volume wave for a smooth surfaced wedge.

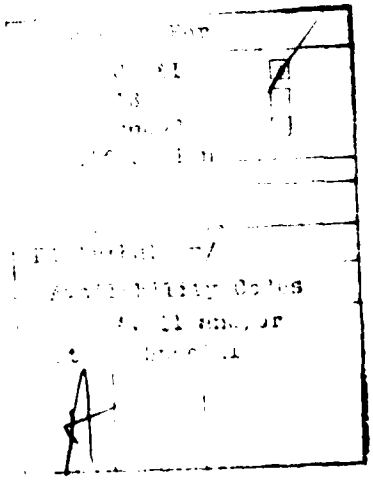

Approved for public release; distribution unlimited

THE PROPAGATION OF A SCATTERED ACOUSTIC BOUNDARY WAVE OVER A ROUGH WEDGE

by

Stephen Joe Hollis
Lieutenant, United States Navy
B.S., Southwest Missouri State University, 1972
M.S., George Washington University, 1978

Submitted in partial fulfillment of the requirements for the degree of

MASTER OF SCIENCE IN ENGINEERING ACOUSTICS

from the

NAVAL POSTGRADUATE SCHOOL
December 1980

Author 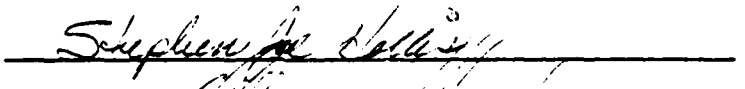

Approved by: 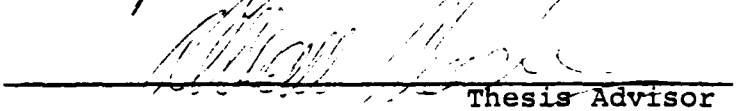
Thesis Advisor

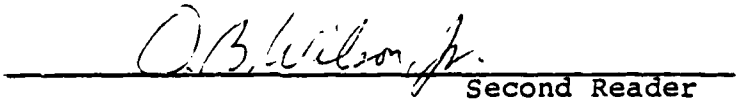
Second Reader

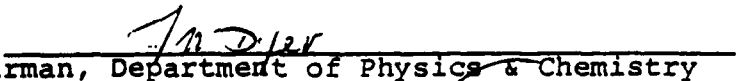
Chairman, Department of Physics & Chemistry


Dean of Science and Engineering

ABSTRACT

The theory for the generation of a scattered acoustic boundary wave over a slightly rough planar surface has been developed by I. Tolstoy [J. Acoust. Soc. Am., 66 1135-1144 (1979)] and experimentally verified by Medwin et al., [J. Acoust. Soc. Am., 66 1131-1134 (1979)]. In the present experiment the propagation of the boundary wave over a wedge is studied. It is found that the boundary wave and the geometrically spreading volume wave diffract from the crest in the same manner. The amplitude ratio of the boundary wave to the diffracted volume wave, where the growth of the boundary wave from the crest is due to a phased line source at the crest caused by the diffracting volume wave, was found to have an average frequency dependence, f^2, and an average range dependence, $R^{+0.5}$. The amplitude ratio of boundary wave to diffracted volume wave due to propagation over the rough wedge gave an average frequency dependence of f^2 and an average range dependence of $R^{0.3}$. Low wave number grazing propagation over a wedge produces a boundary wave whose amplitude can be many times that of a diffracted volume wave for a smooth surfaced wedge.

TABLE OF CONTENTS

LIST OF TABLES

LIST OF FIGURES

FIGURE

FIGURE

ROUGH WEDGE

FIGURE

FIGURE

ACKNOWLEDGMENTS

The writer wishes to thank Professor Herman Medwin, Physics Department of the Naval Postgraduate School, for the opportunity to have prepared this thesis under his experienced guidance and for his friendship and encouragement through these difficult times. The computer assistance of Miss Emily Childs is greatly appreciated. Special thanks to Mr. R. Moeller for the construction of the wedges and to Ken Smith for his help in correcting electronic casualties. Thanks to Lt. Wilson B. Decker, USN, for his assistance in the preparation of the surfaces and for his friendship during many frustrating times. Finally, thanks to my wife for her unending patience and to my whole family for their encouragement and support.

The financial support of the Office of Naval Research is acknowledged.

I. INTRODUCTION

The formation of a boundary wave due to coherent multiple Rayleigh scatter above a slightly rough planar surface was predicted in a theory developed by Tolstoy [Ref. 1] and verified experimentally by Medwin et al., [Ref. 2]. The major importance of this development, from an applications point of view, is that the amplitude of the boundary wave becomes larger than the spherically diverging volume wave at large ranges and frequencies. The theory for diffraction at the crest of a rigid plane wedge by sound radiated from a point source has been developed by Biot and Tolstoy [Ref. 3] and simplified for high frequencies by Medwin [Ref. 4]. This experiment observed the behavior of the boundary wave as it is generated, diffracted, and continues to grow over a rough wedge.

The boundary wave amplitude over a rough wedge results from three components; first, the boundary wave grows as a result of generation from the source to the crest; second, the boundary wave continues to grow after it diffracts at the crest; and third, the diffracted volume wave generates a boundary wave as it propagates beyond the crest.

It is the aim of this paper to be able to predict the behavior of the boundary wave as it propagates over a rough surfaced wedge. To achieve this, first, the behavior of the

boundary wave as it diffracts over the crest must be understood, and second, how the boundary wave continues to grow as a result of a source composed of the diffracted boundary wave and diffracted volume wave.

II. THEORY

At present there is no theory which describes the behavior of the scattered acoustic boundary wave as it diffracts over a slightly rough surfaced wedge. There do exist, however, two separate theories which individually describe difference aspects of the phenomenon.

The first aspect is the diffraction of acoustic energy over a smooth wedge. In 1957, Biot and Tolstoy presented a closed form solution by the use of normal coordinates for the diffraction of a pulse by an infinite rigid wedge [Ref. 3]. This solution modified for a delta function point source by Medwin [Ref. 4] gives the diffracted pressure as:

$$p(t) = \frac{-S\rho c}{4\pi\theta_\omega}(\beta)[rr_0 \sinh y]^{-1}[\exp(-\pi y/\theta_\omega)] \qquad (1)$$

$$\beta = \frac{\sin[(\pi/\theta_\omega)(\pi \pm \theta \pm \theta_0)]}{1-2\exp(-\pi y/\theta_\omega)\cos[(\pi/\theta_\omega)(\pi \pm \theta \pm \theta_0)]\exp(-2\pi y/\theta_\omega)} \qquad (2)$$

$$y = \text{arc cosh}\left[\frac{c^2t^2 - (r^2 + r_0^2 + z^2)}{2\,r\,r_0}\right] \qquad (3)$$

where

S = Delta function source (m^3/sec)

ρ = density of medium

c = speed of sound. (See Figure 1)

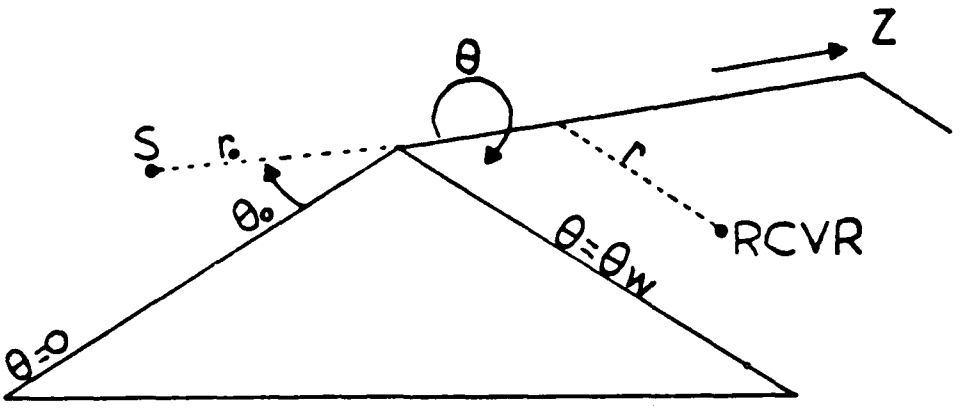

θ_w = fluid filled region above the wedge

θ_0 = angle between the wedge side and the source

θ = angle between wedge side and the receiver

r_0 = distance from source to wedge apex

r = distance from wedge apex to receiver

z = distance out from the least time travel path along the wedge apex

Figure 1. Geometry Diagram For Biot-Tolstoy Theory

The term $(\pi \pm \theta \pm \theta_0)$ is written for simplicity, but in actuality is the sum of four terms composed of all the different combinations of angles.

The interaction of the diverging spherical wave with the crest of the wedge results in a reradiated cylindrically spreading wave. The strongest point of the diffracted wave from the crest exists around the least time path, therefore, this is the area of most concern. The least time path is:

$$\tau_0 \equiv [(r + r_0)^2 + z^2]^{1/2}/c \qquad (4)$$

The other principal energy paths occur at times shortly after τ_0.

$$\tau = t - \tau_0 << \tau_0$$

Then

$$P_s(\tau) = S\rho\beta/[4\pi\sqrt{2}\theta_\omega(\tau\tau_0 r r_0)^{1/2}] \qquad (5)$$

when

$$\tau/\tau_0 << 1$$

Rewriting $P_s(\tau) = A\tau^{-1/2}$

$$A = S\rho\beta/[(4\pi\theta_\omega)(2\tau_0 r_0 r)^{1/2}] \qquad (6)$$

Transforming this equation for times small compared to least time

$$P_s(f) = (A/2)(1+i)f^{-1/2} \qquad (7)$$

Therefore looking at the diffracted wave amplitude (DWA) for times small compared to the least time

$$|P_{DWA}| = S\rho\beta/(4\pi\theta_\omega)(2\tau_0 r_0 r)^{1/2}\sqrt{2}\, f^{1/2} . \qquad (8)$$

The second aspect is the propagation of acoustic energy at grazing incidence over a slightly rough plane surface. Again a theory laid by Biot and extended by Tolstoy [Ref. 1], predicts this behavior. This theory is unique in the fact that it allows for multiple Rayleigh scatter and accounts for the coherent addition at near grazing incidence. Additionally, this theory is first order in εk rather than second order as in other theories. The roughness parameter ε has the dimensions of length and is proportional to the volume of roughnesses per unit area of plate. It takes account of the close interaction effect. For close-packed hemispherical bosses ε/h = 4.44 E-2 where h is the separation of bosses. The published theory describes the scattering over small rigid hemispheres of radius a, separated by h, such that $ka < kh \leq 1$, insonified by near-grazing radiation from a point source.

The normalized spectrum of the total scattered wave at far field, near-grazing conditions kr >> 1 and θ << 1 is: [Ref. 2]

$$P_s = \frac{\varepsilon}{2\pi} k^2 [\theta^2 + \frac{2\pi}{kr} \exp[-2\varepsilon k^2 (z + z_0)] + 2(\frac{2\pi}{kr})^{1/2} \theta \sin(kr - \frac{\pi}{4}) \exp[-\varepsilon k^2 (z + z_0)]]^{1/2} \quad (9)$$

where

$$\theta = \tan^{-1}[(z - z_0)/r] \quad (10)$$

This expression contains a volume scattered wave, a boundary scattered wave, and a cross term. The normalized spectrum of an impulsive point source embedded in the surface is:

$$P_s = (2\pi R)^{-1} \quad (11)$$

where

$$R = (z^2 + r^2)^{1/2} \quad (12)$$

Since the source and receiver are on the surface, z_0 = z = 0 and r = R therefore the boundary wave amplitude (BWA) is

$$P_{BWA} = \varepsilon (2\pi R)^{-1/2} k^{3/2} \quad (13)$$

The ratio of the boundary wave pressure amplitude to that of the spherically spreading volume wave is:

$$P_{BWA}/P_s = \varepsilon(2\pi R)^{1/2} k^{3/2} . \qquad (14)$$

III. RESEARCH FACILITIES

A. ANECHOIC CHAMBER

The experiment was conducted in the Naval Postgraduate School anechoic chamber. The low signal levels necessitated that the experiment be run in a noise isolated environment. The anechoic chamber is designed as a "floating" room-within-a-room construction to minimize outside noise. The outer 12" concrete wall is separated from the inner wall and floor by a 2 inch blanket of fiberglass or cork. Fiberglass wedges which are 40 inches deep surround the ceiling, floor, and wall of the inner room which has a volume of 5000 cubic feet. These wedges trap the incident sound and absorb approximately 99% of the energy of frequencies greater than 100 Hz. Tests to determine noise in the chamber by comparing a Bruel & Kjaer (B&K) receiver 4134 (with no source) to the receiver blocked by two 1/4" aluminum plates showed noise level differences of approximately .1 dB or less over frequency range 2-30 kHz (see Figure 2).

B. DATA ACQUISITION AND PROCESSING EQUIPMENT

The signals were sent by coaxial cable from the anechoic chamber to the adjacent room for collection and real time processing. This was accomplished by using a digital computer system designed by the Special Projects Section of the Naval Air Development Center in conjunction with Pinkerton Computer

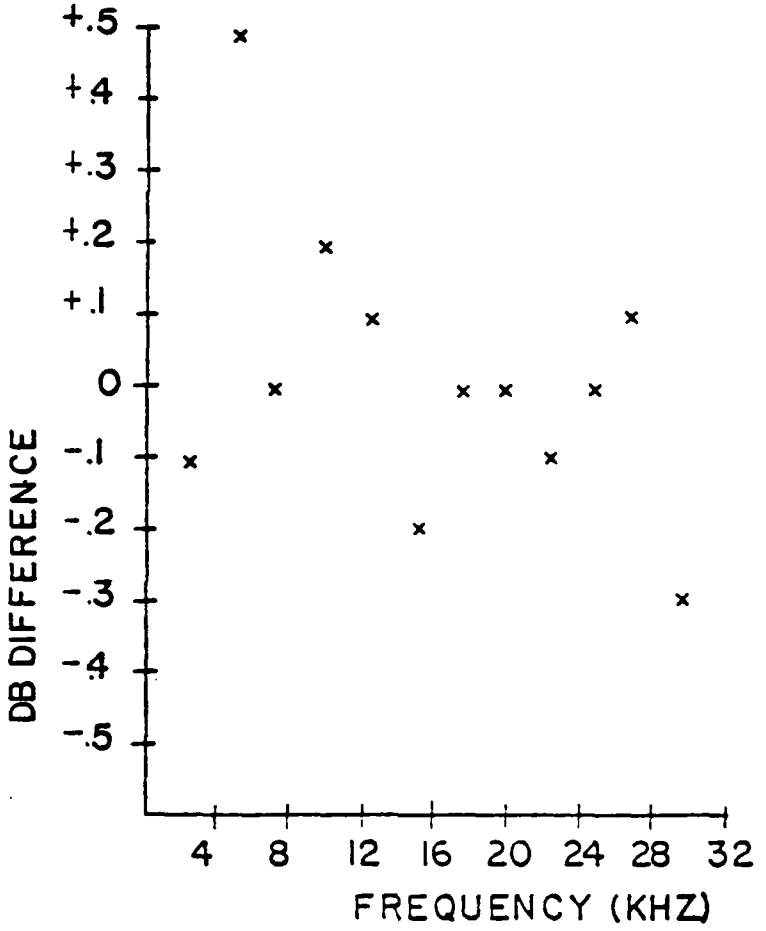

Figure 2. Anechoic chamber noise; dB difference (uncovered receiver-covered receiver) with no source

Consultants, Inc., of Warminister, Pennsylvania. The system consists of four primary components interfaced to provide high speed analog to digital conversion, digital processing, data storage, and data printout. The entire system is shown in Figure 3. The following major components are:

1. Interdata Model 70 Computer

This minicomputer is a digital design with a 64 thousand byte memory and is programmable in FORTRAN or BASIC. In addition to core memory, data can be stored on floppy discs for subsequent processing.

2. Phoenix Analog to Digital Converters, Model ADC 912

The Model ADC 912 is a very high speed, high accuracy analog voltage to digital converter capable of encoding ±10 volt input signals into twelve binary bits of data, with a resolution of one part in 4,095 at a maximum rate of 2 microseconds per conversion. It measures the input voltage against an internal precision reference voltage source with an accuracy of ±0.025% of full range. The input will settle to within specified accuracy within 100 nanoseconds after the application of a step function of full range magnitude. This fast settling time and the successive approximation encoding process will accommodate a typical commutating through-put rate of 476,190 channels per second, including input settling time. The sampling frequency is generated by using a General Radio 1312 Decade Oscillator, whose stability is .001%, being applied via a sampling circuit.

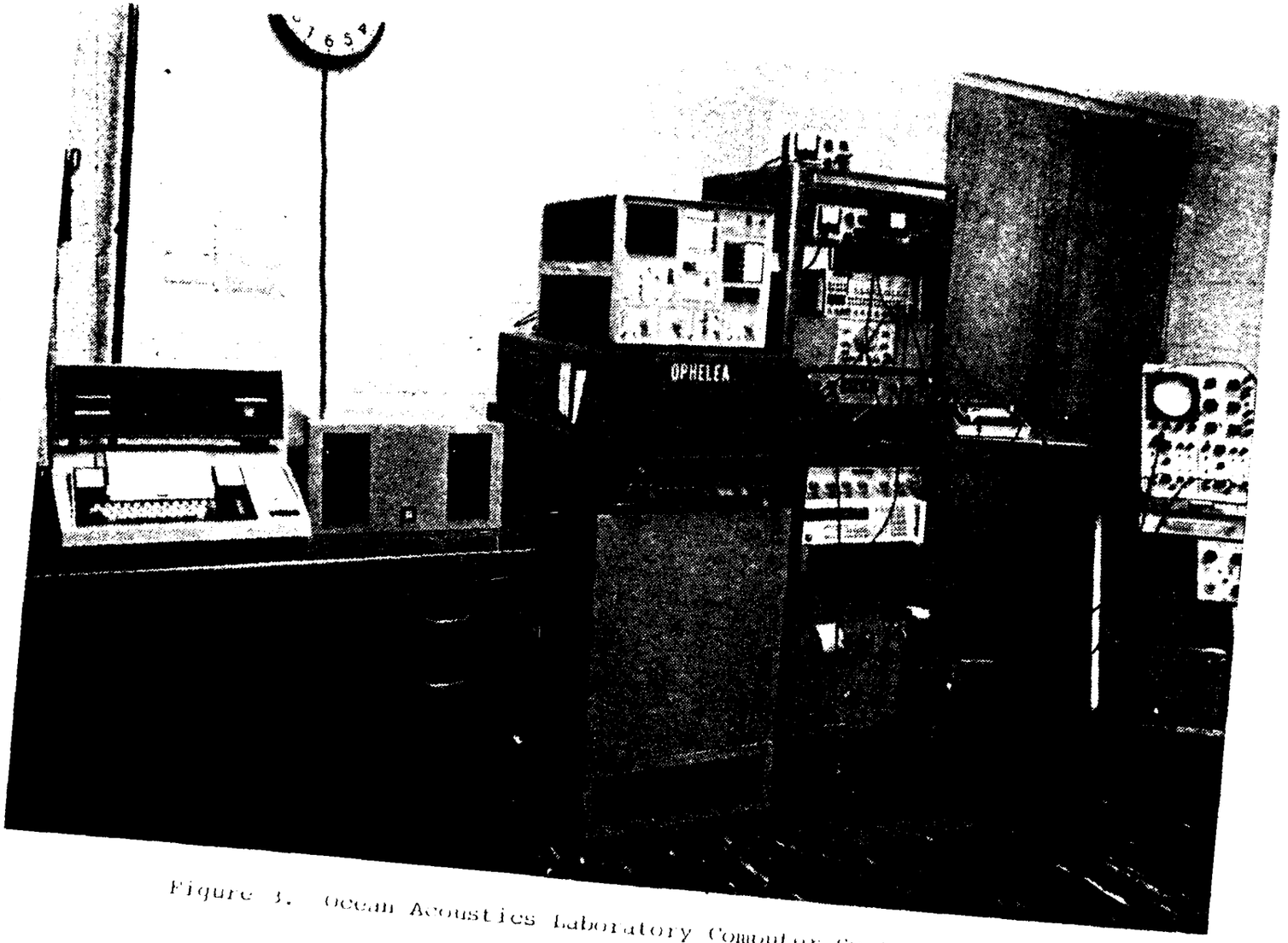

Figure 3. Ocean Acoustics Laboratory Computer System

3. Texas Instruments Silent Electronic Data Terminal, Model 733

The TI-733 consists of a keyboard used as a programming input/output control device, a printer, and a transmit/receiver mechanism going to a peripheral disc drive unit.

4. Orbis Model 76 Diskette Drive

The Orbis Model 76 Diskette Drive is a small, portable, direct access, 256 kilobyte floppy disc data storage device. The magnetic discs provide the capability of storing large quantities of data for later computer analysis.

The overall system allows for the fast collection and processing of any desired analog signal. This system was utilized primarily to do frequency analysis by a Fast Fourier Transform algorithm.

C. *EQUIPMENT LIST*

Abbreviation	Description
Scope	Tektronic Type 551 Dual-Beam Oscilloscope
Frequency Synthesizer	General Radio 1312 Decade Oscillator
Timing Simulator	Interface Technology Timing Simulator/Word Generator, Model RS-648
Frequency Counter	Hewlett Package Model 5223L Electronic Counter
Filter HP	Krohn-Hite Frequency Filter, Mode 3342
Filter LP	Krohn-Hite Frequency Filter, Model 3322

PAR Amplifier	Princeton Applied Research Amplifier, Model 113
Source	Bruel and Kjaer Type 4145 Condenser Microphone
Receiver	Bruel and Kjaer Type 4133 Condenser Microphone
MIC Power Supply	Bruel and Kjaer Microphone Power Supply, Model 2804
ARB	Wavetek Arbitrary Waveform Generator, Model 175
MIC Preamp	Bruel and Kjaer Model 2619
Power Supplies	Hewlett Packard Model 721A
Power Amplifier	Kilowatt Amplifier Model L2 Instruments, Inc.
Oscilloscope	Hewlett Packard Model 140A Oscilloscope

IV. EXPERIMENTAL DESIGN AND PROCEDURES

A. WEDGE CONSTRUCTION

The experiment required the construction of two identical plane wedges. One wedge was to be used as the smooth surface reference and the other to be converted into a rough surface. Each wedge was constructed of two one-fourth inch aluminum plates, 152 cm. wide and 60 cm. long, joined together at an angle of 152 degrees. Aluminum was chosen as the building material due to its rigidity and its reflection coefficient of almost unity. A one inch hole to be used for the source was drilled along the centerline 20 cm. from the crest of the wedge. On the opposite side of the wedge, one-half inch holes for the receiver were drilled at 5 cm. intervals from 5 to 35 cm. Additionally, one receiver hole was drilled 20 cm. in back of the source (see Figure 4). A threaded plug and two non-conducting threaded sleeves were machined to hold the source and receiver rigid. Also the rough plate had a metal border one-half inch high placed 35 cm. from centerline on the sides and along the back of the wedge to facilitate the packing of the spheres (see Figures 5 and 6).

The Tolstoy theory calls for a rough surface to be composed of hemispherical bosses with a maximum hexagonal packing density. To achieve this, it was proposed to submerge a layer of #9 chilled lead shot, two millimeters in diameter, in some kind of adhesive material. The material was required

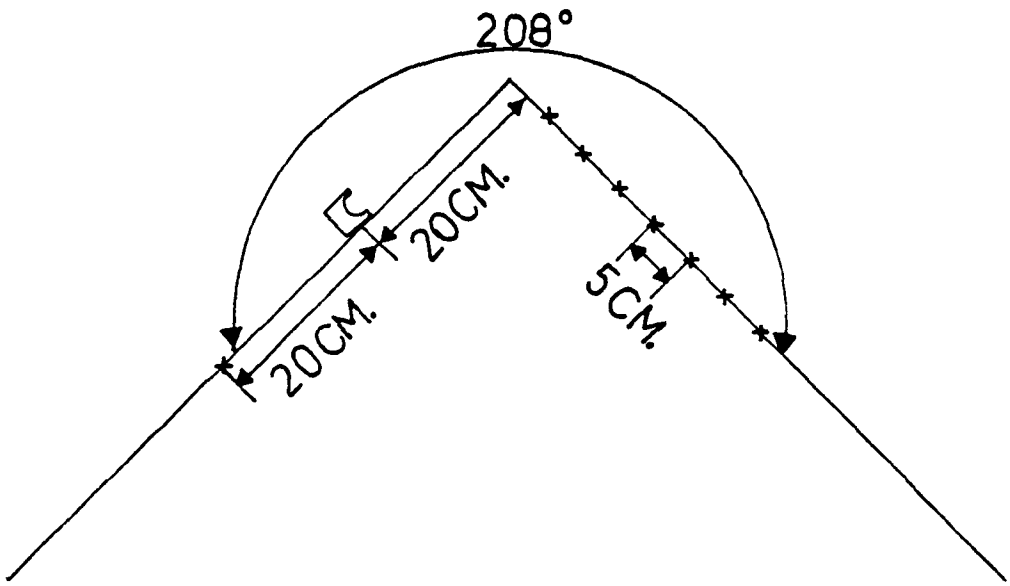

✖ = Receiver Positions

Figure 4. Diagram of Wedge Construction

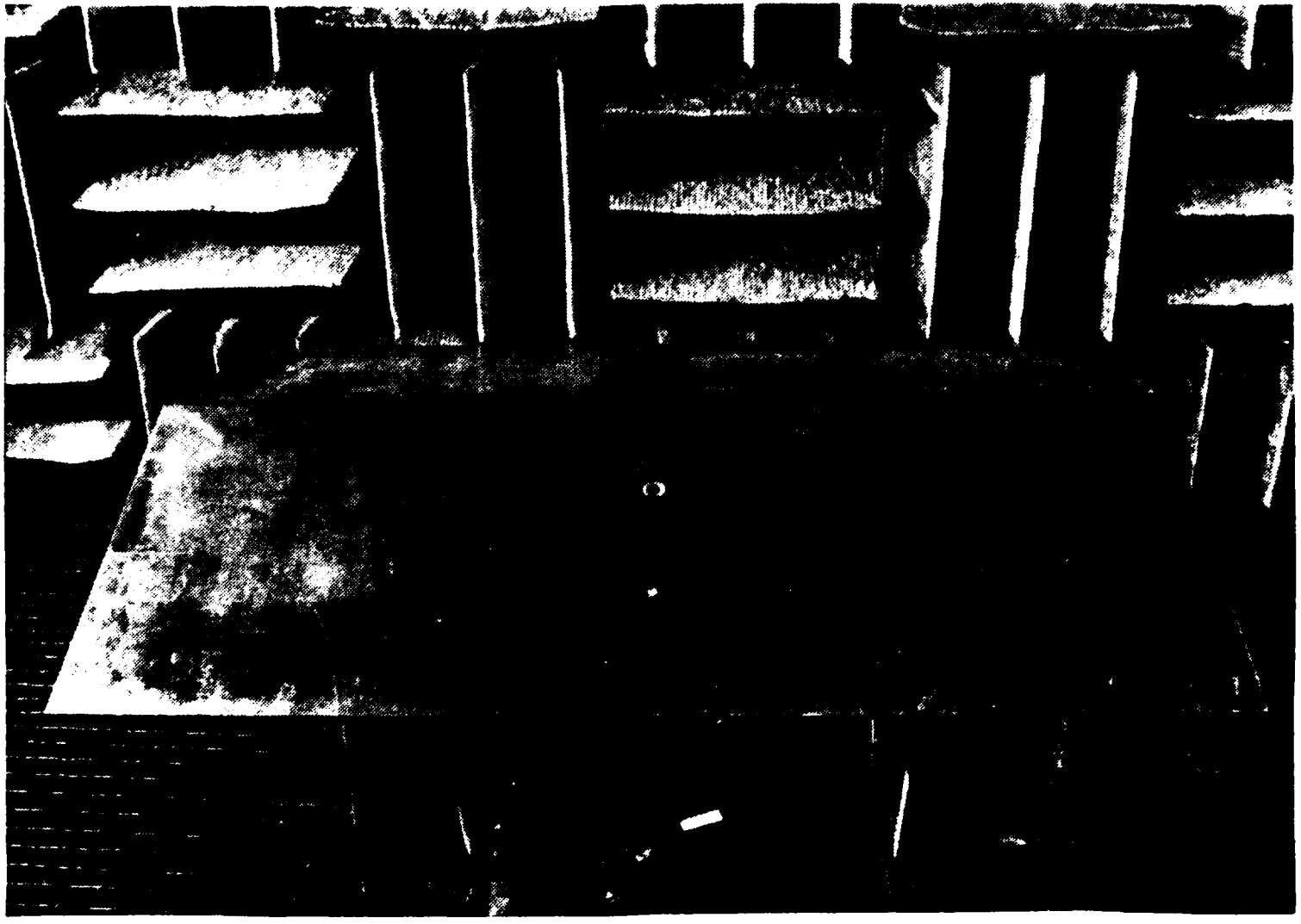

Figure 5. Smooth Wedge

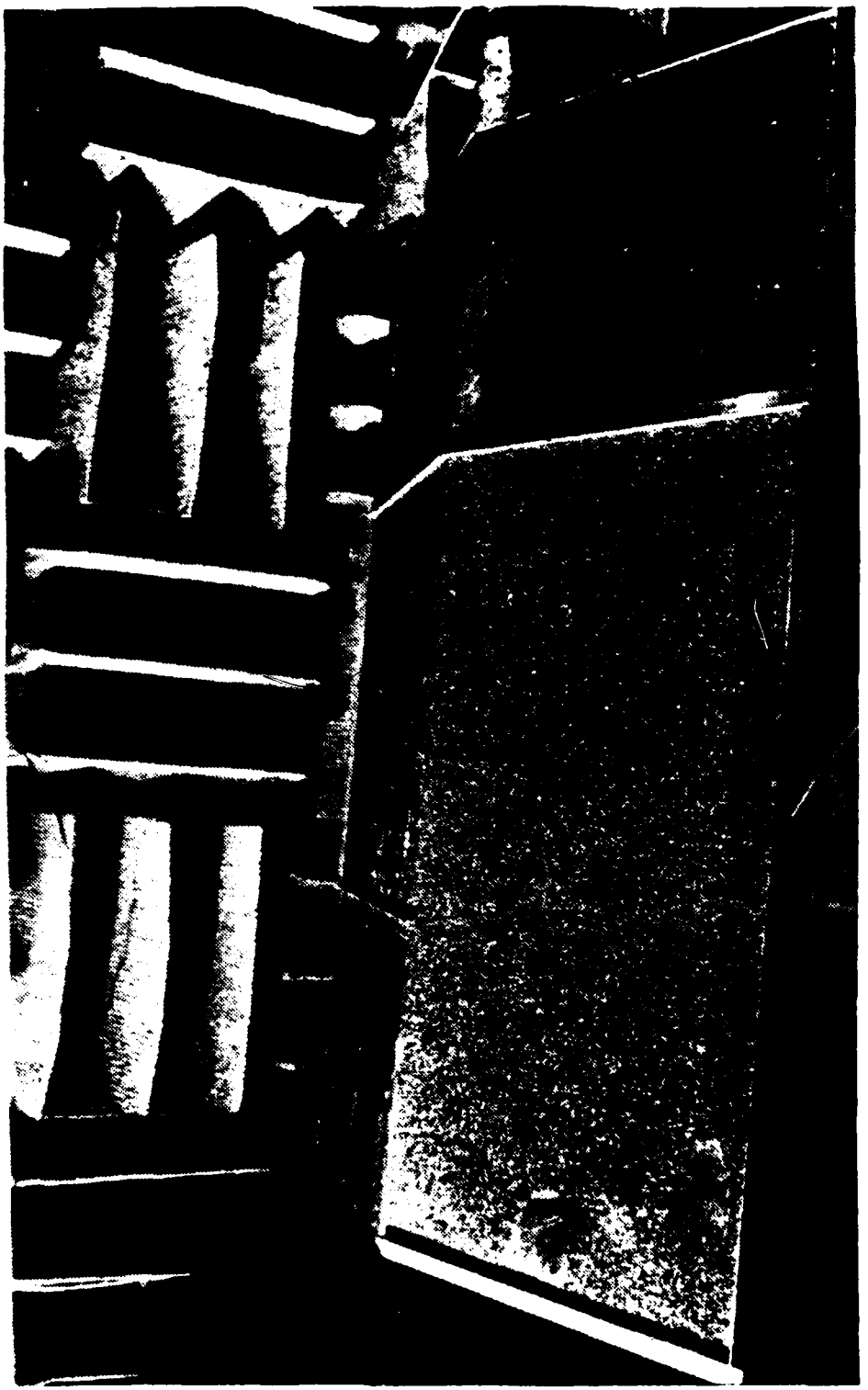

Figure 6. Keough Bridge

to be free of air cavities and to be strong enough to hold the bosses in place. Bailey [Ref. 5] had previously used rubber cement, however, the probability of glue drying with air cavities was thought to be high. Therefore, different varnishes thinned to different thicknesses were tried. The varnishes, however, tended to dry leaving bare areas around the bosses. Also, the liquid tended to push the closely packed hemispheres apart and, furthermore, it was difficult to keep from covering the tops of some of the spheres.

A new approach was tried where the material could be applied, allowed to harden, and then the shot rolled on and pressed in. The material chosen was paraffin, because of its low melting point and ease of application. The procedure used was to melt the paraffin and apply a thin coat over the entire surface to be covered. The paraffin solidifies quickly and with the use of metal rulers can be shaved to .75 mm. thickness, which was the experimentally determined height required to cover the spheres to their equator of 1.0 mm. The shot was then placed into position by a combination of shaking and handpacking. Approximately 200,000 shot were required to cover each surface. With the shot in position the paraffin was heated very slowly in spots by the use of a hand air blower and allowed to sink. This method, while time consuming, results in the formation of a uniform hemispherical surface (see Figure 7).

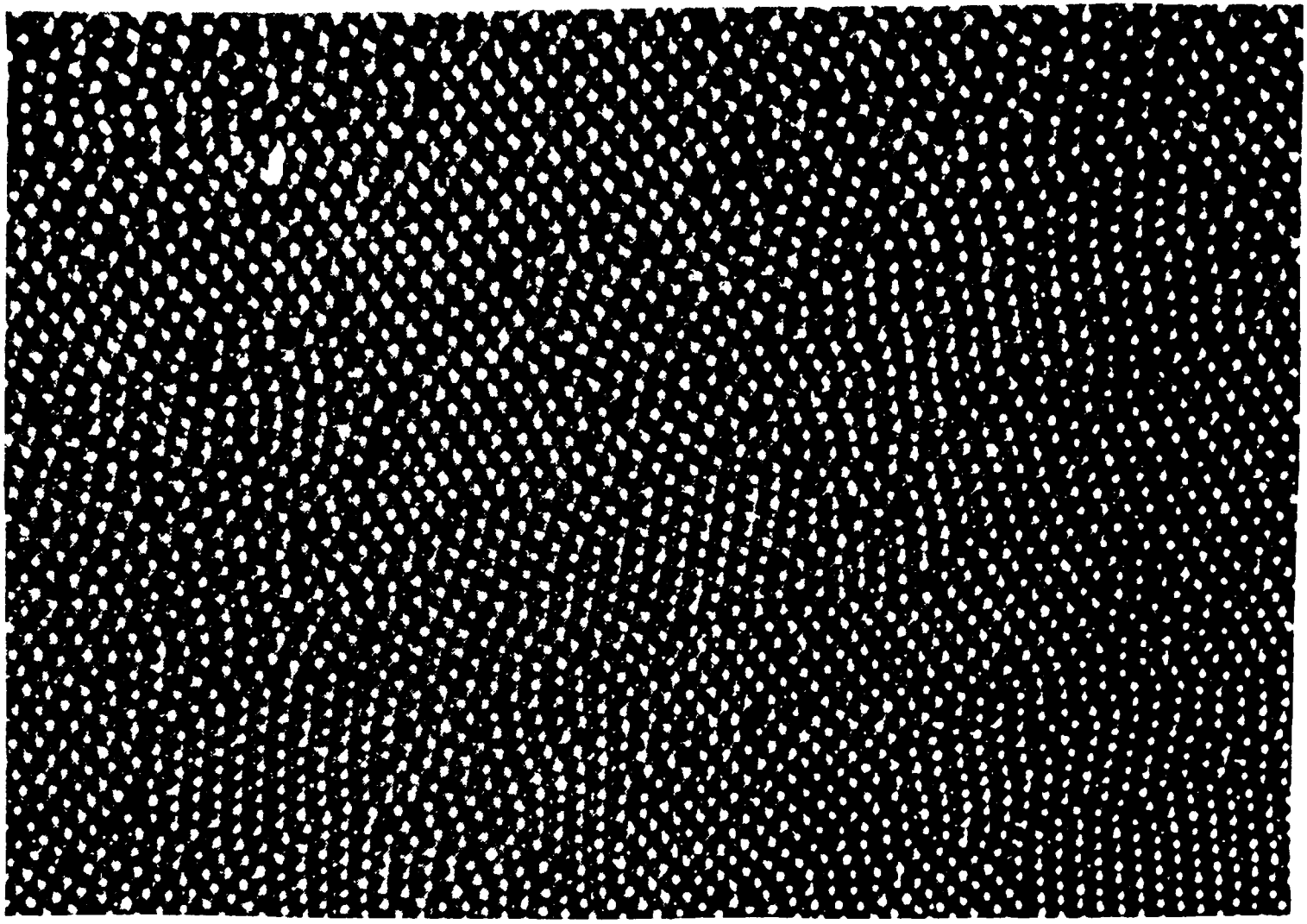

Figure 7. Hemispherical Surface

B. SOURCE/RECEIVER SELECTION

The Tolstoy theory requires a point source which radiates spherically symmetrical waves. To meet this requirement a radiater must have dimensions small compared to a wavelength, in other words, $ka' << 1$ where k is the wave number and a' is the radius of the source. The selection of a source is further complicated by the need for a strong signal to give sufficient diffracted energy over the wedge. Particle velocities at small distances from point sources become very large with the result that a small source of sound is inherently incapable of generating spherical waves of large intensities. Likewise, it is impossible to construct a sound source of moderately small size that is capable of radiating large amounts of power at low frequencies.

An attempt was made to construct a microphone which could meet the previous requirements. Prior work by Bremhorst had shown that B&K microphones, while of high quality, were limited in amplitude by driving voltage and also gave an undesired ringing response when an impulse signal was applied. Four electrostatic transducers, two 3 inch diameter and two 1 inch diameter, were fabricated in accordance with reference 6. Mylar was to be replaced by PVF_2, Polyvinylidene Fluoride, if successful. The microphones were constructed with an adjustable large air cavity to control stiffness and thus improve sensitivity. Also the backplates were designed from reference 7 of different roughness. The backplates were

constructed of concentric rings .23 mm. wide and separated by 4 mm. The rings were 1 and 10 micrometers thick to give a different roughness effect. These microphones also gave a ringing response to an impulse signal. Even more critical was their lower amplitude and lack of stability. The response tended to decay slowly over several weeks which was attributed to the weakening of the glue holding the Mylar secure. It was then decided to continue to use the B&K's. The B&K model 4145 one inch diameter microphone was chosen, because of its greater source strength. The flush mounting of the source created a problem in signal strength due to the directivity of the microphone. As a result of the mounting, the majority of the energy (at grazing incidence) over the plate is radiated from side lobes. Consequently, the desired extra signal strength from larger sources was not fully realized because of increasing directivity with increasing microphone size. To correct this problem a brass circular cap, 7 mm. high with a 5 mm. diameter hole on the periphery, was manufactured. The cap was filled with tackey wax as shown in Figure 8. To avoid standing wave interference, the dimensions of the cap were kept small compared to the smallest wavelength, 8.625 mm. for a 40 kHz signal. The resulting gain in signal strength at higher frequencies was quite pronounced as shown in Table I.

The power amplifier, Model LL by Instruments Inc., allowed more flexibility in AC driving voltage and less distortion than the North Hills Pulse Transformer used by Bailey. The

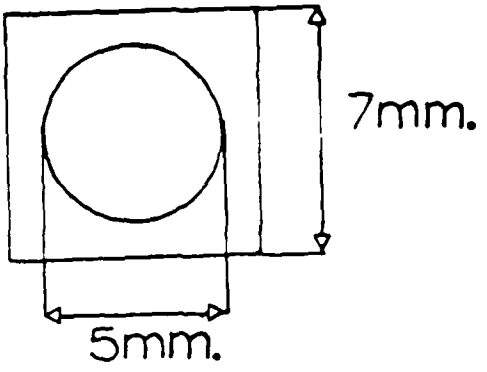

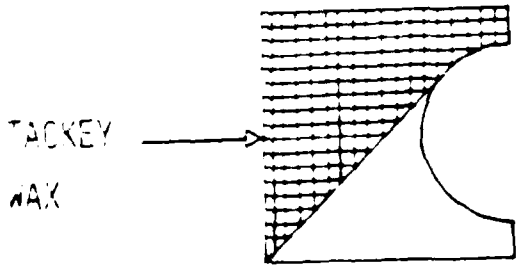

Figure 8. Diagram of source cap construction

Table I.

Net Gain of Signal Resulting from Source Cap

Freq. (kHz)	1" source no cap (dB)	1" source with cap (dB)	Net (dB) effect improvement
2	34.9	42.2	+ 7.3
4	40.1	43.7	+ 3.6
6	34.9	38.8	+ 3.9
8	34.6	36.3	+ 1.7
10	36.0	37.5	+ 1.5
12	35.4	33.5	- 1.9
14	33.9	29.3	- 4.6
16	39.5	27.8	- 1.7
18	22.3	25.1	+ 2.8
20	15.7	20.7	+ 5.0
22	9.34	17.7	+ 8.36
24	- .957	13.8	+14.76
26	4.16	13.3	+ 9.14
28	2.91	14.6	+11.69
30	5.19	13.6	+ 8.41
32	2.77	12.4	+ 9.63
34	- 4.48	10.3	+14.78
36	-13.7	8.83	+22.53
38	-15.4	9.22	+24.62
40	- 6.54	9.70	+16.24

Measurement taken 90° to axis of source over a smooth plate at a range of 20 cm.

microphone 4145 can be driven with a maximum of 250 volts DC plus AC peak [Ref. 8]. The combination of 150 volts DC plus 100 volts AC peak gave the strongest signal.

The choice of receiver had to be balanced between desired frequency range and sensitivity. The 1/2 inch B&K model 4133 was selected as the optimum choice. The 4133 has an open circuit frequency response flat within ±2 dB from 3.9 Hz to 40 kHz and an open circuit axial sensitivity -38 dB re 1V/Pa. Since the receiver was flush mounted, it was necessary to have the face of the transducer small compared to a half wavelength for the highest frequency to avoid pressure averaging over the face. To accomplish this, an 8 centimeter long probe tube of outer diameter 3.2 millimeters was selected. A compatible B&K Model 2804 DC microphone power supply was used in conjunction with a B&K Model 2619 preamplifier for this 1/2 inch condenser microphone. The power supply runs on batteries and is therefore electrically quieter; additionally, there is no heating element for the microphone thus reducing thermally induced signal fluctuations.

C. SIGNAL PROCESSING

1. Source Signal

The experimental procedure was to take two sets of measurements propagating over the smooth wedge and two sets over the rough wedge. These runs were then assumed to be independent and four different combinations of data could be calculated. The source always remained at a fixed position

of 20 cm. from the crest and the receiver positions were varied from 5 to 35 cm. on the opposite side of the wedge. Once the source and receiver were positioned, the Wavetek Arbitrary Waveform Generator (ARB) was triggered to generate a 2.0 kHz half triangular pulse. This waveform was chosen because its frequency spectrum consists of the fundamental and all its harmonics. This enables the analysis of a broad range of frequencies. The signal then goes through a power amplifier which inverts the signal and brings the amplitude to 100 volts AC peak. The 100 volts AC is sent via a junction box (Figure 9) which combined the AC signal with 150 volts DC biasing voltage. The total maximum allowable voltage of 250 volts DC plus AC peak was then sent to the B&K Model 4145 source.

2. Received Signal Processing

The signal received by the B&K Model 4133 is amplified by a PAR Model 113 preamp with a gain of 10K. The signal is then band passed through a series of filters, the Krohn Hite 3342 and Krohn Hite 3322, which were set to be high pass and low pass respectively. Both filters had their left and right channels connected in series to give 96 and 48 dB attenuation per octave. The signal is then passed through another PAR 113 whose gain for each data position was adjusted to approximately ±10 volts of signal output to maximize the use of the dynamic range of A/D converter (see Figure 10). In addition to increase reproducibility of high frequency data over the

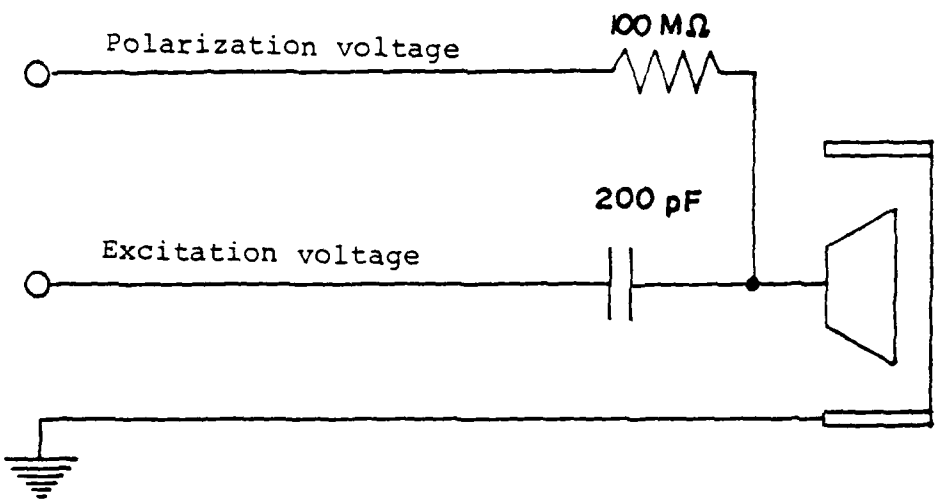

Figure 9. Junction Box for Polarization

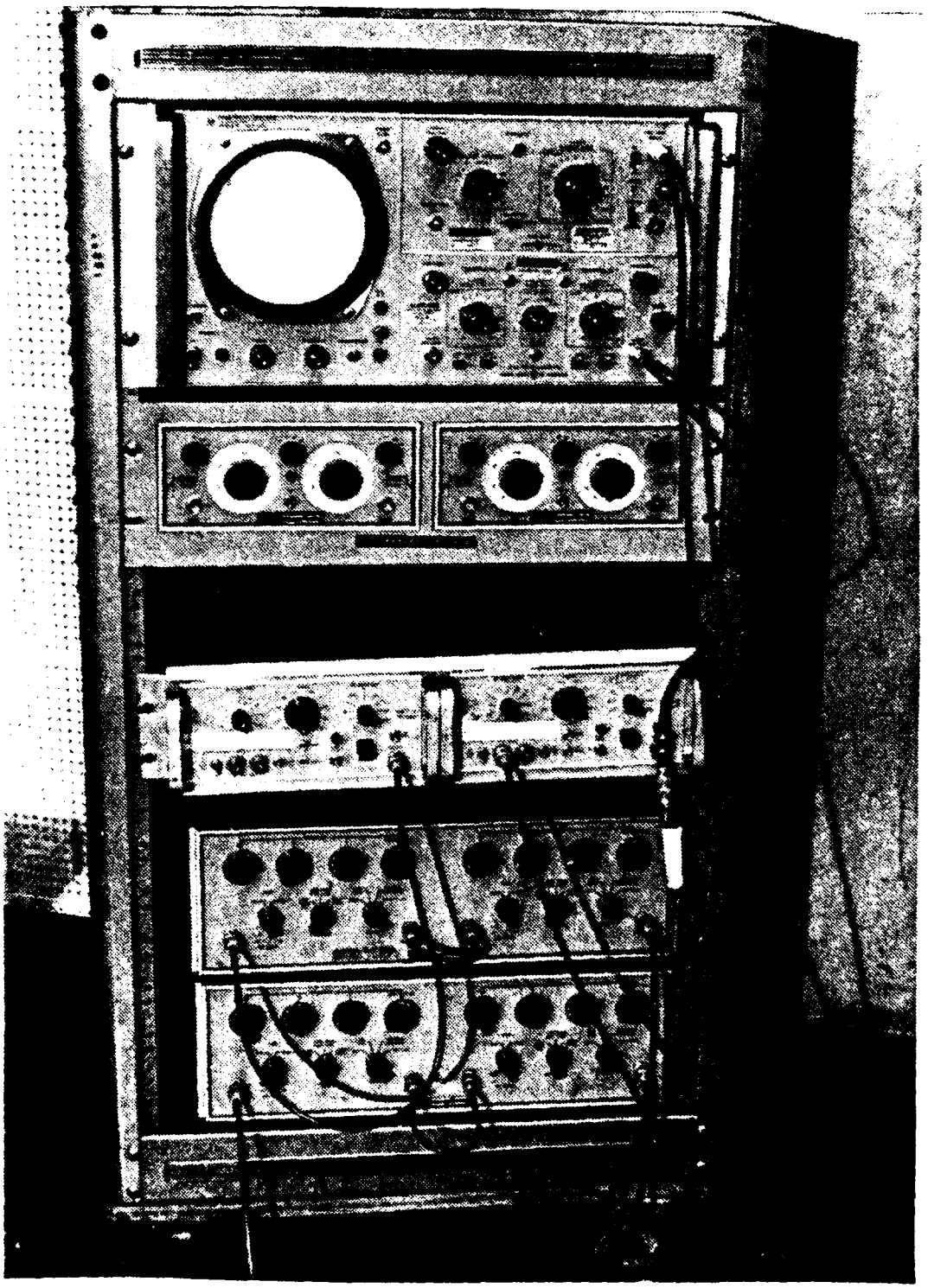

Figure 10. Received Signal Filtering and Amplification Rack

wedge, the high frequencies were bandpassed from 16 to 42 kHz. This enabled the signal to be amplified more and with the aid of increased averaging achieved greater reproducibility (see Table II).

3. Experimental Control

The Interface Technology timing simulator acted as the command and control device for the experiment. The timing simulator was programmed to trigger the ARB once every 22 milliseconds and then through a sampling circuit established the sampling window. The sampling window could be left on for any predetermined time and then gated off with 100 nanosecond accuracy.

In order to have a source of very stable frequency, a sampling circuit was designed (Figure 11). The sampling circuit was constructed of two IC devices, two DC power supplies, and a General Radio 1312 Decade Oscillator. The oscillator has the stability characteristics of a crystal oscillator, therefore providing a constant frequency source to the A/D converter. The circuit operates in the following manner. The oscillator generates a constant frequency sine wave which goes through a LM 710 CN, voltage comparator, which changes the sine wave into a square wave, which is required by the A/D converter. This output along with the output from the timing simulator goes to the two inputs of the 7408 AND gate. As long as the positive trigger from the timing simulator is received the AND gate is open and allows the sampling frequency

Table II

Increases in Reproducibility due to Signal Processing

Freq. kHz	Parameters (1) Run 1/Run 2		Parameters (2) Run 1/Run 2		Parameters (3) Run 1/Run 2		Parameters (4) Run 1/Run 2	
2	41.1	41.1	xxx	xxx	41.0	41.0	xxx	xxx
4	46.2	46.2	xxx	xxx	46.5	46.5	xxx	xxx
6	47.6	37.6	xxx	xxx	37.5	37.4	xxx	xxx
8	37.1	37.2	xxx	xxx	37.3	37.3	xxx	xxx
10	41.5	41.4	xxx	xxx	42.5	42.5	xxx	xxx
12	38.3	38.3	xxx	xxx	39.5	39.4	xxx	xxx
14	32.2	32.3	xxx	xxx	33.2	33.2	xxx	xxx
16	28.2	28.2	33.7	33.7	29.6	29.6	35.7	35.7
18	22.1	22.2	34.0	34.1	29.4	24.4	36.5	36.5
20	15.4	16.7	29.2	29.2	19.4	19.4	32.1	32.2
22	13.4	14.3	26.0	26.8	18.8	18.9	29.7	29.7
24	8.69	8.95	19.5	18.8	13.6	13.5	22.8	22.6
26	-1.47	.256	13.0	11.2	-2.47	-1.67	15.4	14.5
28	2.13	1.61	17.3	16.7	11.2	11.6	21.8	21.4
30	6.17	4.35	16.5	19.5	11.7	11.7	20.4	20.1
32	6.56	7.12	18.8	17.0	10.6	10.4	19.5	19.4
34	9.20	8.96	20.0	18.1	6.03	5.68	19.1	19.3
36	4.92	5.69	17.1	15.7	15.7	-20.8	17.8	17.7
38	-2.08	-2.71	13.8	13.5	3.25	3.79	16.8	16.9
40	-13.0	-9.27	10.6	9.97	6.49	6.73	12.2	11.8

Parameter 1 - R = 10, R = 20/Bandlimit 1.5-42 kHz/1000 averages/ Amplification 200k/Smooth Wedge

Parameter 2 - R = 10, R = 20/Bandlimit 16-42 kHz/1000 averages/ Amplification 1000k/Smooth Wedge

Parameter 3 - R = 10, R = 20/Bandlimit 1.5-42 kHz/9999 averages/ Amplification 200k/Rough to Smooth Surface Wedge

Parameter 4 - R = 10, R = 20/Bandlimit 16-42 kHz/9999 averages/ Amplification 1000k/Rough to Smooth Surface Wedge

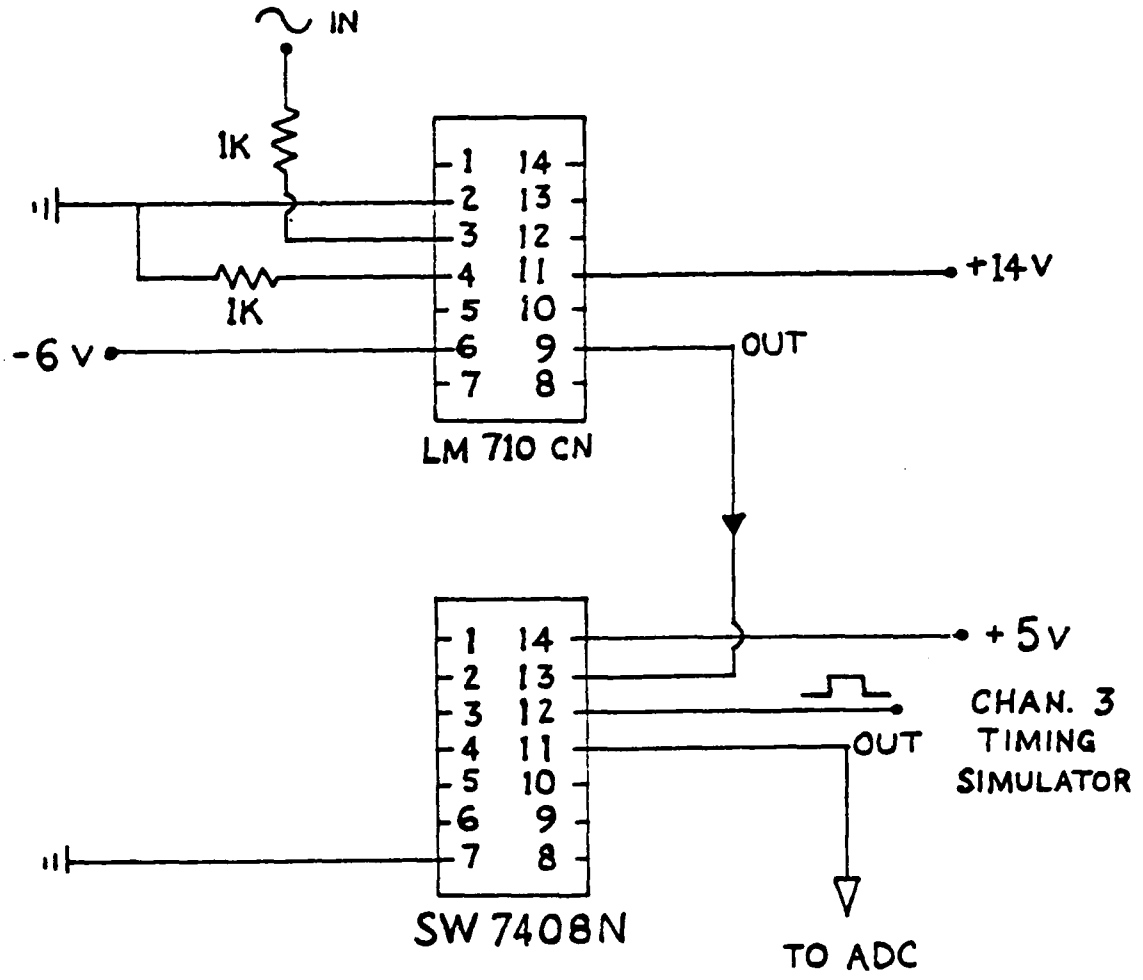

Figure 11. Sampling Circuit

to pass. The length of the positive trigger which is programmable, establishes the sampling window (see Figure 12).

4. Computer Processing

The computer Fast Fourier Transform (FFT) algorithm requires that the number of samples be a power of two, i.e., 64, 128, 256, etc. To avoid truncation errors and eliminate sidelobes, the samping frequency and ARB frequency were sent to the frequency counter and an exact integral ratio to five significant figures of the number of samples was obtained. The input signal was bandlimited to 42 kHz, therefore a sampling frequency of 256 kHz was chosen which is three times greater than the Nyquist rate required to avoid aliasing. The ratio of sampling frequency to ARB frequency allows for 128 samples which gives a sampling window of 5 milliseconds and a frequency resolution of 2 kHz.

To improve the signal to noise ratio, signal averaging was incorporated into software prior to doing the FFT. The data could be averaged for a maximum of 9,999 samples which required 22 minutes to complete. The improvement received as a result of averaging is 10 log $\sqrt{N}$ where N is the number of samples averaged. As a result 20 dB gain in signal to noise ratio is achieved. Additionally, bandlimiting the signal to either the band 1.5 to 40 kHz or 16 to 40 kHz, a higher S/N was possible for these bands.

The procedure used for collecting and processing data was to take two data runs for each bandwindow at a specific

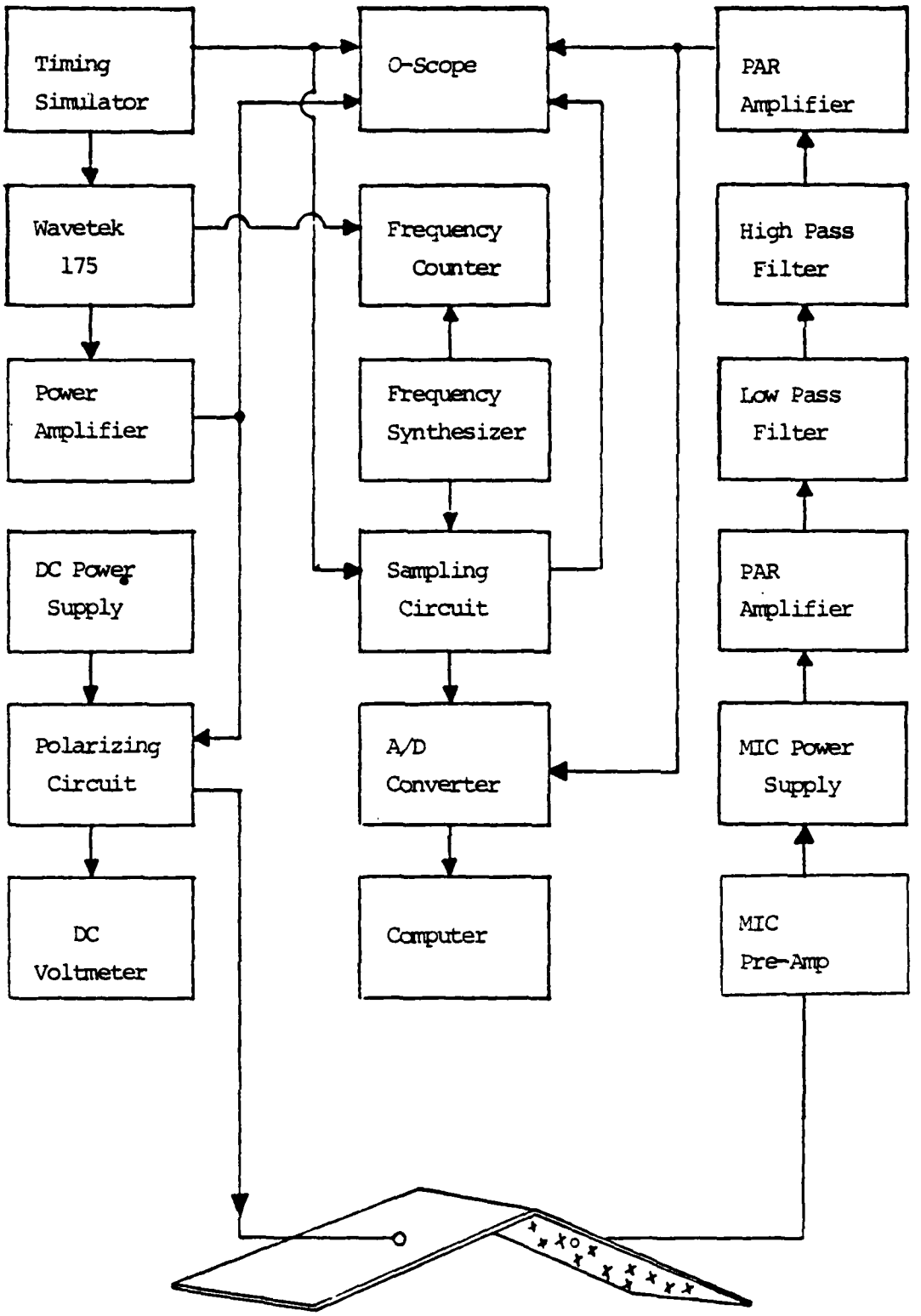

Figure 12. Equipment Diagram

range over the rough and smooth wedges or plates. 9999 samples of data were averaged and then Fourier transformed. The Fourier transformed data was printed out and stored on magnetic disc for each frequency from 2 to 40 kHz in 2 kHz increments. The information was then printed out in four columns for each frequency. These columns were titled, amplitude, phase angle, A (real part) and B (imaginary part) of the complex form. To determine the magnitude and phase angle of the boundary wave, a computer program was written which would subtract the smooth surface, real and imaginary components, from those of the rough surface. The differences were then the complex components of the boundary wave. To obtain the amplitude of the boundary wave, these individual components are each squared, added, and the square root taken. The phase angle was calculated from the arc tangent of the imaginary component divided by the real component. The boundary wave amplitude (BWA) was then divided by the volume wave amplitude (VWA, for planar surface) or the diffracted wave amplitude (DWA, for wedge) to determine the ratio of BWA/(VWA or DWA) for each corresponding frequency. Additionally the difference in phase between the BWA and (VWA or DWA) was calculated for each value. These data points were then compared to the theoretical curves.

V. EXPERIMENTAL RESULTS AND ANALYSIS

Four tasks were identified for this experiment. The first task was to verify Bailey's [Ref. 5] work in order to be assured that the wave propagating towards the crest of the wedge agreed with the Tolstoy theory. This step verifies the exactness of the construction of the closely packed hemispherical surface to theoretical requirements and also insures the proper functioning of the equipment. The second task was to measure the effect of a boundary wave propagating on a rough surface and diffracting over the crest of the wedge onto a smooth surface. The third task was to determine the boundary wave growth generated by the phased line source at the crest which is associated with a spherical wave interacting with the wedge. The fourth task and the goal of this experiment is to determine the characteristics of a boundary wave propagating and diffracting over the wedge from one rough surface to another.

A. REVERIFICATION OF PROPAGATION OVER A ROUGH PLANAR SURFACE

This part of the experiment was run at a range of 20 cm. from source to receiver over the rough planar surface. It was desired to have both source and receiver height to be 0 cm. as specified in the theory. To determine the point on the source to be used as a reference for the height above the bosses was complicated by the hole in the brass source

cap. It was found that the correct positioning of the source was essential for the experiment to come within close agreement with theory and previous results. Figure 13 shows the results of 1 mm. variations in height of the source. The position where the bottom of the hole of the source cap is 1.12 mm. down from the top of the hemisphere was chosen because it more closely agreed with theory (see Figures 14 and 15). The receiver probe was experimentally determined to be not as sensitive to variations in height as was the source. The receiver probe was placed level with the top of the hemispheres. The amplification factor of the signal was 20 thousand through PAR I and 2 thousand through PAR II. The signal was bandlimited from 1.5 to 42 kHz and 9999 averaging was used. Figure 16 shows data from three runs taken on two separate days. The agreement with theory is very close up to f = 24 kHz, Kh = 0.9. An oscillation effect at lower frequencies which was present in the Bailey experiment [Ref. 2] is now absent. This is attributed to the paraffin being a better material for avoiding air cavities and the improved S/N of the present experiment. A graph of the phase difference between the boundary wave and volume wave is presented in Figure 17. The graph demonstrates that with increasing frequency the scattered component lags farther behind the incident wave.

At frequencies greater than Kh = 1, it was observed that the boundary wave was larger than the volume wave at this

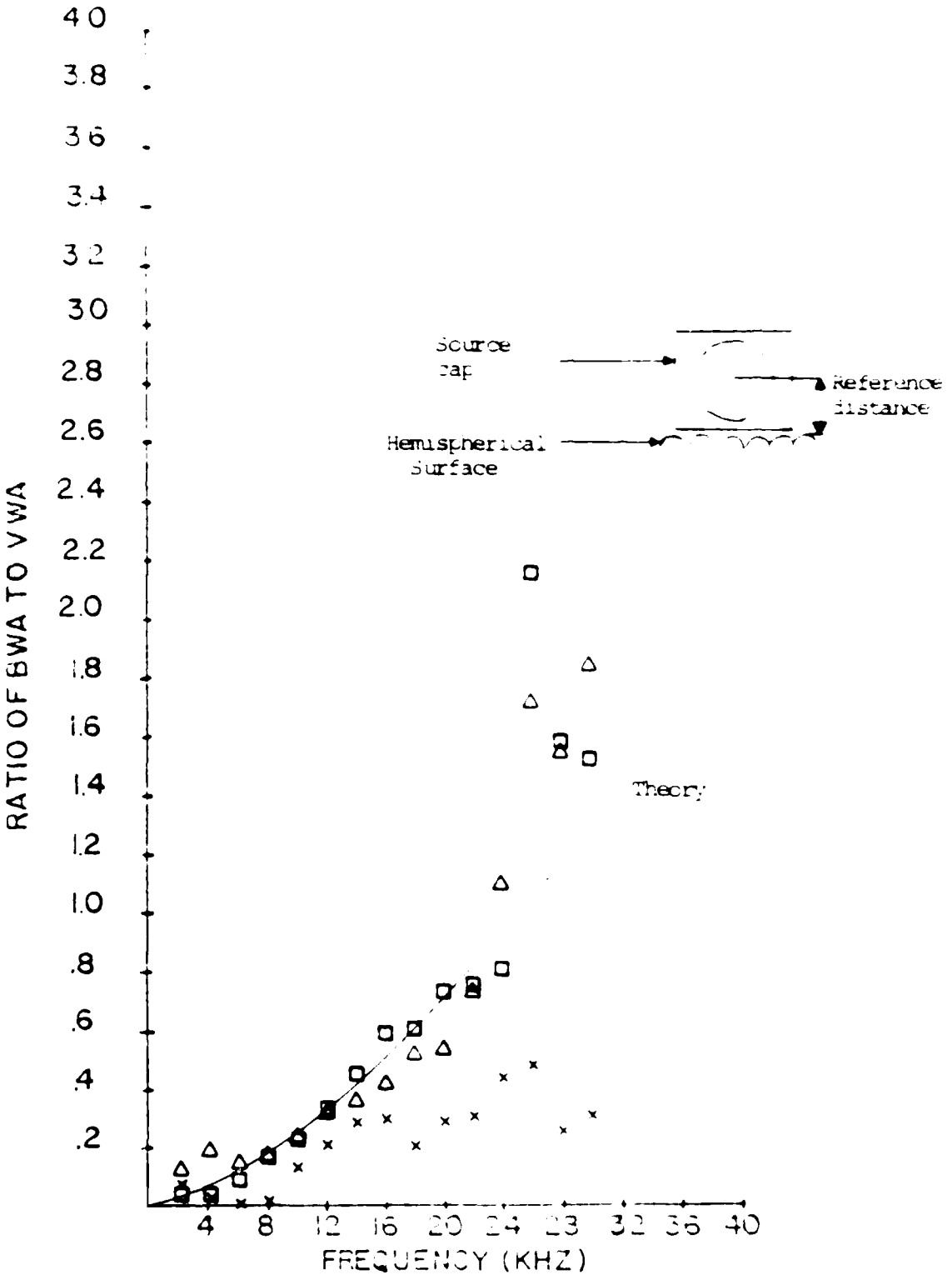

Figure 13. Graph of Source Height Sensitivity; R_0 = 20 cm., rough planar surface, x = 2.38 mm., □ = 1.38 mm., and △ = .38 mm.

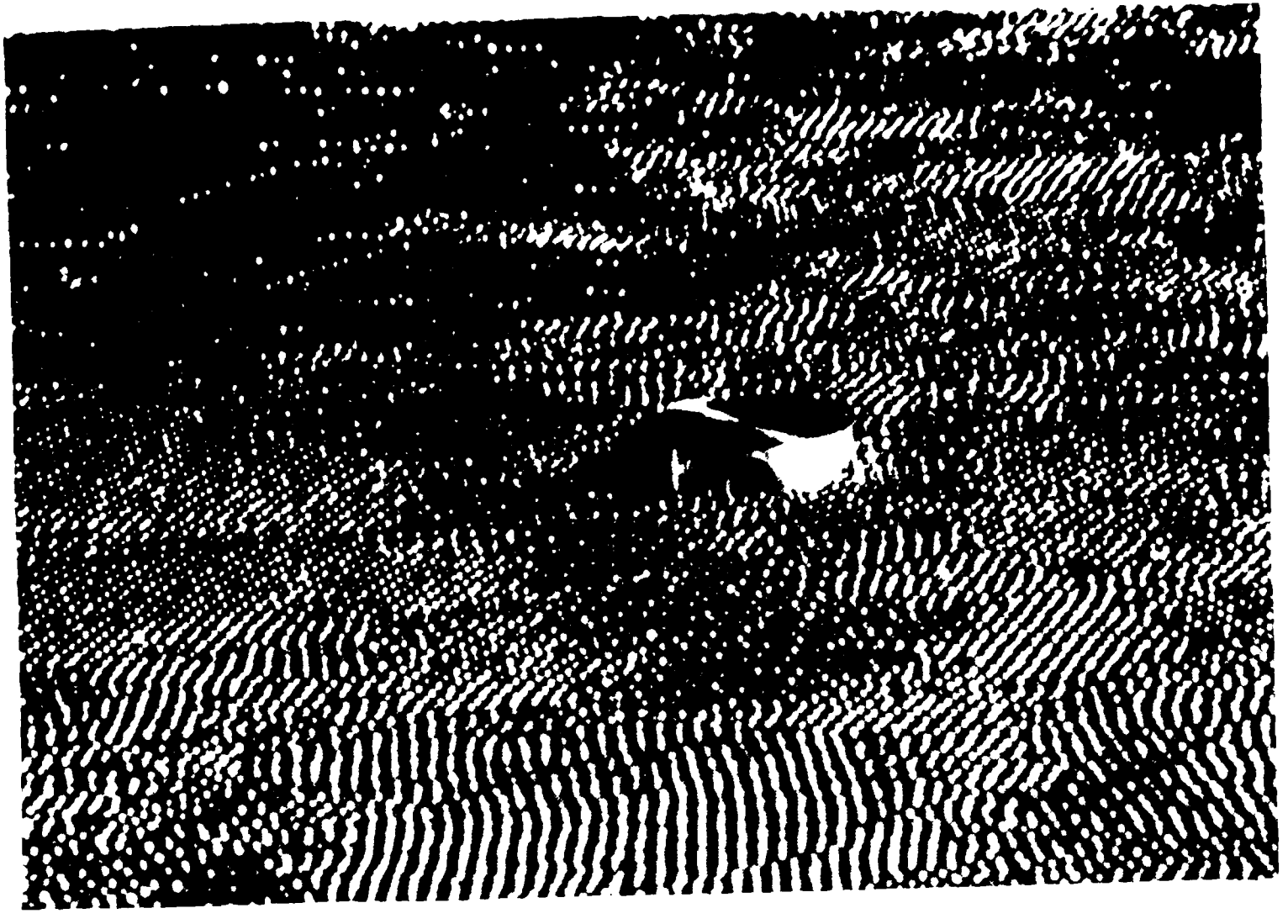

Figure 11. Screen Mounted in Rough Plate

Figure 15. Source Mounted In Wedge

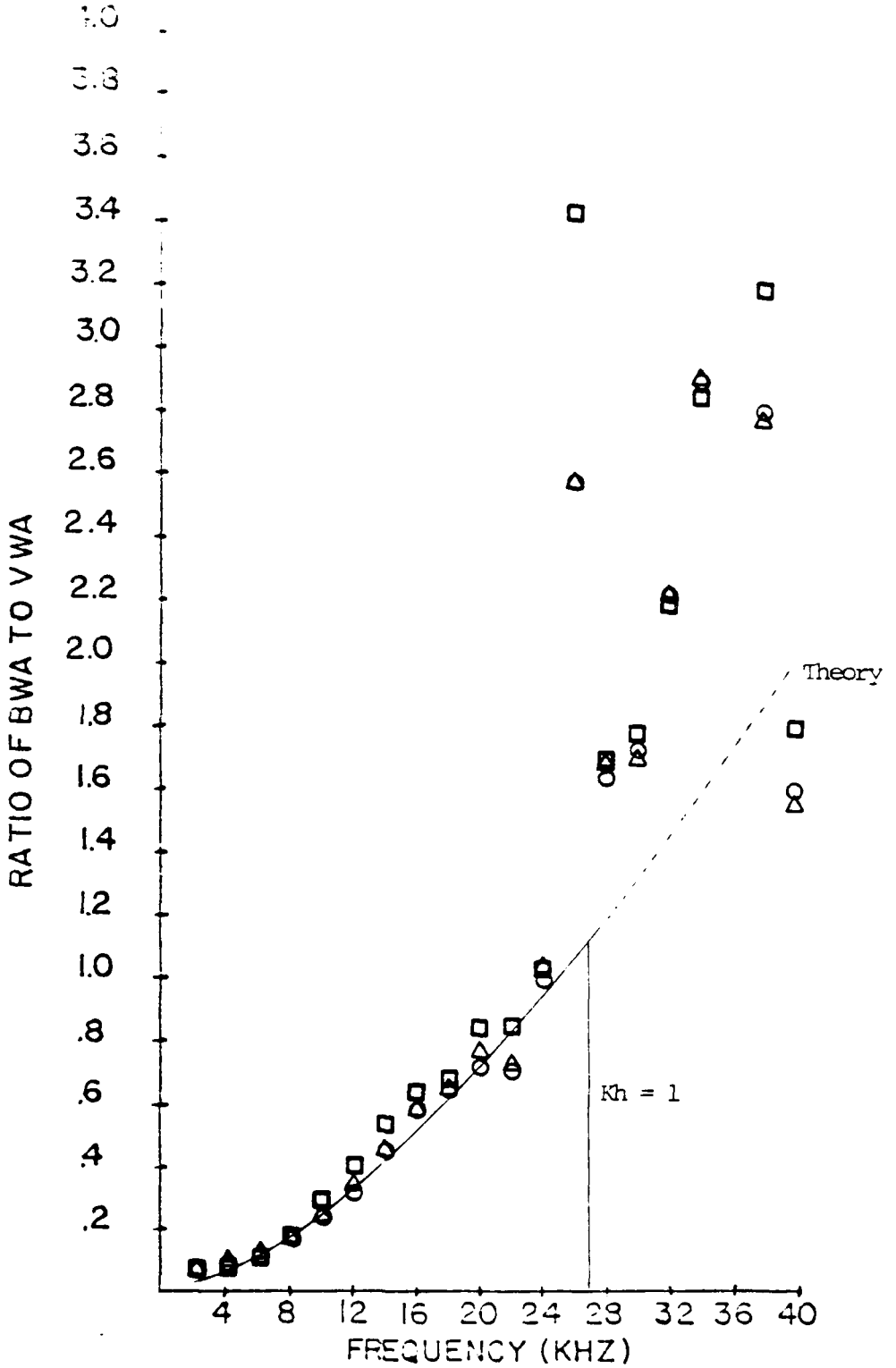

Figure 16. Ratio of BWA to VWA vs. Frequency (R_0 = 20 cm); rough planar surface, 0 = Run I, △ = Run II, and □ = Run III. — = Tolstoy theory for sound propagation over a rough planar surface at a range of 20 cm.

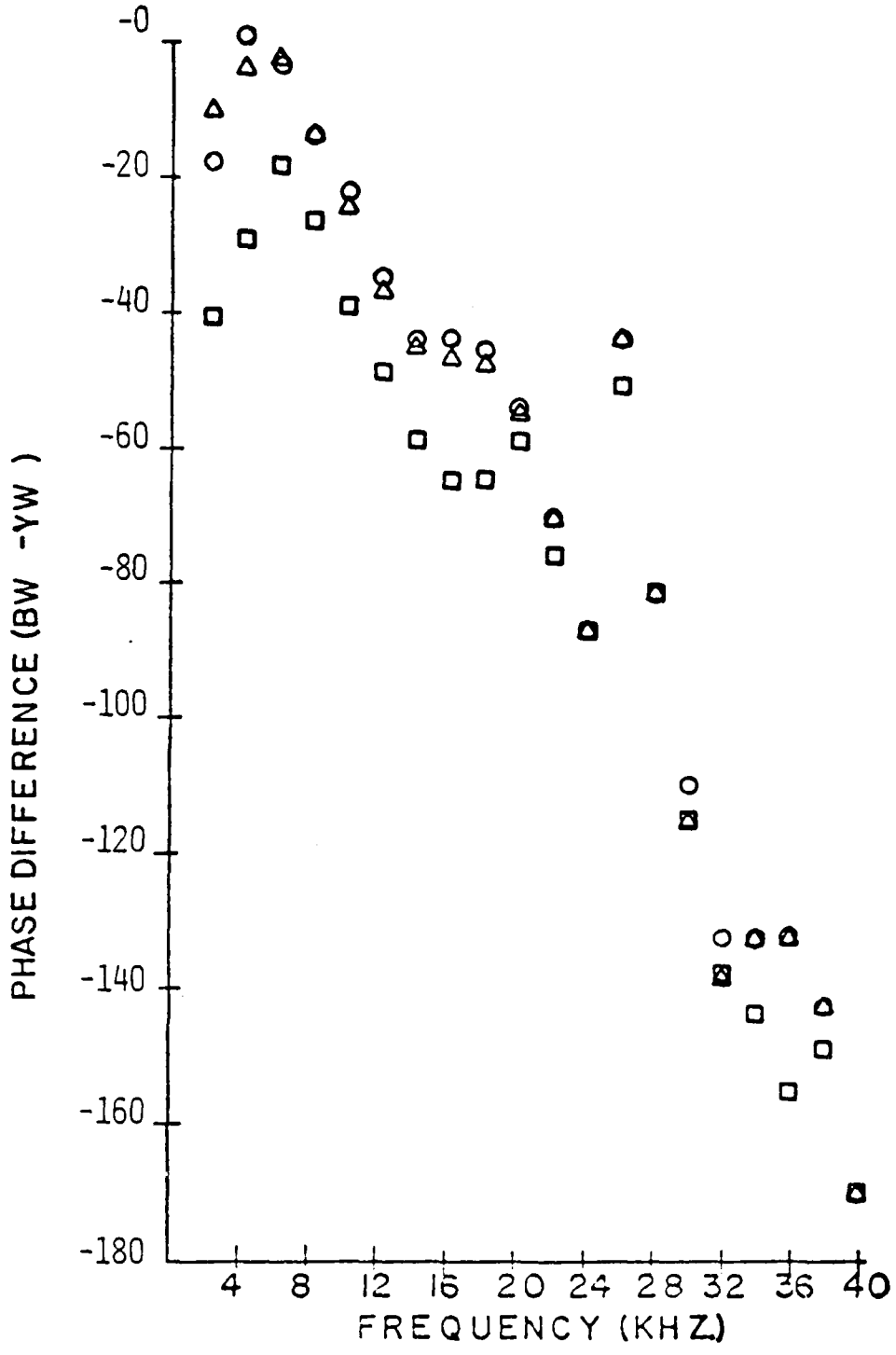

Figure 17. Phase Difference (BW-WW) vs. Frequency (R_0 = 20 cm); rough planar surface; Z = Z_0 = 0.0 cm, O = Run I, Δ = Run II, and □ = Run III.

range (20 cm.). These results are beyond the limits of the theory; and are considered important from an application point of view. The data for the entire experiment was therefore taken out to 40 kHz which was essentially the limit of the equipment in order to maintain reproducibility in the presence of the remaining background noise.

It was then desired to observe the effects of varying the receiver height from 0 to 3.0 cm. above the surface of the bosses. This measure essentially gives the effective height of the scattered boundary wave. The results of these variations (z in equation 9) are plotted in Figures 18, 19, and 20. In Figures 18 and 19, the results are compared to the theory line for height 0. It can be seen that as the receiver is moved away from the boundary surface the boundary wave becomes weaker. Figure 20 shows that at low frequencies and small values of Z the experimental data agree well with theory but at higher frequencies and $Z > 0.5$ cm. the two deviate more as the height of the receiver is increased. The reason for the deviation is that in addition to the constraint $Kh \leq 1$, the theory holds only for $\theta << 1$ (that is for $Z_0+Z << R$), therefore, at R = 20 cm. for $Z < 2.0$ cm. Figures 21 and 22 demonstrate the behavior of the phase as the height of the receiver was change Again it is seen that at higher frequencies the phase difference (BW-VW) is larger.

In summary, experimental data agreed closely with the Tolstoy theory for propagation over a rough plane surface.

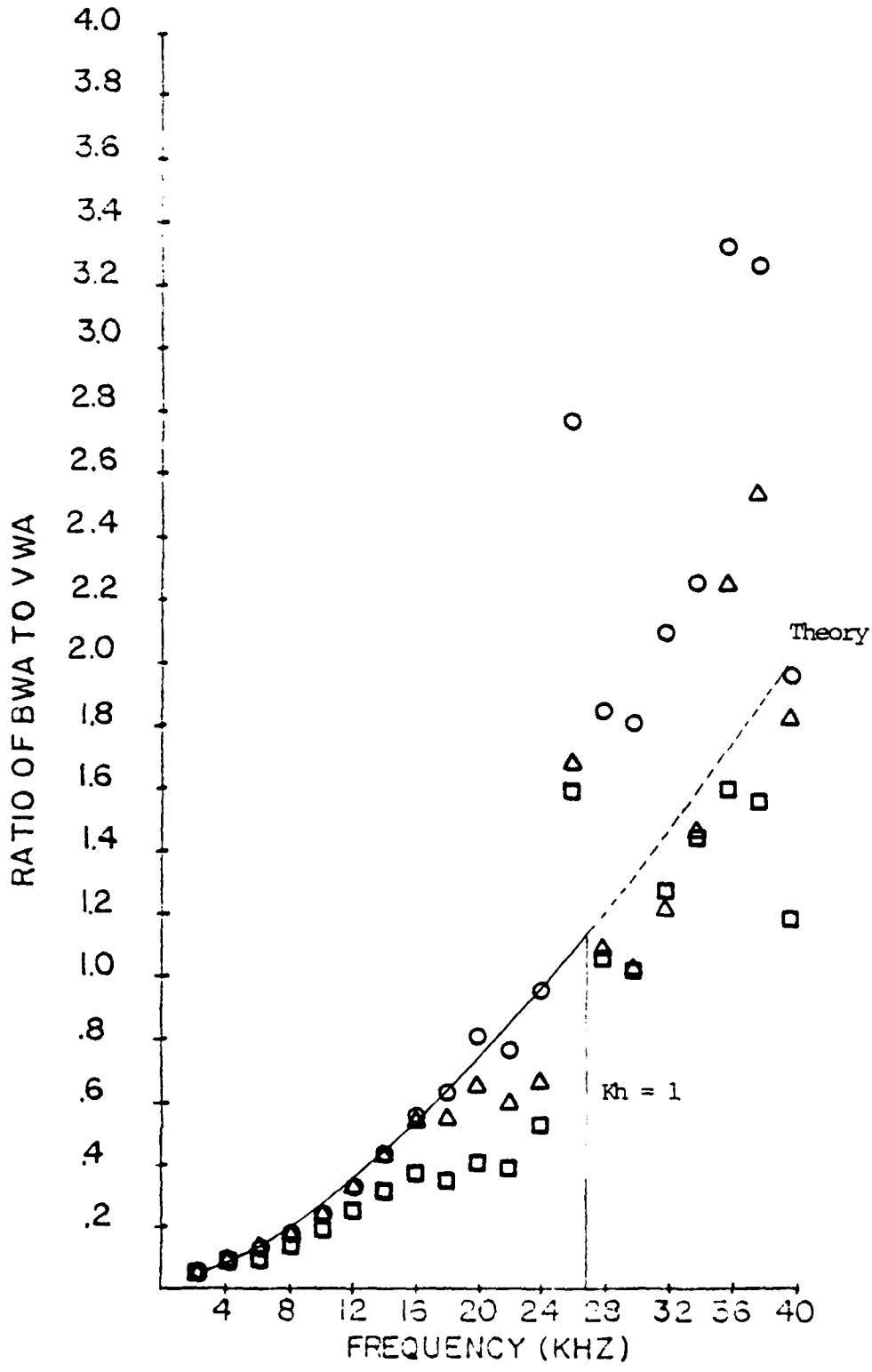

Figure 18. Ratio of BWA to VWA vs. Frequency for Various Receiver Heights; Range = 20 cm, O = 0.0 cm, Δ = 0.5 cm, □ = 1.0 cm, · = Tolstoy Theory Line for Receiver Height Z = 0.0 over 20 cm rough planar surface.

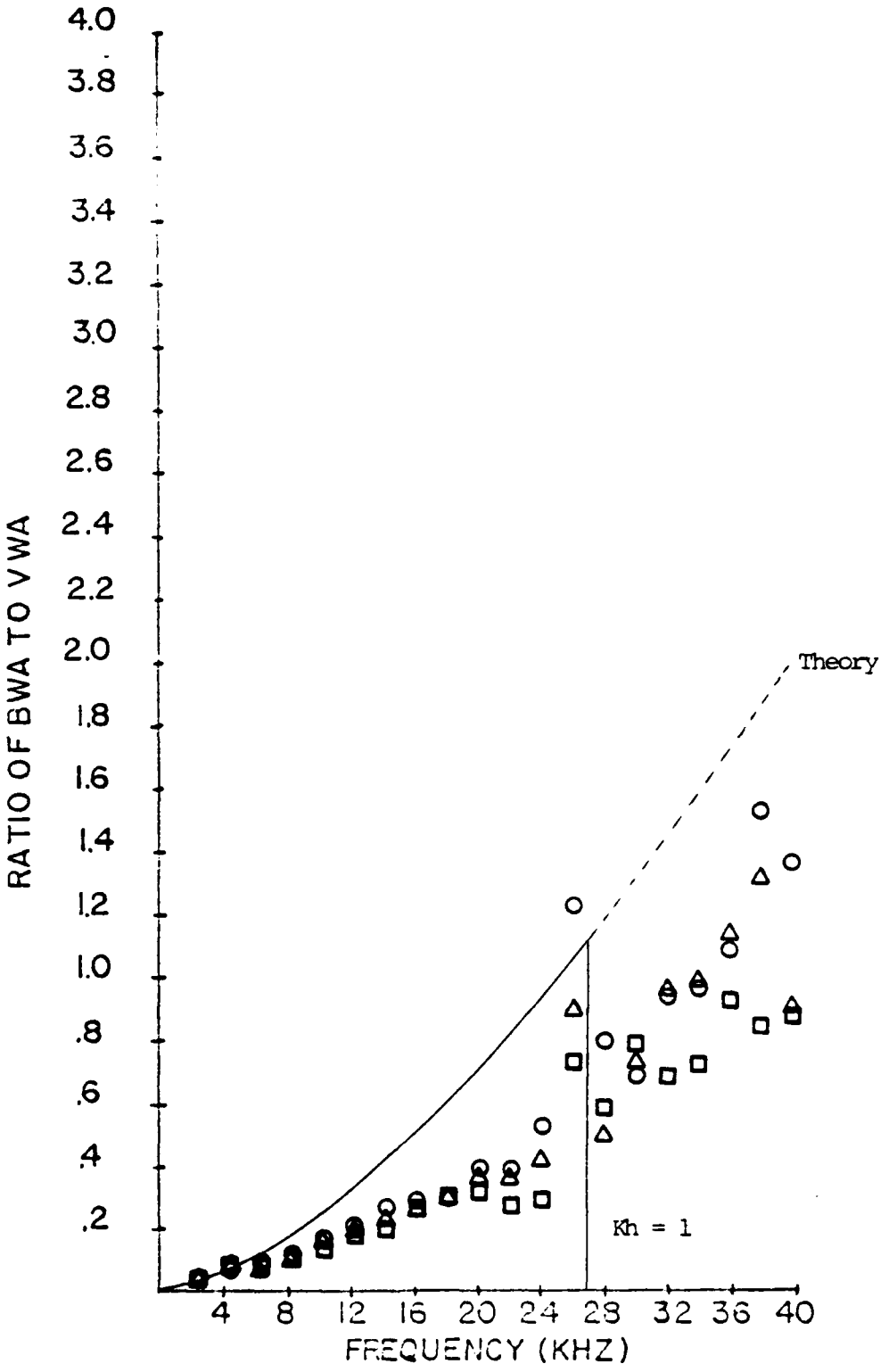

Figure 19. Ratio of BWA to VWA vs. Frequency for Various Receiver Heights; Range = 20 cm, O = 1.5 cm, Δ = 2.0 cm, □ = 2.5 cm, — = Tolstoy Theory Line for Receiver Height Z = 0.0 over 20 cm Rough Planar Surface.

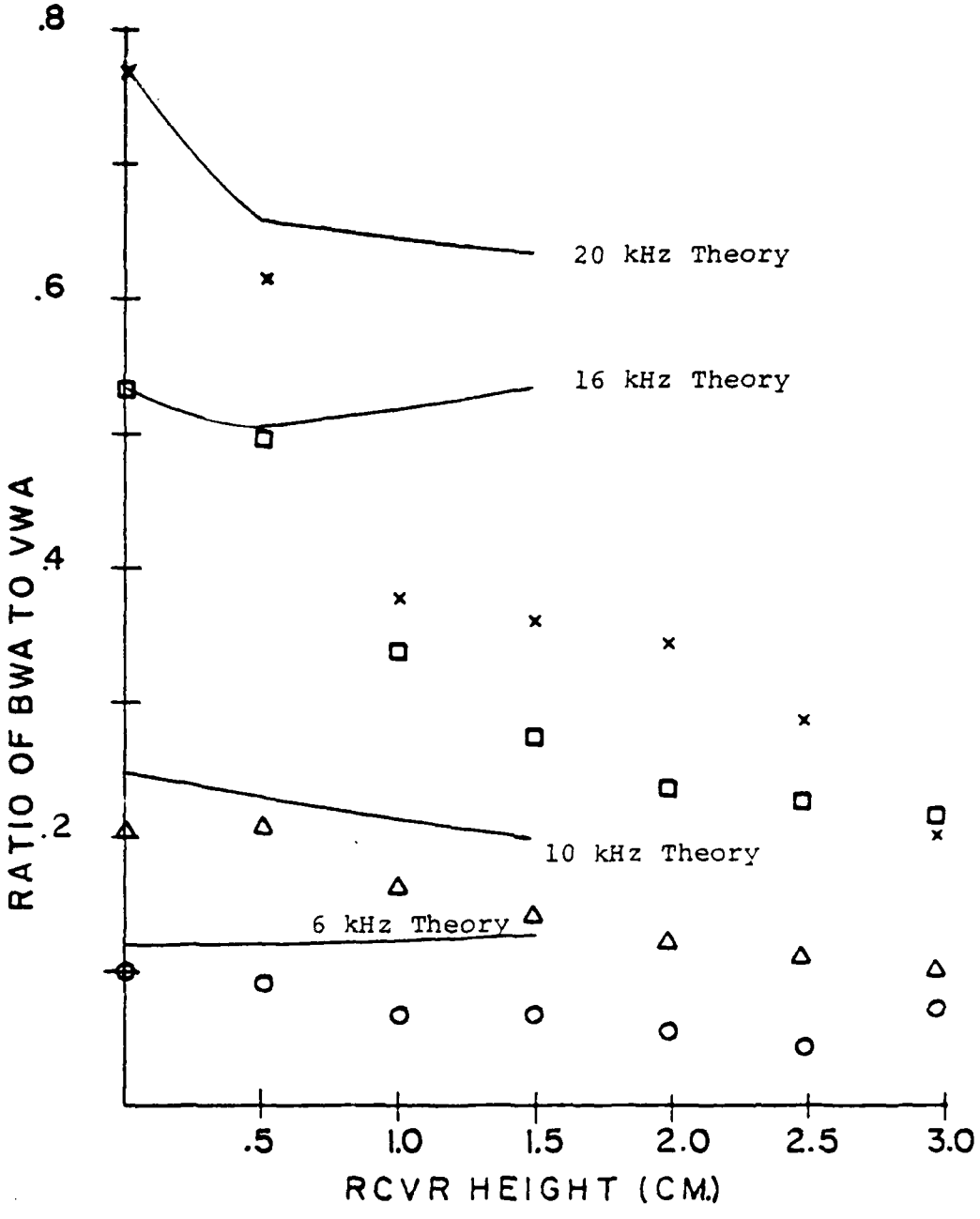

Figure 20. Ratio of BWA to VWA vs. Receiver Heights; R_0 = 20 cm, Rough Planar Surface, o = 6 kHz, Δ = 10 kHz, □ = 16 kHz, and x = 20 kHz. Theory holds only for $\theta \ll 1$, therefore, at R_0 = 20 cm for Z < 2.0 cm.

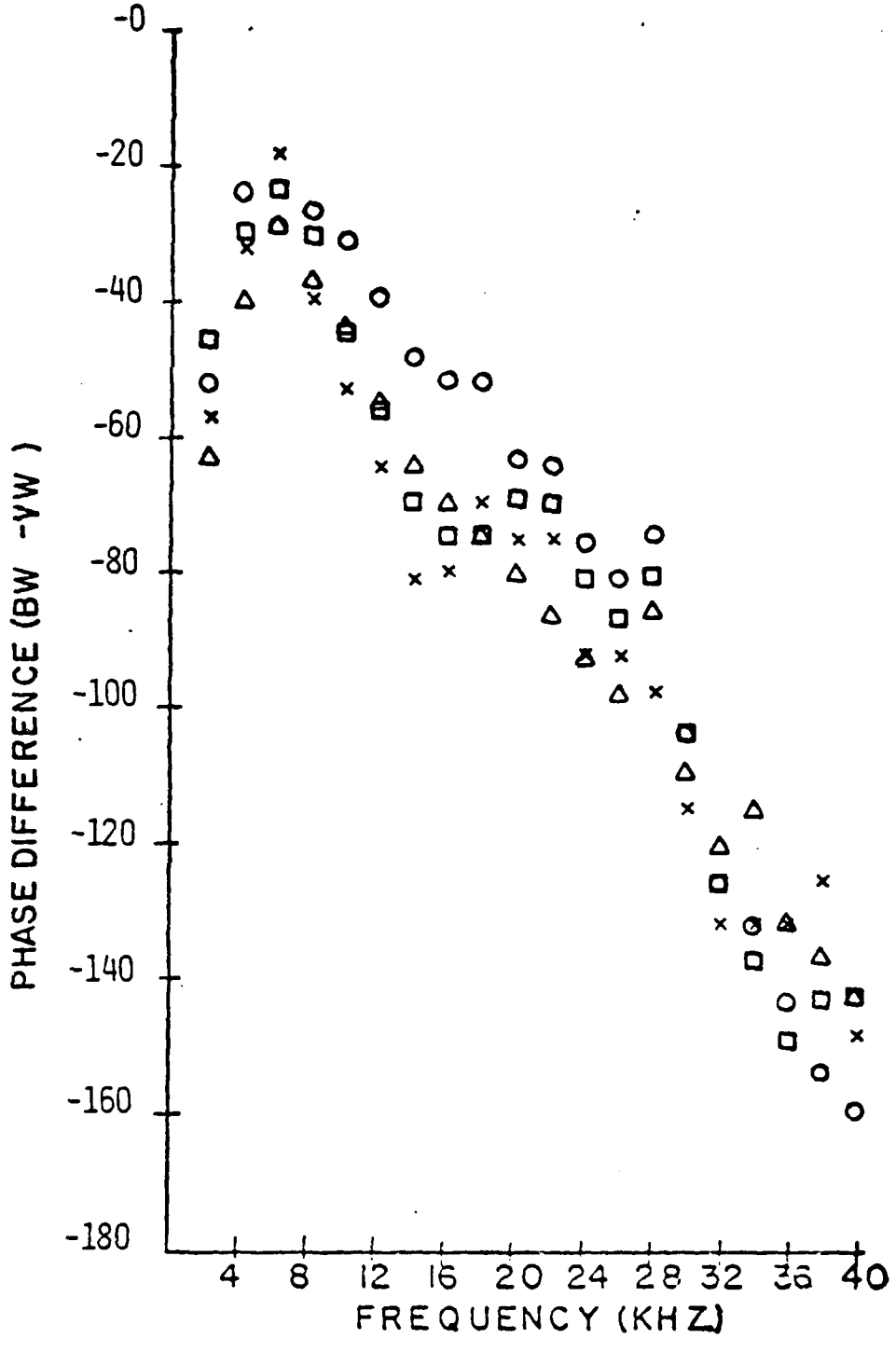

Figure 21. Phase Difference (BW-VW) vs. Frequency for Various Receiver Heights; R_0 = 20 cm, Rough Planar Surface, 0 = 0.0 cm, Δ = 0.5 cm, □ = 1.0 cm, and x = 1.5 cm.

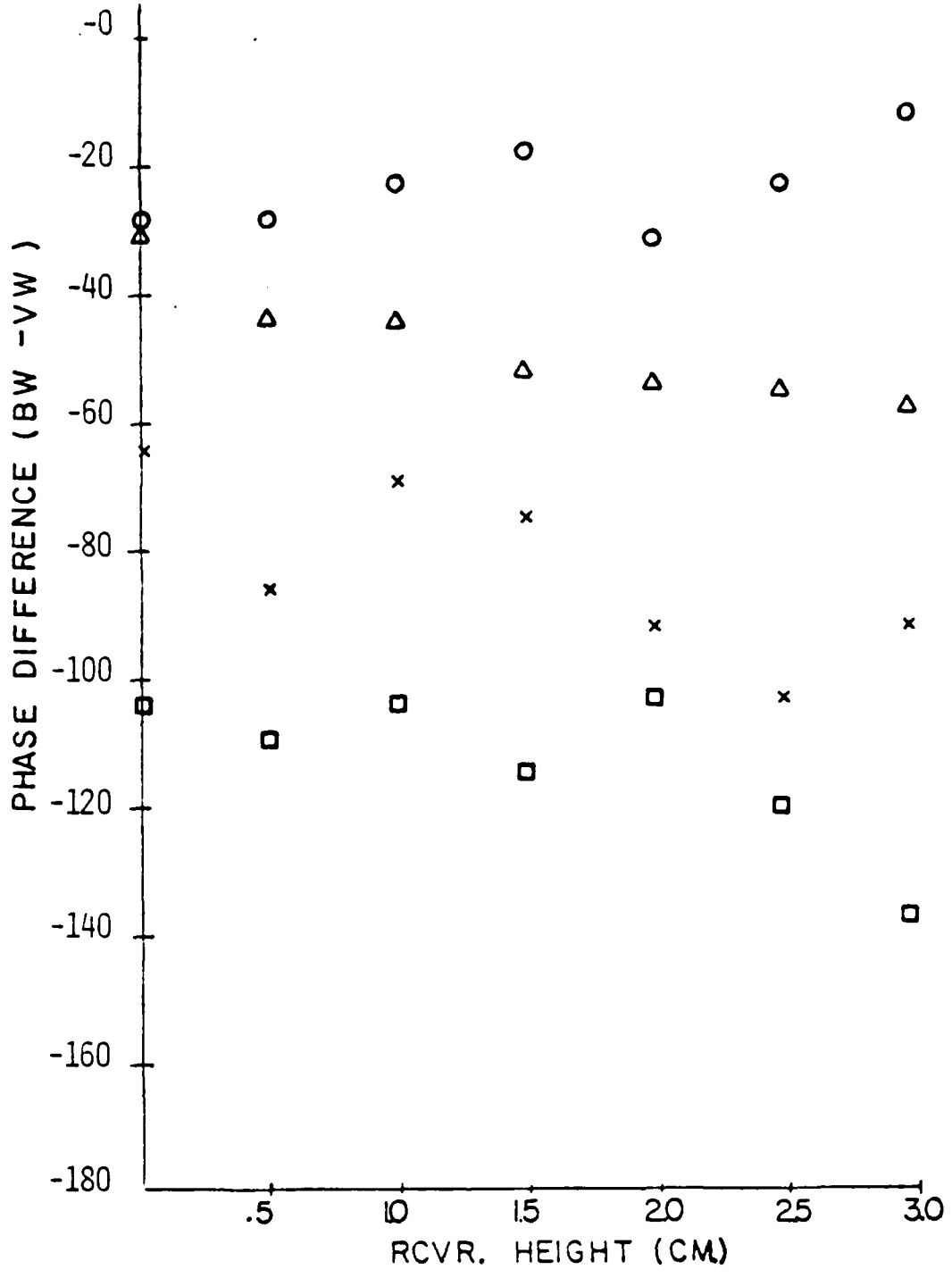

Figure 22. Phase Difference (BW-VW) vs. Receiver Heights; R_0 = 20 cm, Rough Planar Surface, 0 = 6 kHz, Δ = 10 kHz, x = 22 kHz, and □ = 30 kHz.

This agreement confirmed that a satisfactory surface roughness had been achieved and that the equipment was functioning properly. Upon completion of this phase, the experiment proceeded to task two.

B. THE DIFFRACTION AND PROPAGATION OF A ROUGH SURFACE BOUNDARY WAVE OVER A PARTIALLY ROUGH WEDGE

For this trial the front side of the wedge was rough to permit boundary wave growth and the backside of the wedge was smooth. The expected loss in signal strength due to greater ranges and diffraction over the wedge required that the signal be processed differently. From previous observations, it was observed that to have small variations in results the data were required to be reproducible within .1 dB at 2-14 kHz, and .3 dB at 16-40 kHz. The higher tolerance at higher frequencies for 16-40 kHz is made possible by the stronger boundary wave. A band from 1.5 to 40 kHz was run using amplification through PAR I of 10 thousand and through PAR II of 20. The high frequency signal was so much weaker than the lower frequency signals that there was no problem in leaving the bandwidth wide. However, to collect reliable high frequency information it was necessary to have a high frequency passband, 16-42 kHz in order to attenuate the low frequency signals enough for additional amplification to be used. Therefore the Krohn-Hite Model 3342 filter was substituted for the previously used Model 3550 in order to gain an additional 72 more dB attenuation per octave. The amplification factor used for the high frequency bandwindow was 10 thousand through

PAR I and 100 through PAR II. The increase in reproducibility due to amplification alone was not sufficient and additional averaging was required. The averaging was increased from 1,000 to 9,999, which was the maximum limit of the available OPHELEA computer program. Table II demonstrates these effects. The high frequency band at ranges greater than 10 cm. from the crest had a negative signal to noise ratio. To insure the desired signal was being received at maximum range, a run was compared with signal on and signal off. These results are given in Table III and demonstrate the necessity of being able to average the signal many times. The dB reference is .18 Vrms therefore a signal level of 20 dB in the high frequency band represents a signal strength of 1.8 microvolts.

The results of these data runs from 5 to 35 cm. are shown in Figures 23-36. In Figures 23-29, two runs have been plotted out of the possible four combinations for both frequency bands.

In the experiment the data were taken first over the smooth then the rough surface and repeated in that order. Figures 30-36 show the variation in range of the data. At R = 5 cm. there is only 1 run in the (2-14 kHz) band. The reason was that previously this run had been made using 1000 averages and the data had shown a small variation, therefore, at this range the additional averages were not necessary. However, to have all the data to be averaged 9999 times this one run was taken. The R = 5 cm. values from 16-40 kHz do show the range in values from the four possible combinations

Table III

Table of Source ON/OFF Data

Freq. kHz	Parameters - $R = 35$, $R_0 = 20$,/Bandlimit 16-42 kHz/ 9999 averages/Amplification 1000K/ Smooth Wedge		
	Run I	Run II	Run (No Signal)
16	26.1	26.1	-5.50
18	26.1	26.2	.371
20	21.8	21.6	4.88
22	17.6	17.7	1.41
24	11.5	11.4	-1.79
26	6.28	5.97	.430
28	8.99	8.36	1.51
30	9.97	8.55	-2.06
32	9.80	10.8	-3.06
34	10.6	9.27	2.79
36	8.15	8.57	-7.59
38	6.20	6.40	-5.48
40	4.73	4.09	-4.45

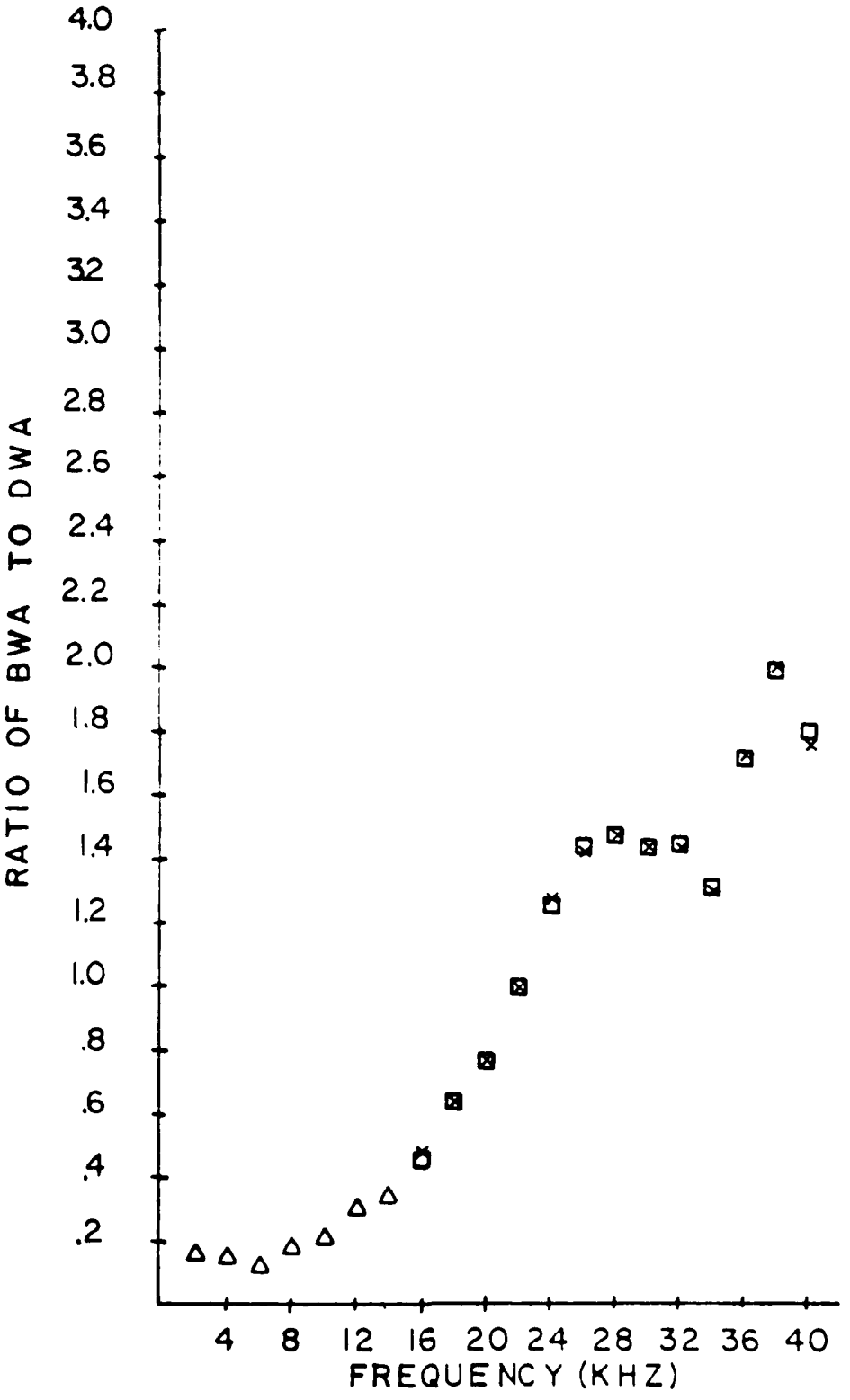

Figure 23. Ratio of BWA to DWA vs. Frequency (R = 5 cm); R_0 = 20 cm, Z = Z_0 = 0 cm, Δ = Run I (1.5-42 kHz), □ = Run II (16-42 kHz), and x = Run II (16-42 kHz).

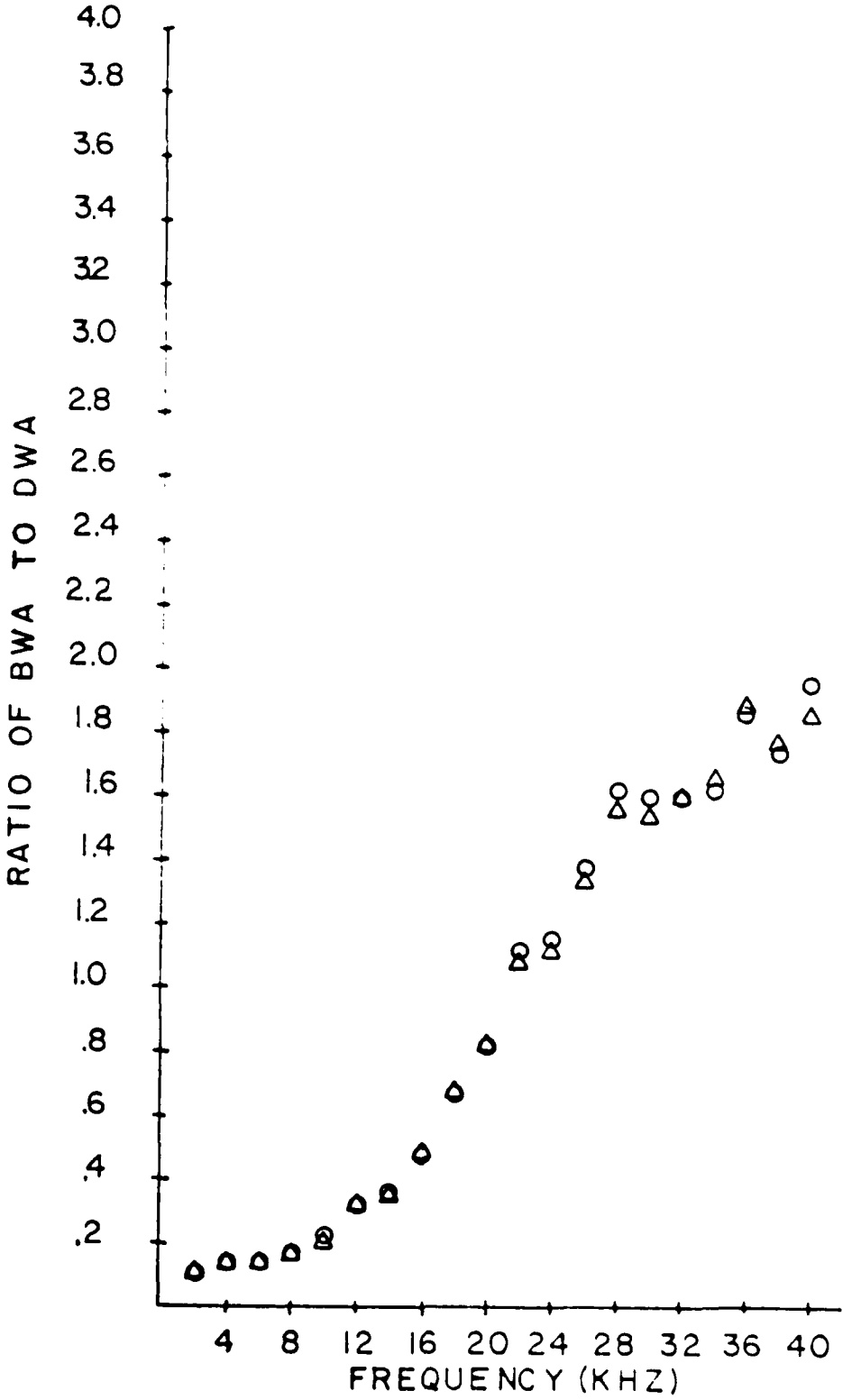

Figure 24. Ratio of BWA to DWA vs. Frequency (R = 10 cm); R_0 = 20 cm, $Z = Z_0 = 0$, 0 = Run I, and Δ = Run II.

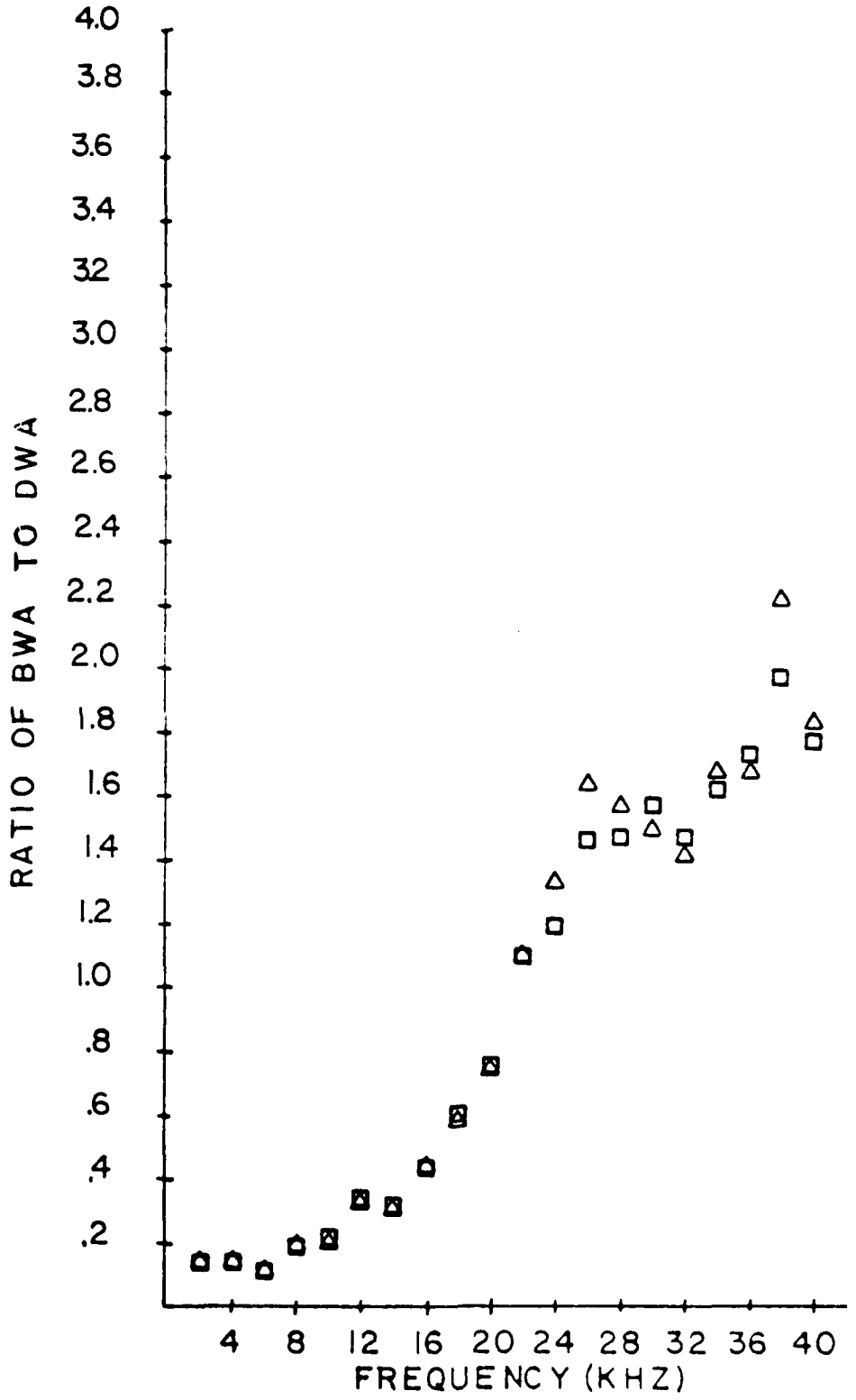

Figure 25. Ratio of BWA to DWA vs. Frequency (R = 15 cm); R_0 = 20 cm, Z = Z_0 = 0, □ = Run I and △ = Run II.

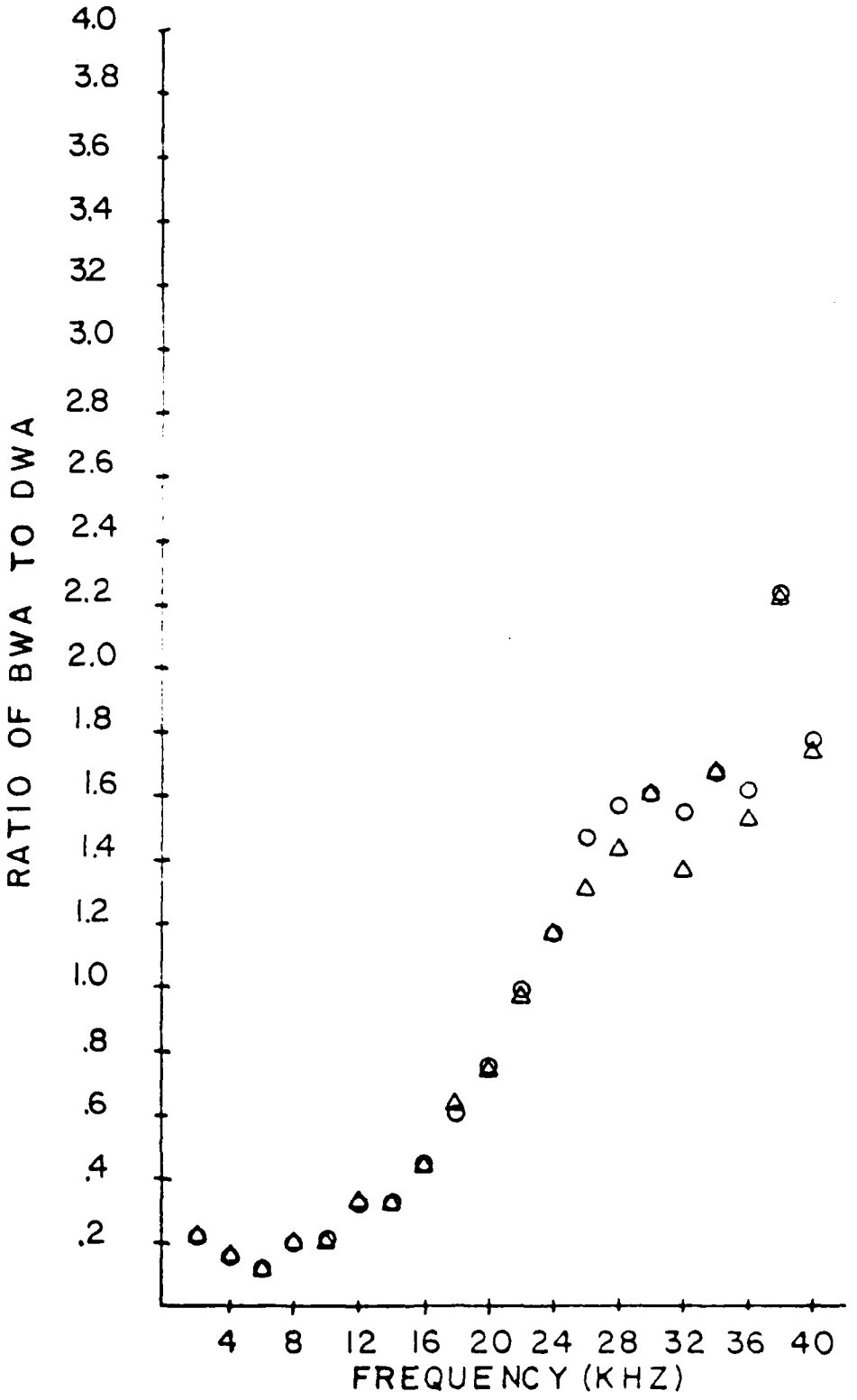

Figure 26. Ratio of BWA to DWA vs. Frequency (R = 20 cm); R_0 = 20 cm, Z = Z_0 = 0 cm, 0 = Run I and Δ = Run II.

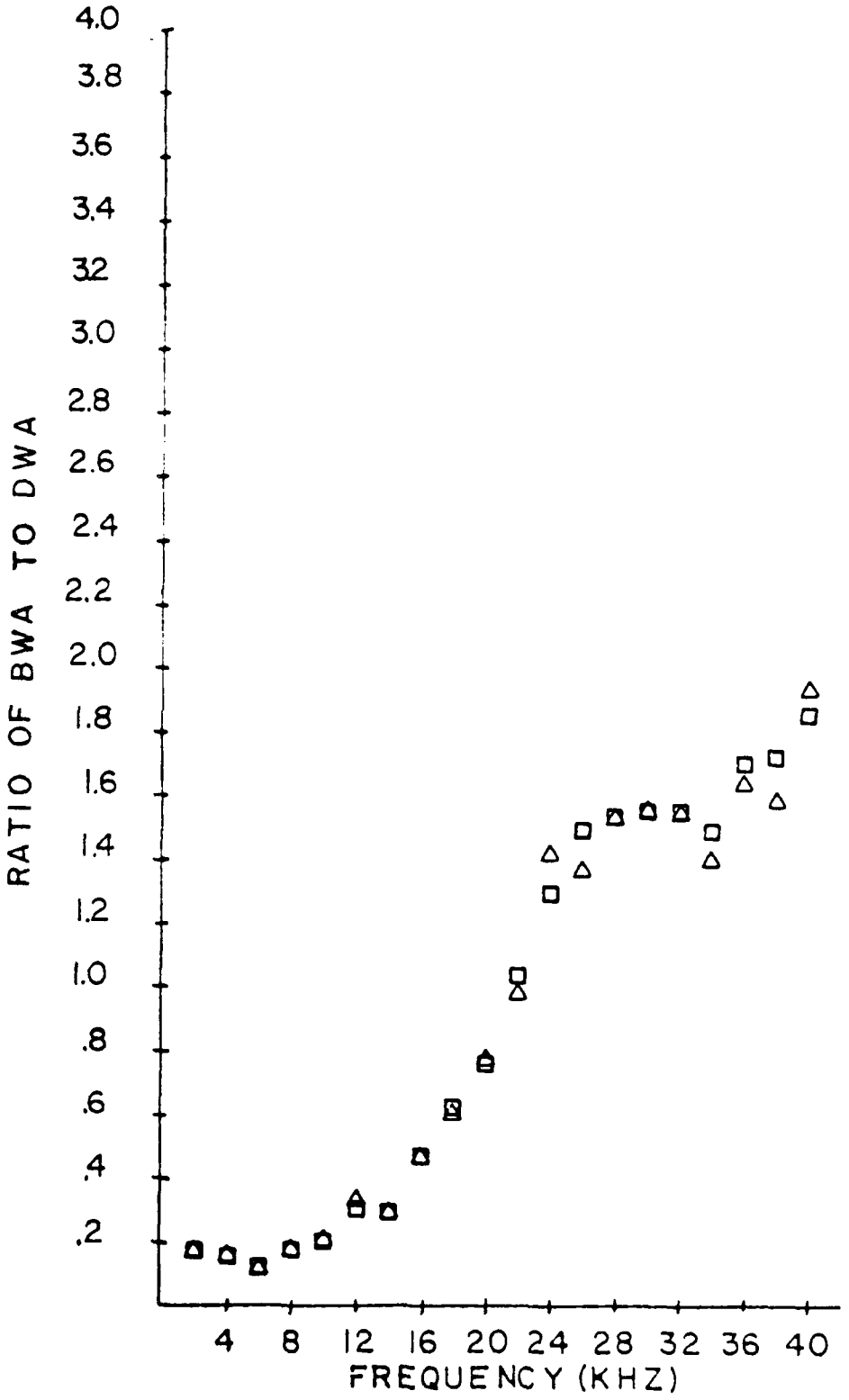

Figure 27. Ratio of BWA to DWA vs. Frequency (R = 25 cm); R_0 = 20 cm, Z = Z_0 = 0.0 cm, □ = Run I and △ = Run II.

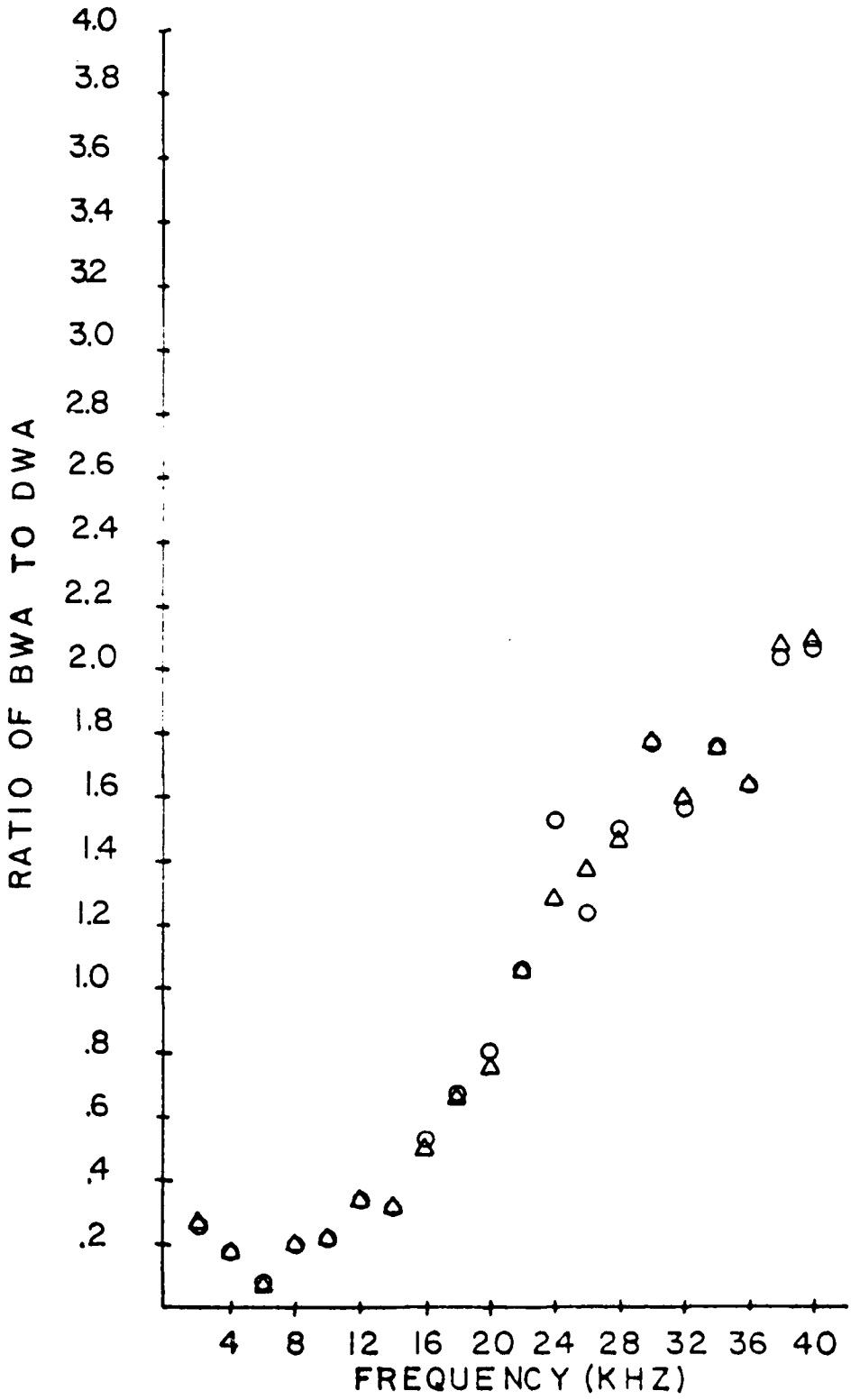

Figure 28. Ratio of BWA to DWA vs. Frequency (R = 30 cm); R_0 = 20 cm, Z = Z_0 = 0.0 cm, O = Run I and Δ = Run II.

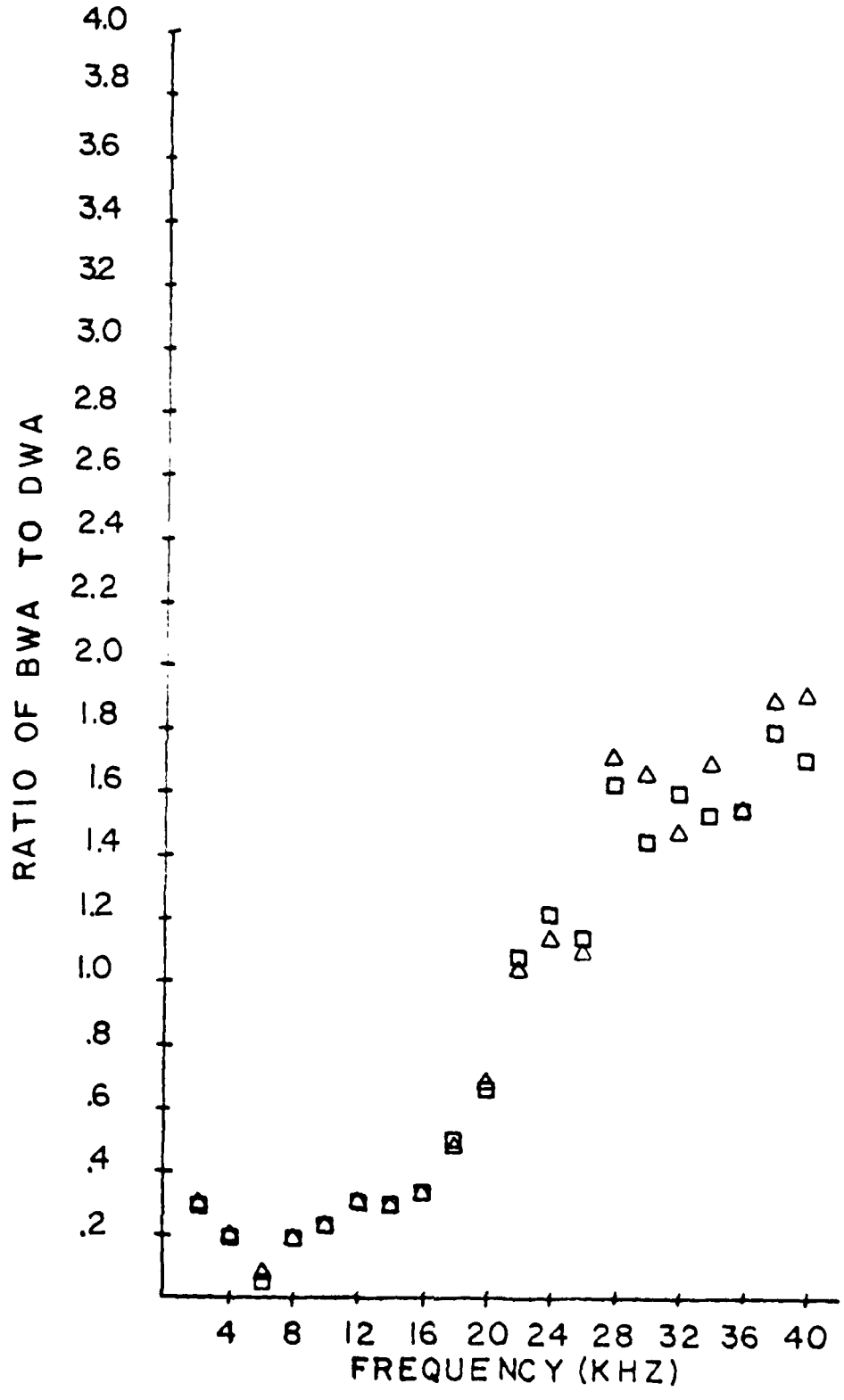

Figure 29. Ratio of BWA to DWA vs. Frequency (R = 35 cm); R_0 = 20 cm, Z = Z_0 = 0.0 cm, □ = Run I and Δ = Run II.

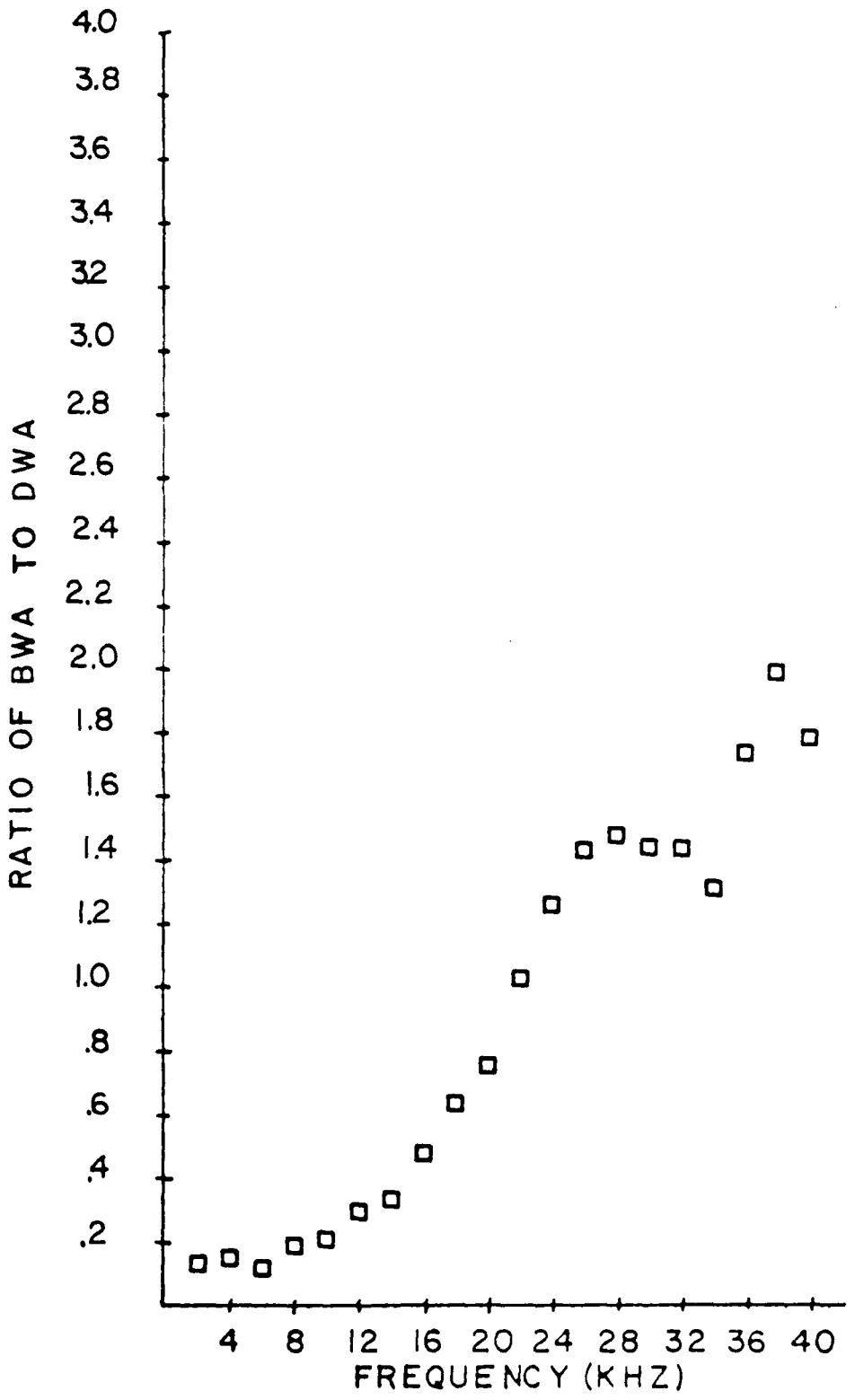

Figure 30. Range of Data Values for Ratio of BWA to DWA vs. Frequency ($R = 5$ cm); $R_0 = 20$ cm, $Z = Z_0 = 0.0$ cm, □ = (2-14 kHz) Run I, and □ = (16-40 kHz), Range of Four Data Values.

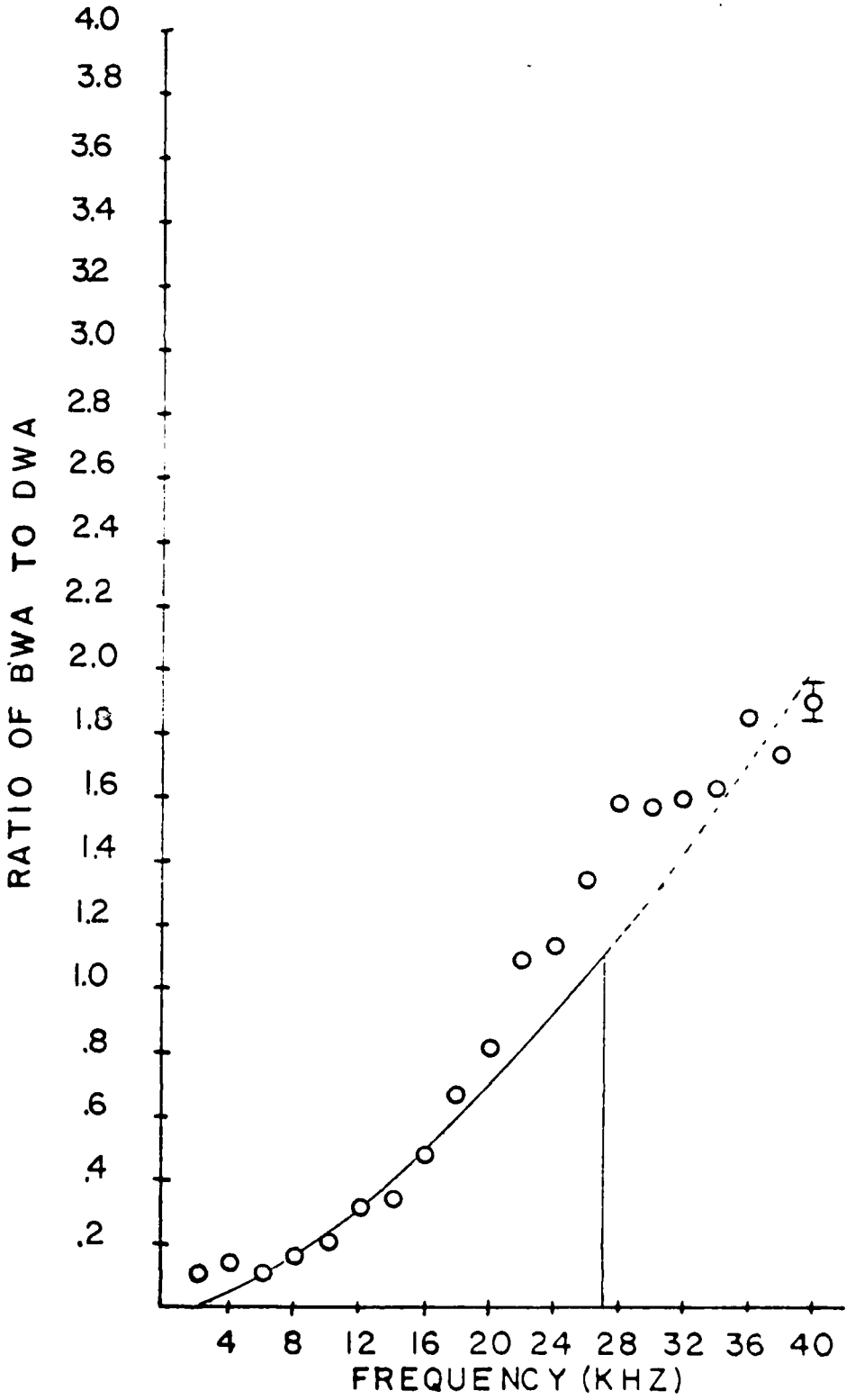

Figure 31. Range of Data Values for Ratio of BWA to DWA vs. Frequency (R = 10 cm); R_0 = 20 cm, Z = Z_θ = 0.0 cm, 0 = (2-14 kHz), Range of Two Data Values, and θ = (16-40 kHz), Range of Four Data Values. Tolstoy Theory Line R_0 = 20 cm over Rough Planar Surface.

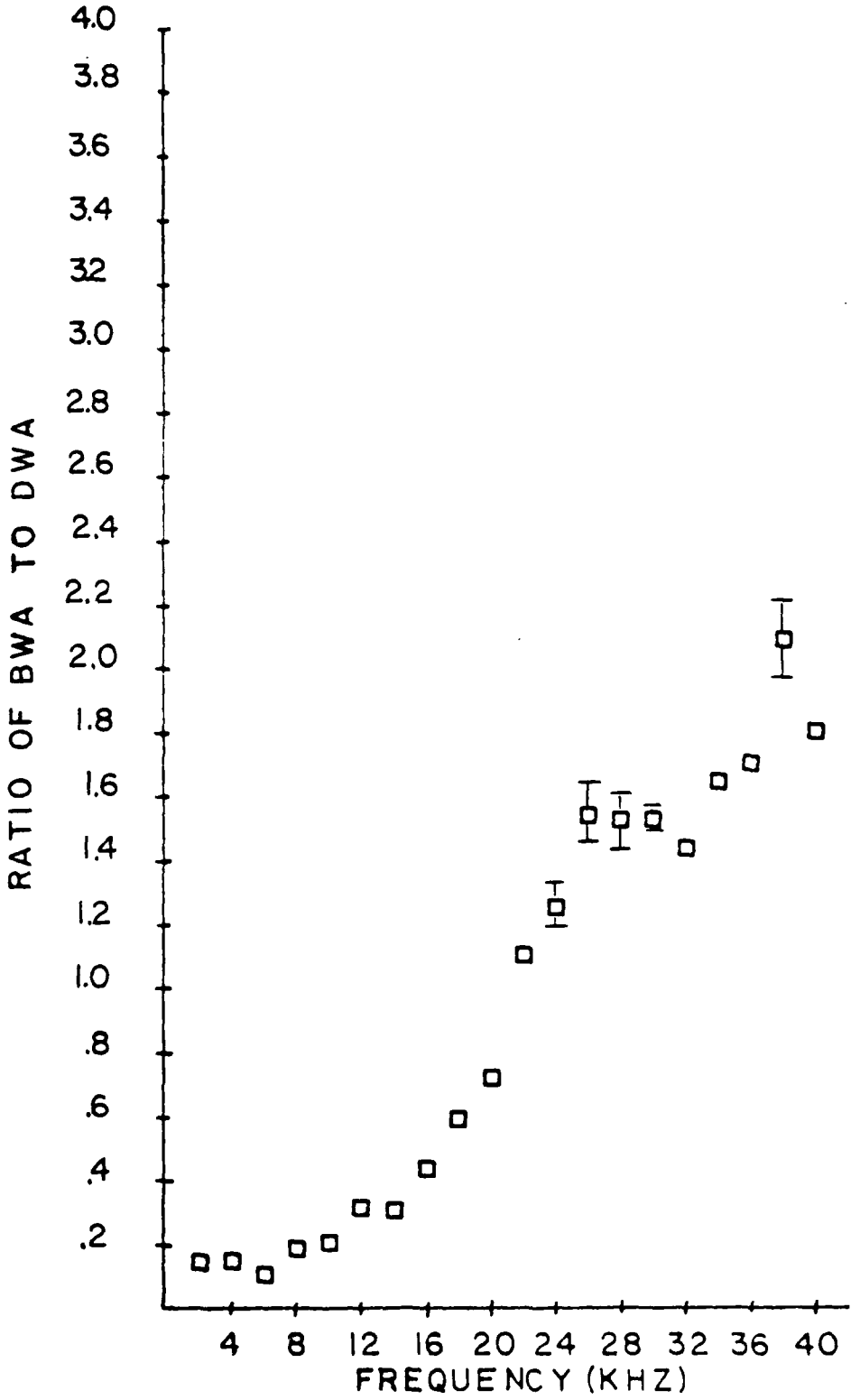

Figure 32. Range of Data Values for Ratio of BWA to DWA vs. Frequency (R = 15 cm); R_0 = 20 cm, Z = Z_0 = 0.0 cm, and □ = Range of Four Values.

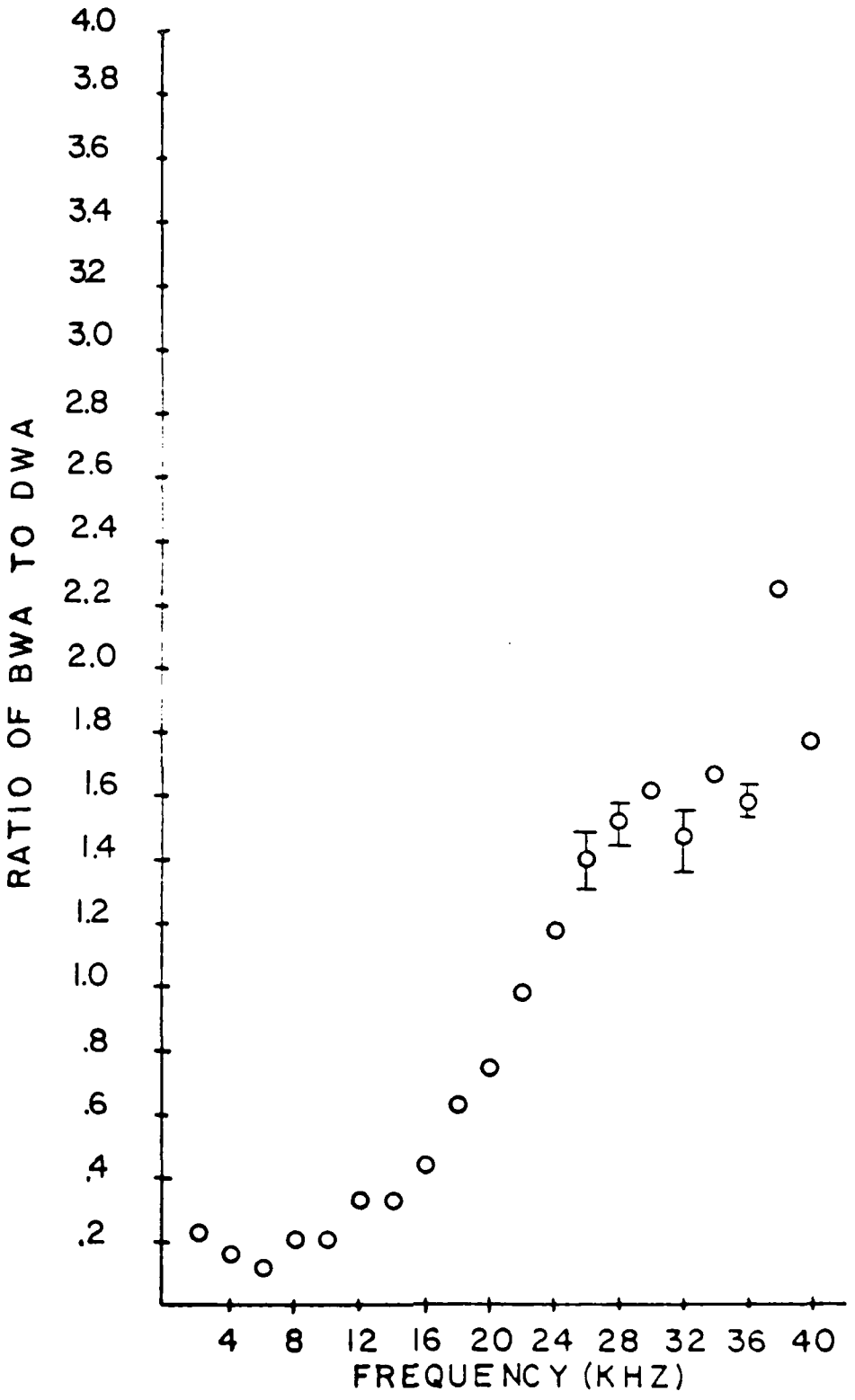

Figure 33. Range of Data Values for Ratio of BWA to DWA vs. Frequency (R = 20 cm); R_0 = 20 cm, Z = Z_0 = 0.0 cm, 0 = Range of Four Data Values.

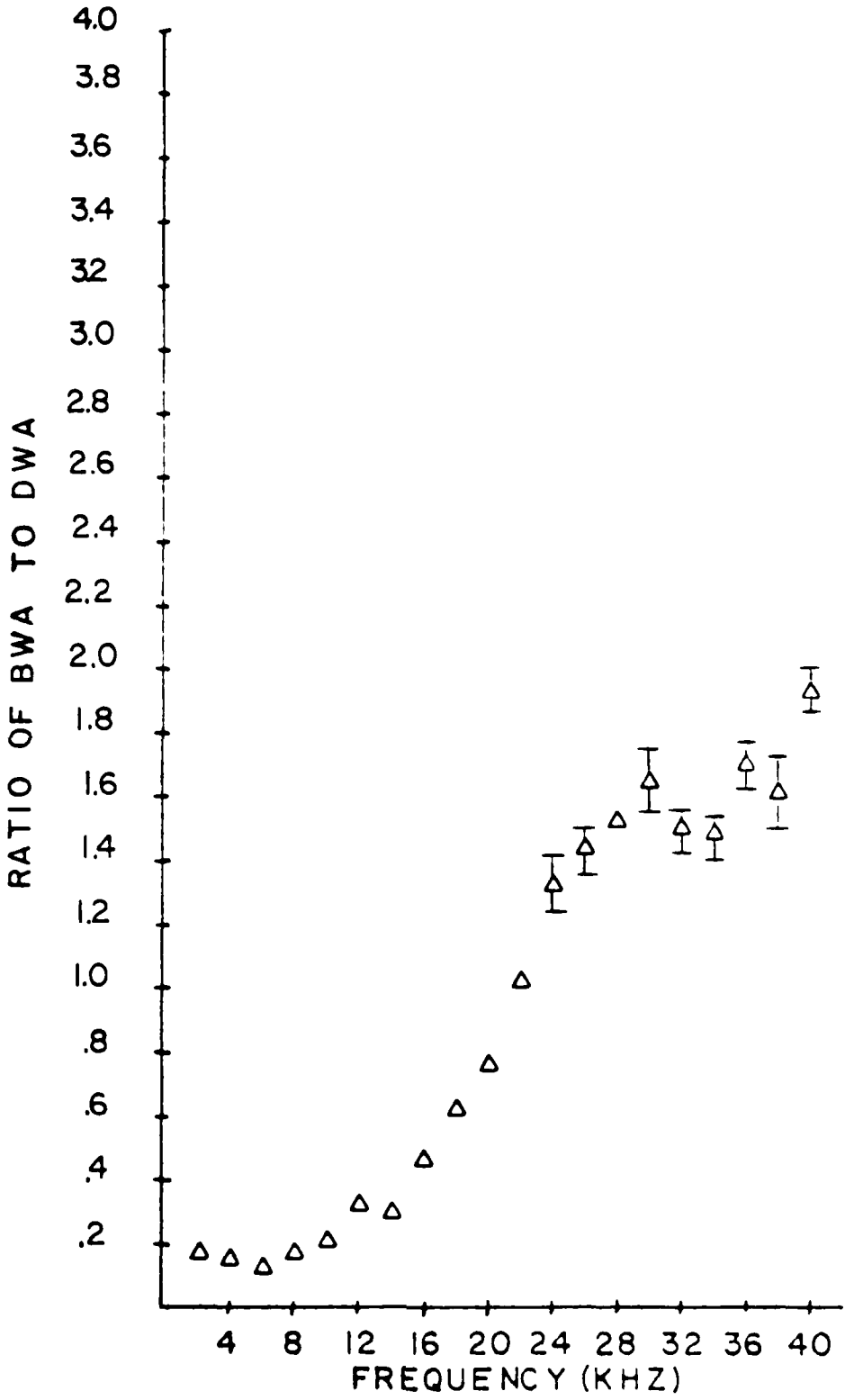

Figure 34. Range of Data Values for Ratio of BWA to DWA vs. Frequency (R = 25 cm); R_0 = 20 cm, Z = Z_0 = 0.0 cm, and Δ = Range of Four Data Values.

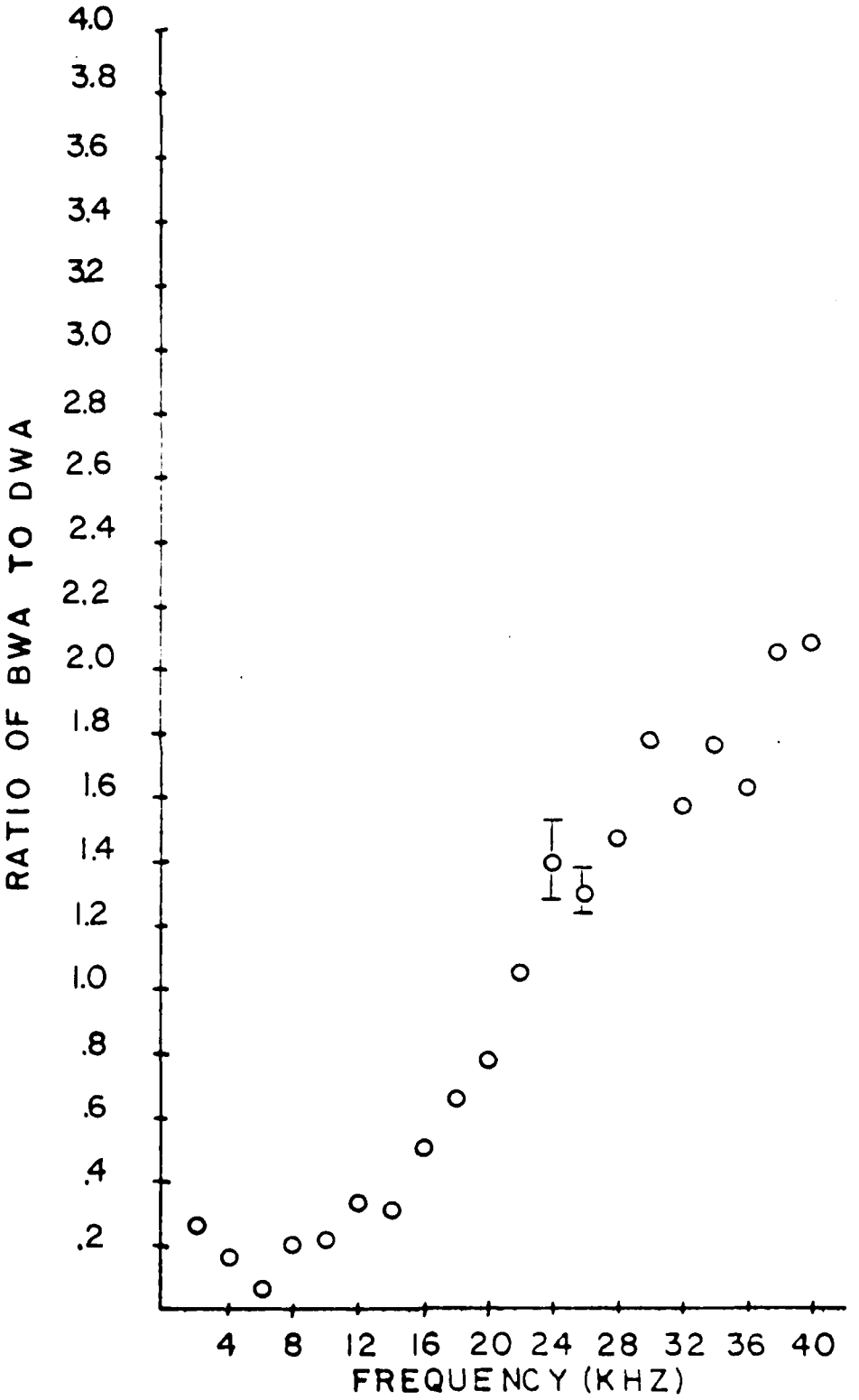

Figure 35. Range of Data Values for Ratio of BWA to DWA vs. Frequency (R = 30 cm); R_0 = 20 cm, Z = Z_0 = 0.0 cm, and 0 = Range of Four Data Values.

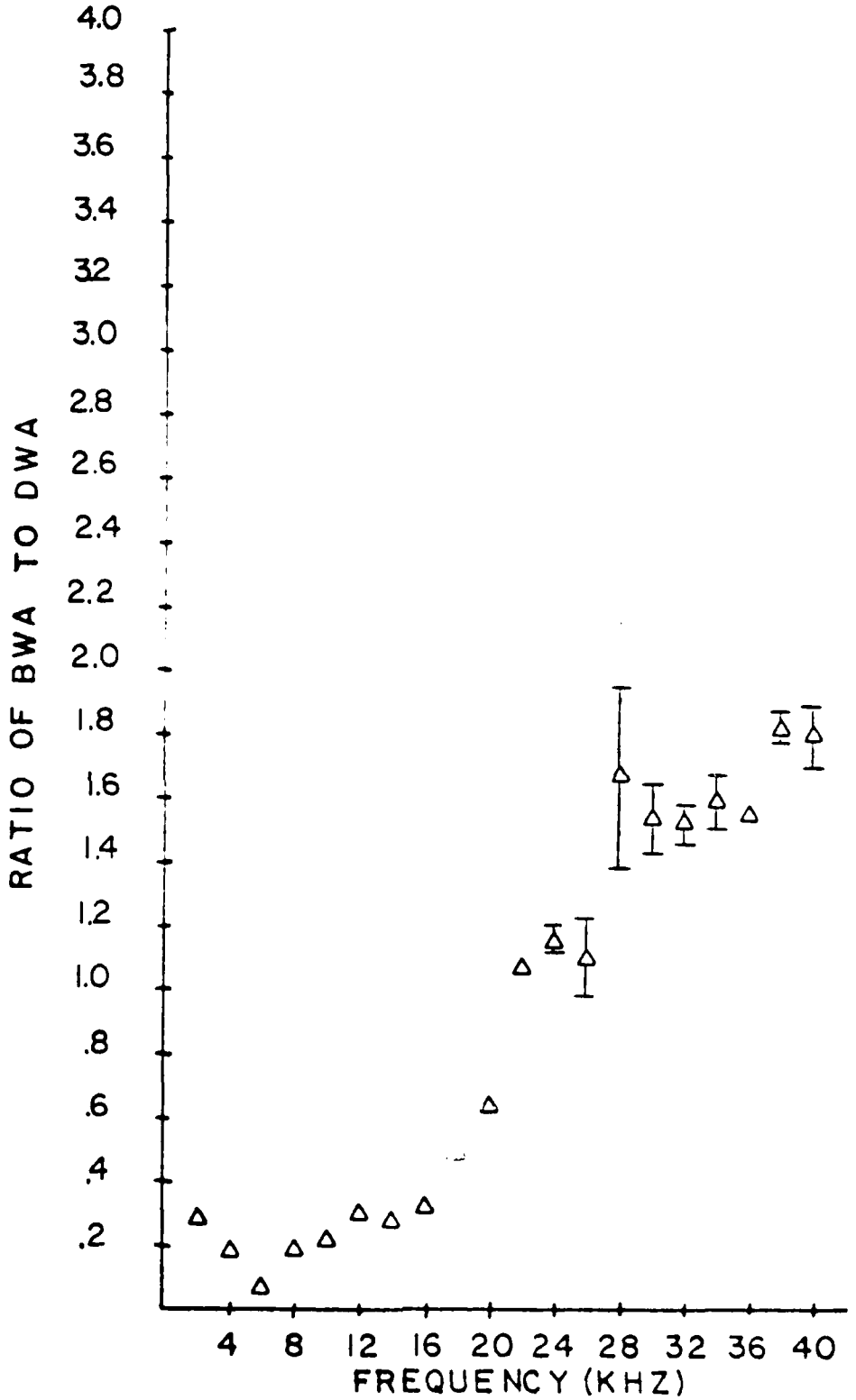

Figure 36. Range of Data Values for Ratio of BWA to DWA vs. Frequency (R = 35 cm); R_0 = 20 cm, $Z = Z_0$ = 0.0 cm., and Δ = Range of Four Data Values.

of data. The R = 10 cm. value has its 2-14 kHz band plotted for only 2 runs, but again the 16-40 kHz was plotted for four runs. All other ranges, 15 through 35 cm., show the deviations of four data combinations in both bands. There is a particularly small range of data values in the important frequency range of 2-24 kHz. The data were compared to theory for propagation over 20 cm. of the rough planar surface. It can be seen that the data agree closely with these theoretical values. Additionally, Figures 37-43 show the log amplitude against log frequency. The average frequency dependence determined by linear regression was 1.7 (see Table V) in comparison with that of the plane rough surface theory of 1.5 (see equation 13). Figure 44, a plot of log amplitude versus log range shows that the amplitude is independent of range beyond the crest (see Table VI). The conclusion is that the boundary wave arriving at the crest diffracts and propagates the same as the volume wave, therefore no net effect is observed in the ratio of the boundary wave to the diffracted volume wave amplitude.

The phase difference between boundary wave and diffracted wave in degrees are plotted in Figures 45 and 46. The phase difference is larger in the low frequencies 2-8 kHz and decreases in the range 10 to 24 kHz. Figure 46 shows that the phase difference for frequencies 10, 16, 22 kHz vary only slightly for the various ranges.

In essence a new source has been created at the crest of the wedge whose amplitude characteristics were determined by

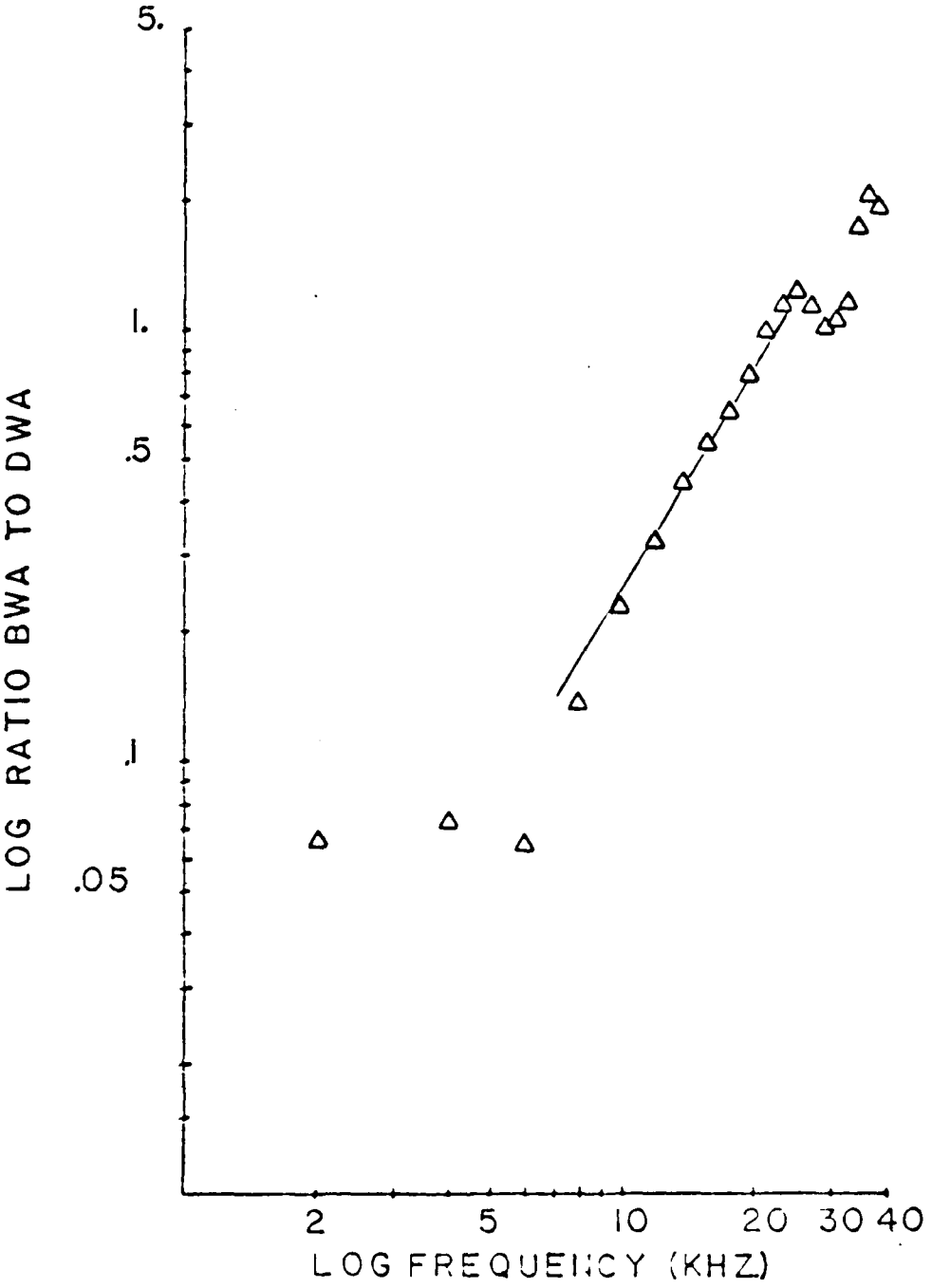

Figure 37. Log Ratio BWA to DWA vs. Log Frequency (R = 5 cm); R_0 = 20 cm, Z = Z_0 = 0.0 cm, Δ = Run I, and — = slope 1.7 (see Table V).

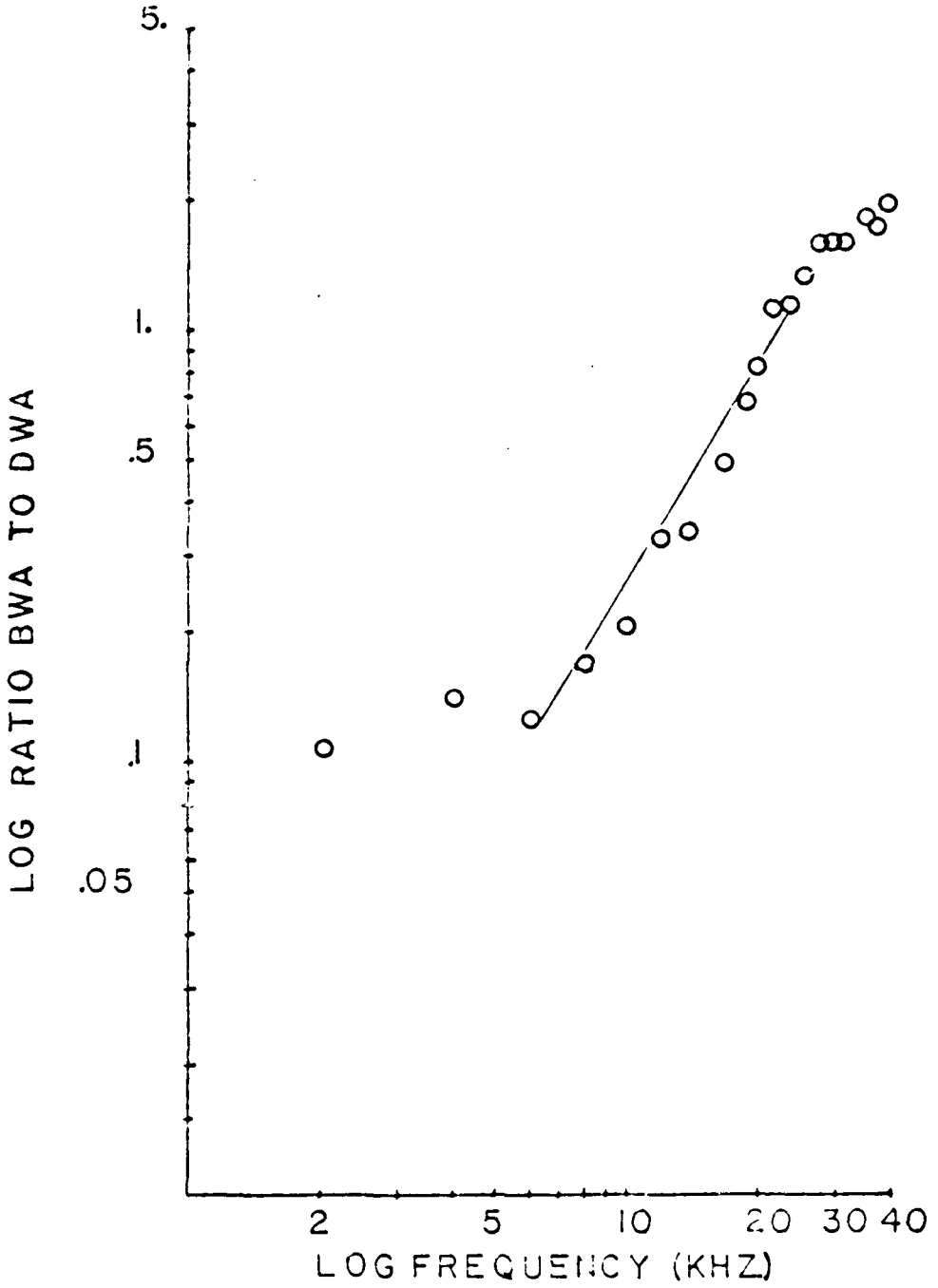

Figure 38. Log Ratio BWA to DWA vs. Log Frequency (R = 10 cm); R_0 = 20 cm, Z = Z_0 = 0.0 cm, 0 = Run I and — = slope 1.7 (see Table V).

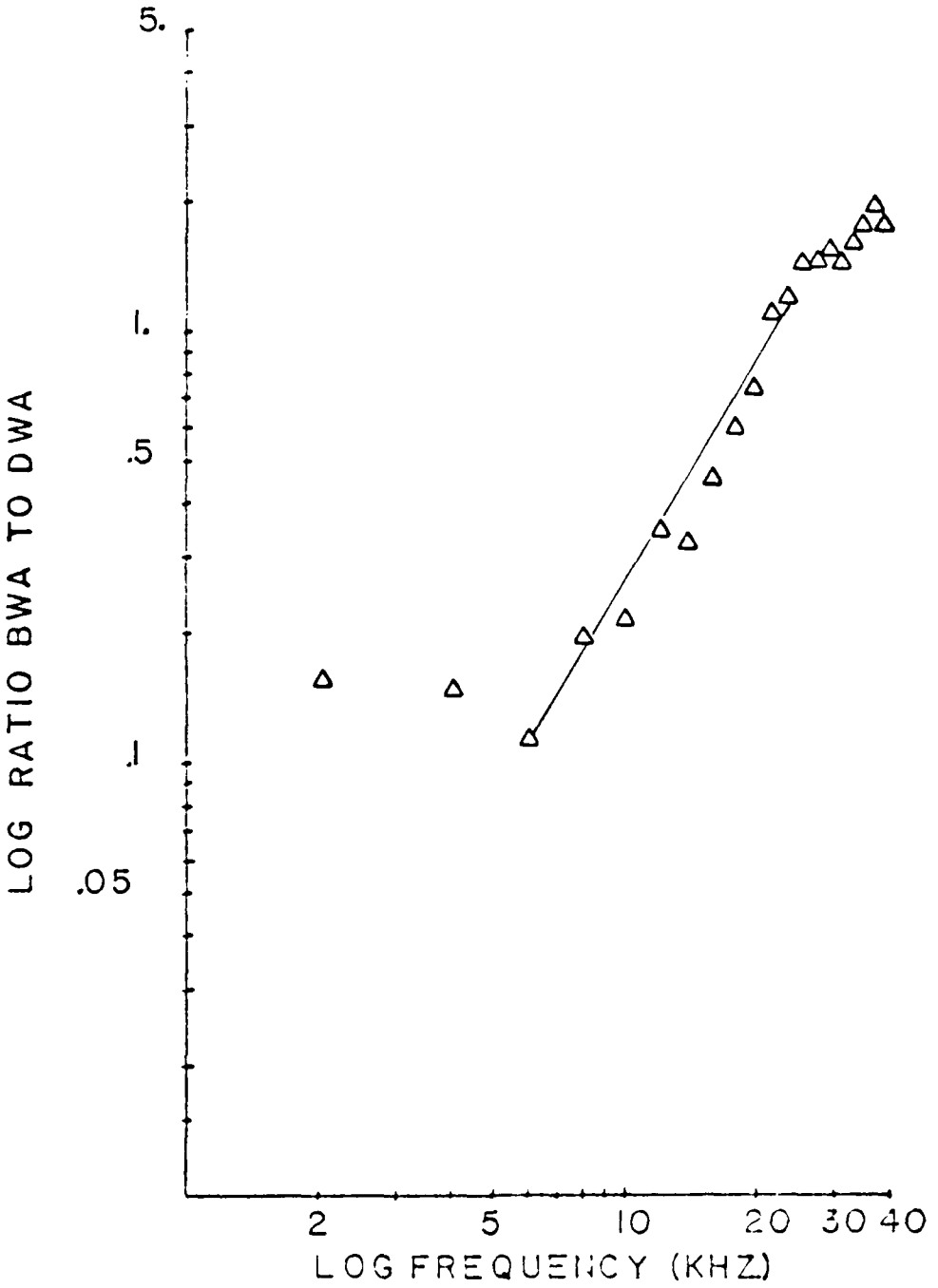

Figure 39. Log Ratio BWA to DWA vs. Log Frequency (R = 15 cm); R_0 = 20 cm, Z = Z_0 = 0.0 cm, Δ = Run I, and — = slope 1.7 (see Table V).

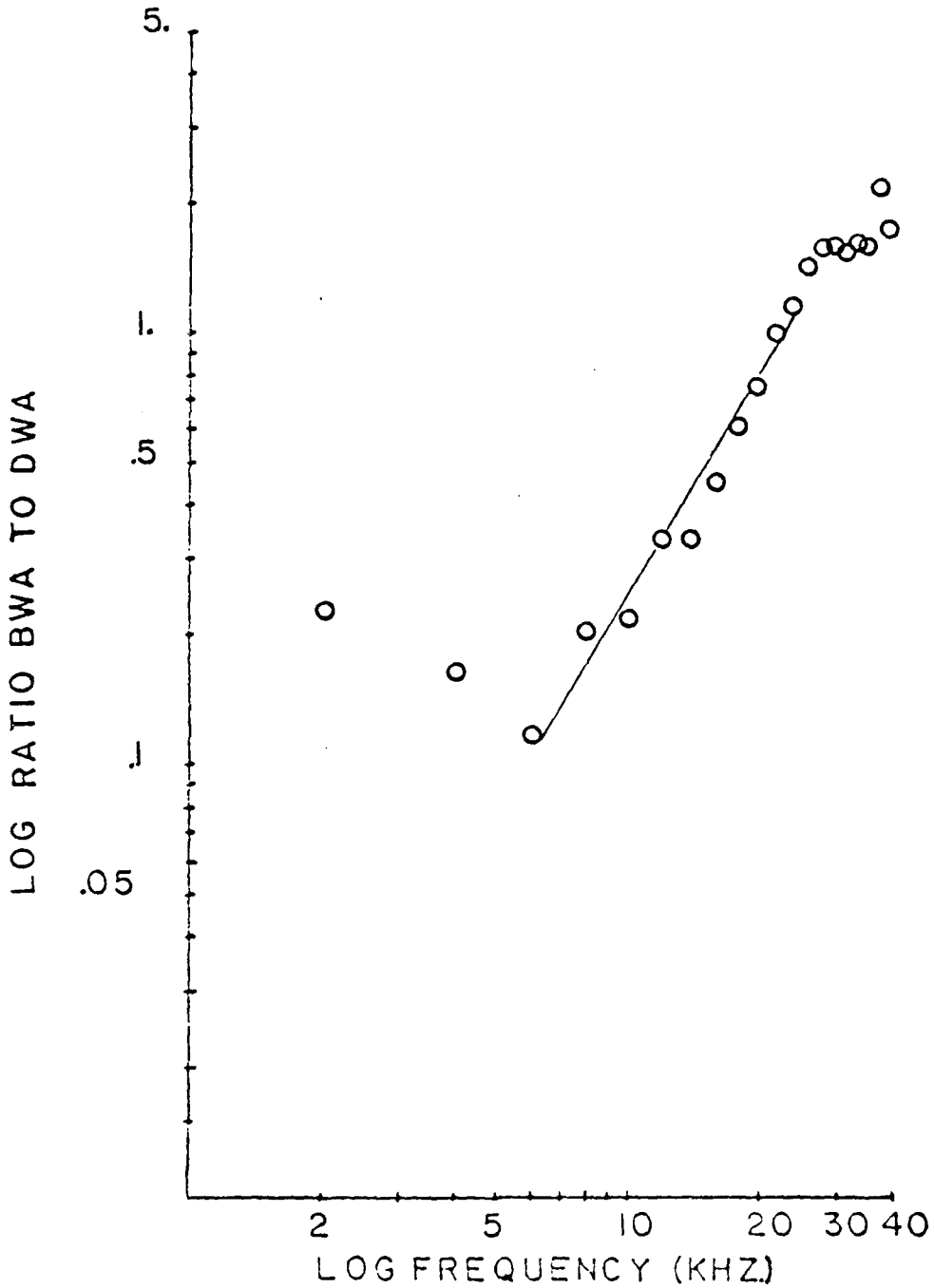

Figure 40. Log Ratio BWA to DWA vs. Log Frequency (R = 20 cm); R_0 = 20 cm, Z = Z_0 = 0.0 cm, 0 = Run I and — = slope 1.7 (see Table V).

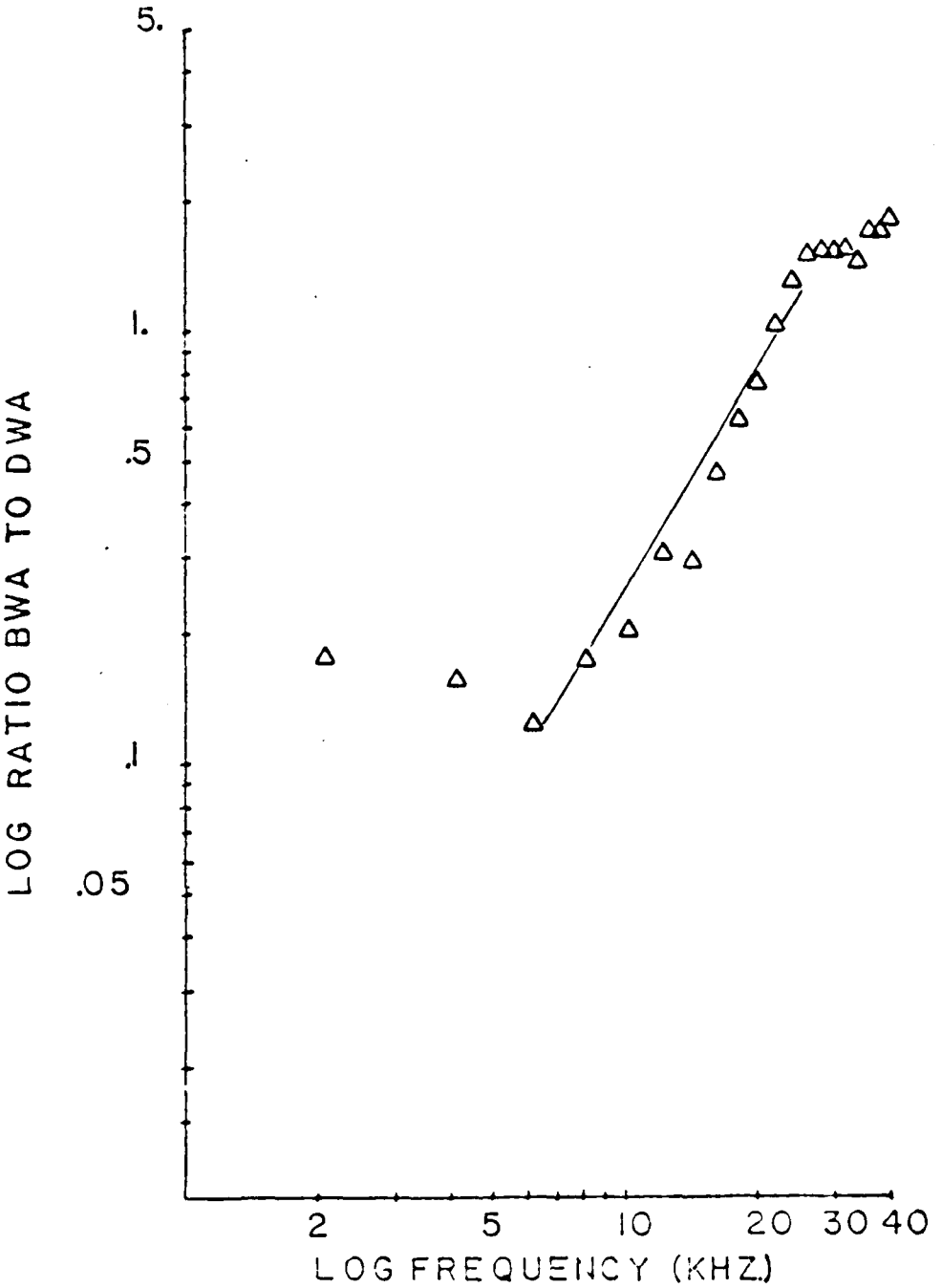

Figure 41. Log Ratio BWA to DWA vs. Log Frequency (R = 25 cm); R_0 = 20 cm, Z = Z_0 = 0.0 cm, Δ = Run I, and — = slope 1.7 (see Table V).

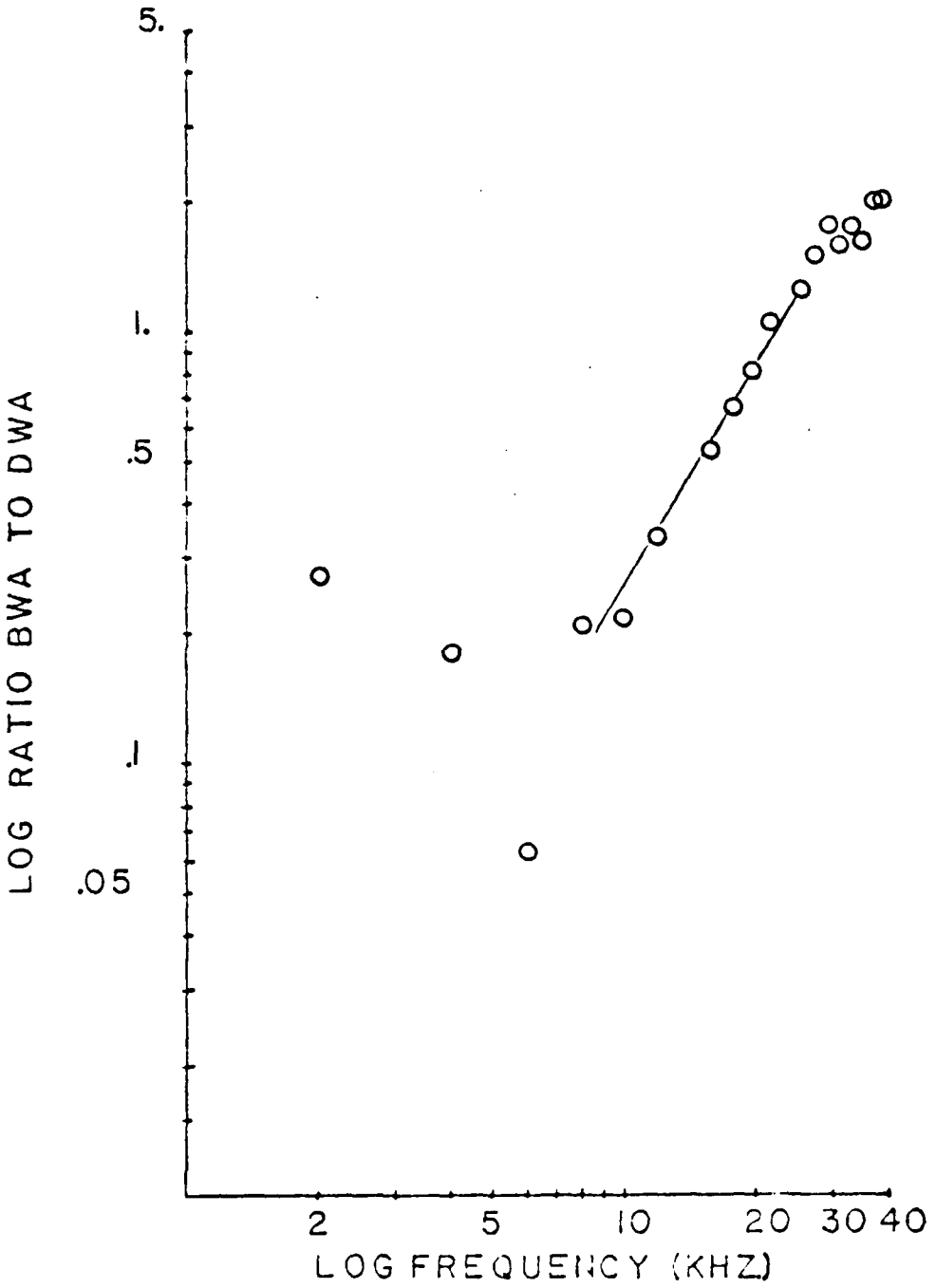

Figure 42. Log Ratio BWA to DWA vs. Log Frequency (R = 30 cm); R_0 = 20 cm, Z = Z_0 = 0.0 cm, 0 = Run I, and — = slope 1.7 (see Table V).

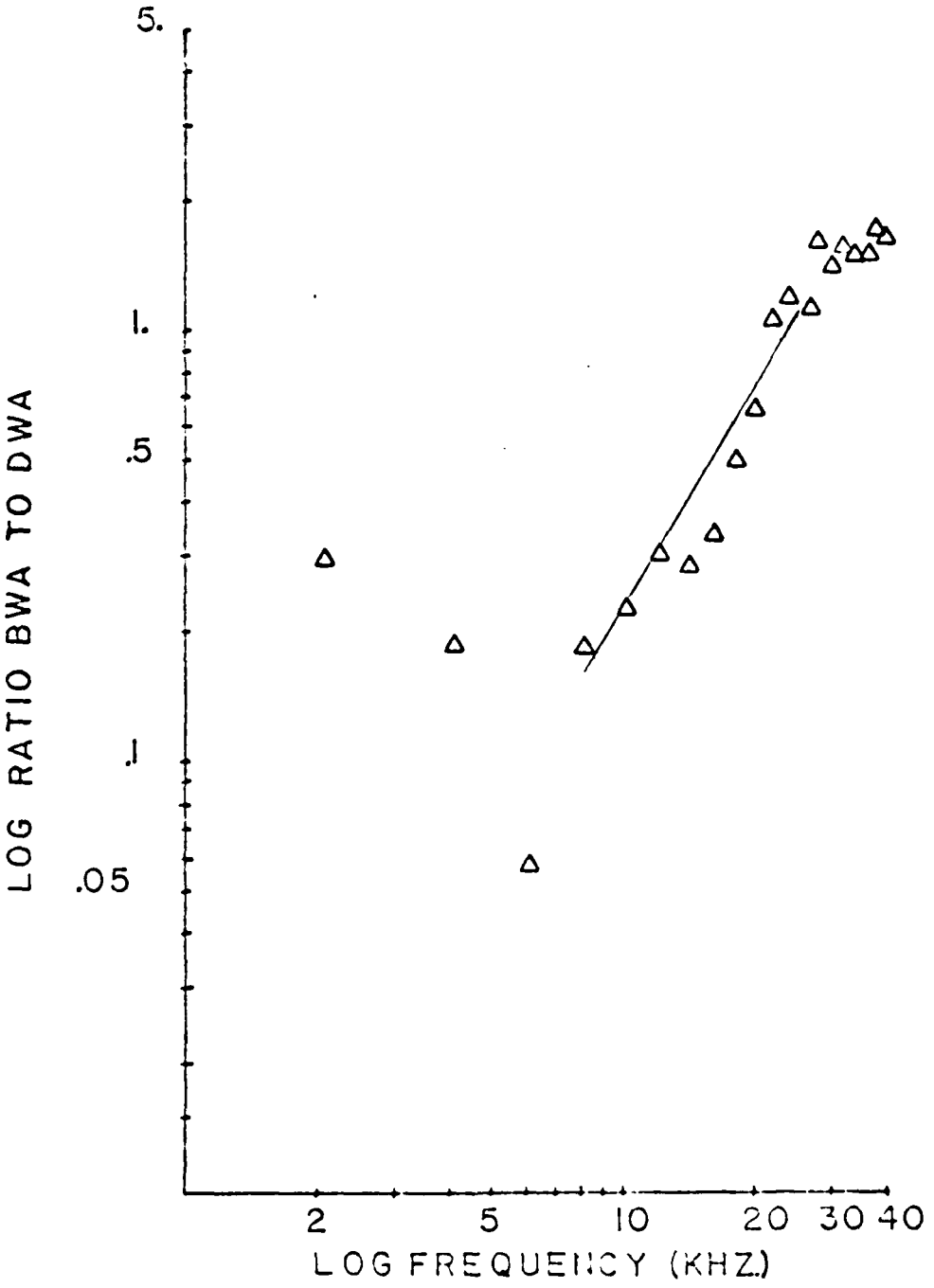

Figure 43. Log Ratio BWA to DWA vs. Log Frequency (R = 35 cm); R_0 = 20 cm, Z = Z_0 = 0.0 cm, Δ = Run I, and — = Slope 1.7 (see Table V).

Table IV

Semi-Empirical Calculations of Ratio
BWA to DWA for Rough Wedge

$$\left|\frac{BWA}{DWA}\right| \approx \frac{4\,\varepsilon\,k^2\,\theta_w\,R_0^{1/2}\,R_{Ref}^{1/2}}{\beta} \qquad \text{(Equation 19)}$$

$\varepsilon = 8.875 \times 10^{-2}$

$\theta_w = 3.630$ radians

$R_0 = 20.0$ cm.

$R_{Ref}(Avg) = 2.493 \times 10^{-3}$ cm. $\pm$ 1.297×10^{-3} cm.

$\beta = 1.993$

FREQ (kHz)	$\frac{BWA}{DWA}$
2	.0192
4	.0766
6	.1724
8	.3066
10	.4790
12	.6898
14	.9388
16	1.226
18	1.552
20	1.916
22	2.318
24	2.759
26	3.238
28	3.755

Table V

Determination of Frequency Dependence
of the Ratio of BWA to DWA

Rough to Smooth Surface Wedge	Range (cm.)	Slope
	5	1.652
	10	1.729
	15	1.680
	20	1.620
	25	1.711
	30	1.859
	35	1.699

Parameters: Ranges 5-25 cm. used frequency range 6-24 kHz, Ranges 30-35 cm. used frequency range 8-24 kHz, Average slope 1.7.

Smooth to Rough Surface Wedge	Range (cm.)	Slope
	5	2.45
	20	1.82
	30	1.71
	35	1.97

Parameters: Determined over frequency range 16-24 kHz, Average slope 1.99 ($\tilde{=}$ 2.0).

Rough to Rough Surface Wedge	Range (cm.)	Slope
	5	1.657
	10	2.085
	15	2.139
	20	1.870
	25	1.857
	30	2.035
	35	2.210

Parameters: Determined over frequency range 6-24 kHz, Average slope 1.98 ($\tilde{=}$ 2.0).

All slopes determined using linear regression for log range versus log amplitude data values.

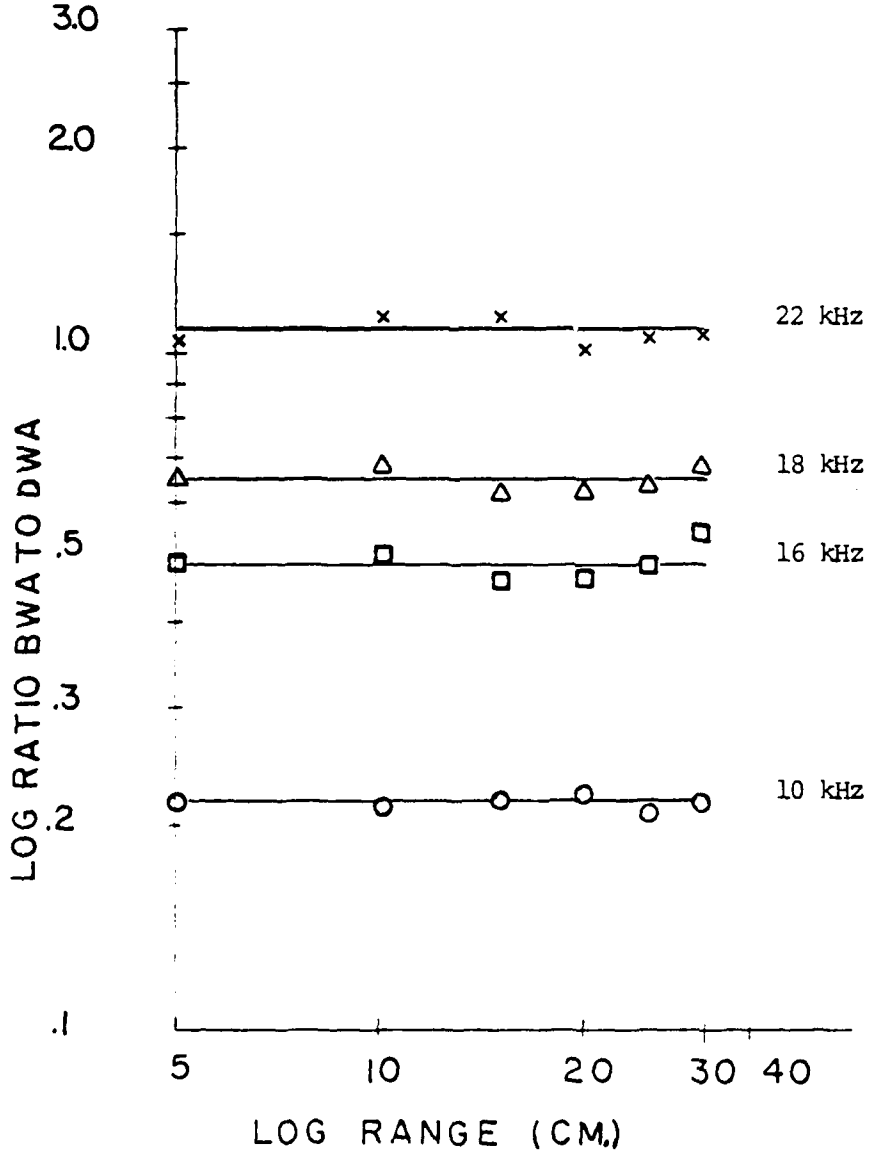

Figure 44. Log Ratio BWA to DWA vs. Log Range; R_0 = 20 cm, $Z = Z_0$ = 0.0 cm, and — = slope $(0.0)^0$ (see Table VI).

Table VI

Determination of Range Dependence
of the Ratio of BWA to DWA

Rough to Smooth Surface Wedge	Frequency (kHz)	Slope
	10	0.02
	16	0.02
	18	0.00
	22	0.01

Parameters: Determined over ranges 5-30 cm. Average slope 0.01.

Smooth to Rough Surface Wedge	Frequency (kHz)	Slope
	10	.33
	12	.21
	14	.21
	16	.66
	18	.68
	20	.62
	22	.56
	24	.56

Parameters: Determined over ranges 5, 20, 30, 35 cm., Average slope .48.

Rough to Rough Surface Wedge	Frequency (kHz)	Slope
	10	0.12
	16	0.27
	18	0.27
	22	0.36

Parameters: Determined over ranges 5-30 cm. Average slope .26.

All slopes determined using linear regression for log frequency versus log amplitude data values.

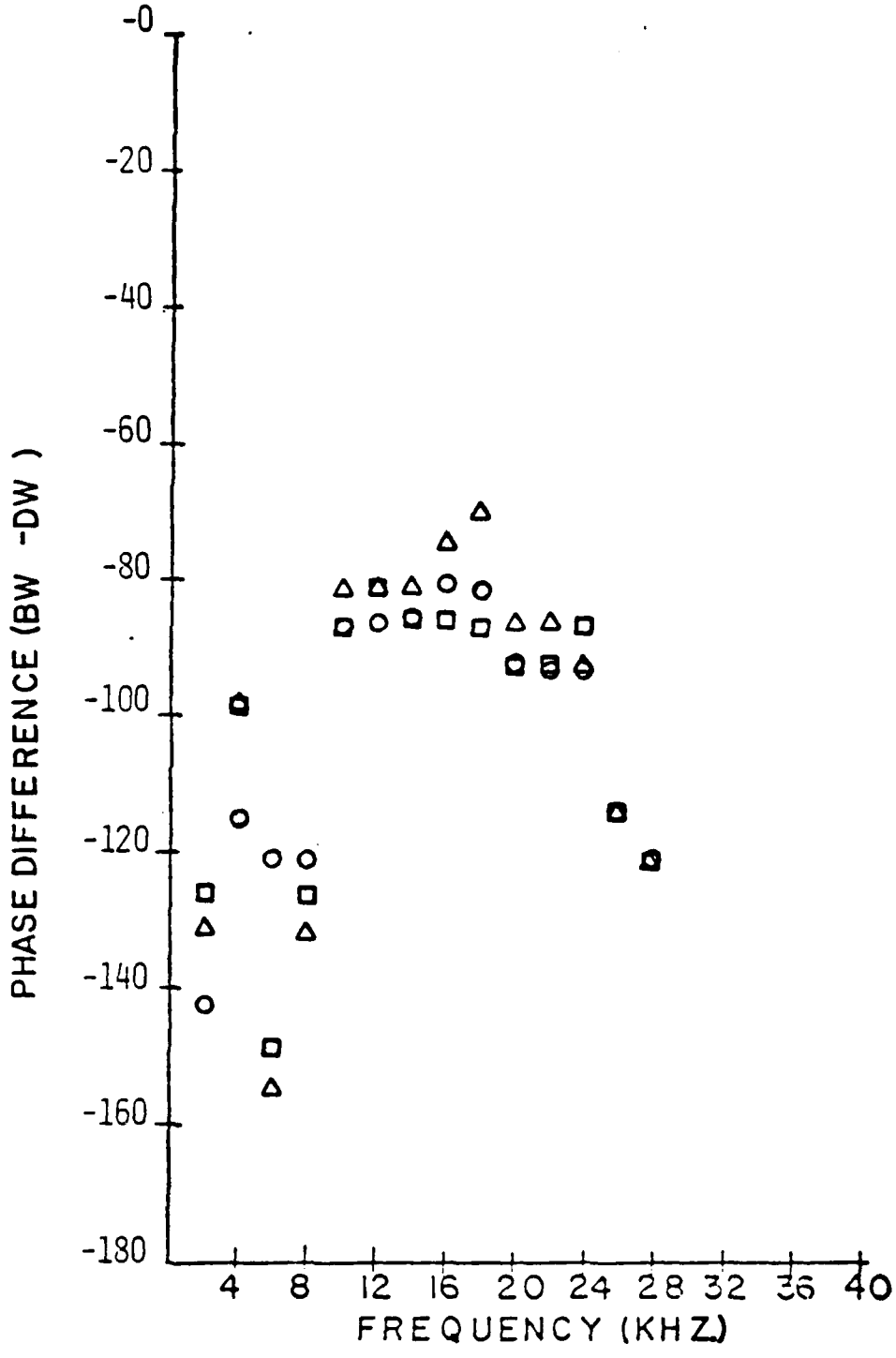

Figure 45. Phase Difference (BW-DW) vs. Frequency; R_0 = 20 cm, Z = Z_0 = 0.0 cm, 0 (R = 10 cm), Δ (R = 20 cm), and □ (R_0 = 30 cm).

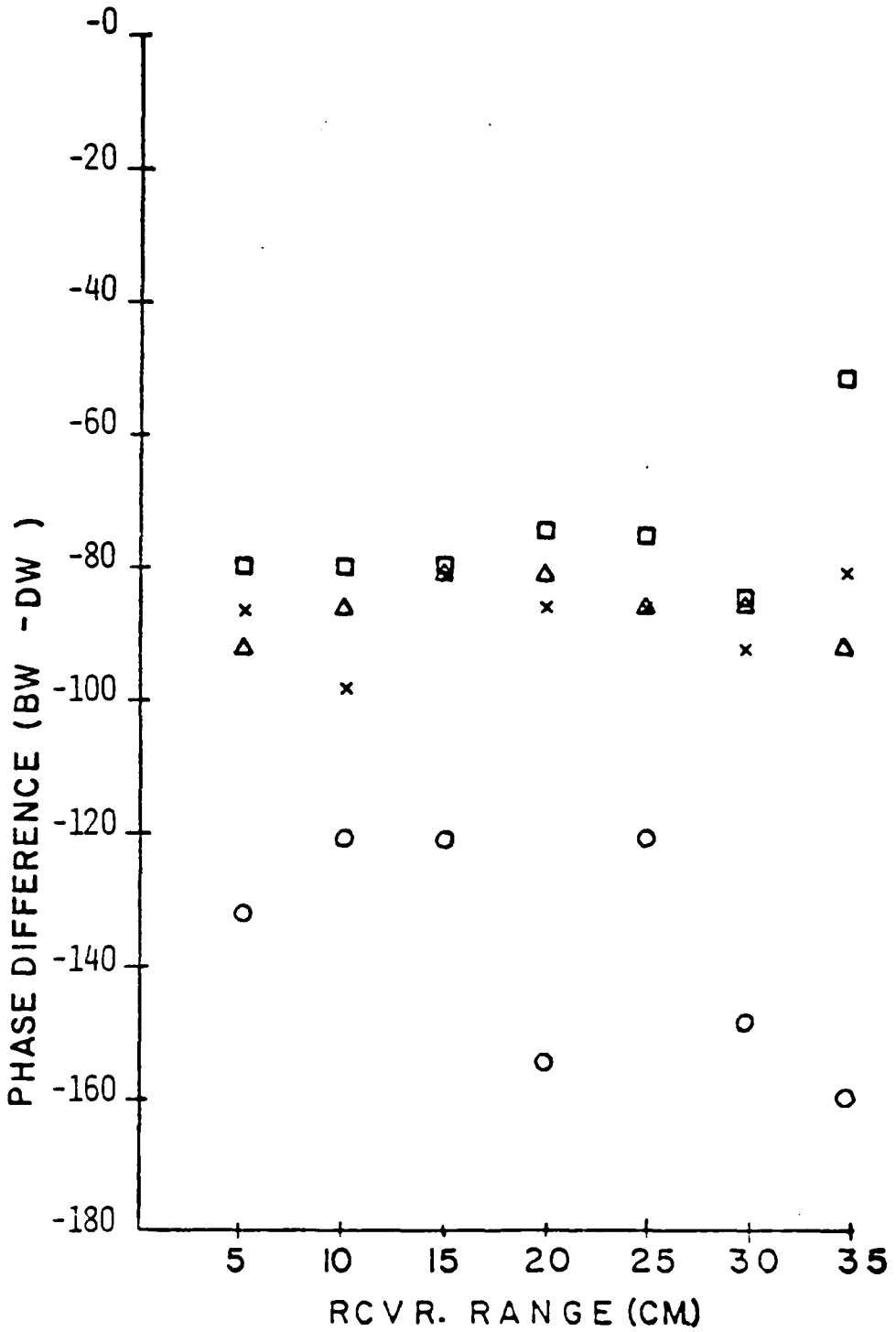

Figure 46. Phase Difference (BW-DW) vs. Range; R_0 = 20 cm, Z = Z_0 = 0.0 cm, 0 = 6 kHz, Δ = 10 kHz, □ = 16 kHz, and x^0 = 22 kHz.

the initial propagation for 20 cm. over the rough surface in agreement with theory (see Figure 47). Having accomplished step two, the next goal was to study the boundary wave propagation over the crest to a rough surfaced back wedge.

C. THE PROPAGATION OF A BOUNDARY WAVE OVER A ROUGH SURFACED WEDGE

This phase of the experiment was run exactly as the preceding case using the same amplifications, bandwindows, and averaging. The results for two data runs at each range are plotted in Figures 48-54. The range of data values for the possible four combinations are plotted in Figures 55-61. Again excellent reproducibility in values was obtained. The ratio of amplitudes was observed to be growing more rapidly with frequency than previous values and in the maximum case the boundary wave amplitude was four times greater than the diffracting wave amplitude. The log amplitude versus log frequency was plotted for one run each in Figures 62-68. These plots show an increase in frequency dependence compared to plane rough surface propagation. The slope of the frequency dependence from 6-24 kHz, using linear regression, showed an average power law of 1.98 for ranges 10 to 35 cm. (see Table V). The plot of log amplitude versus log range, Figure 69, showed a range dependence of $0.3 \pm .1$ (see Table VI).

The phase difference between the boundary wave and the diffracted wave in degrees are plotted in Figures 70 and 71. Figure 70 shows that the phase difference decreases from 2 to

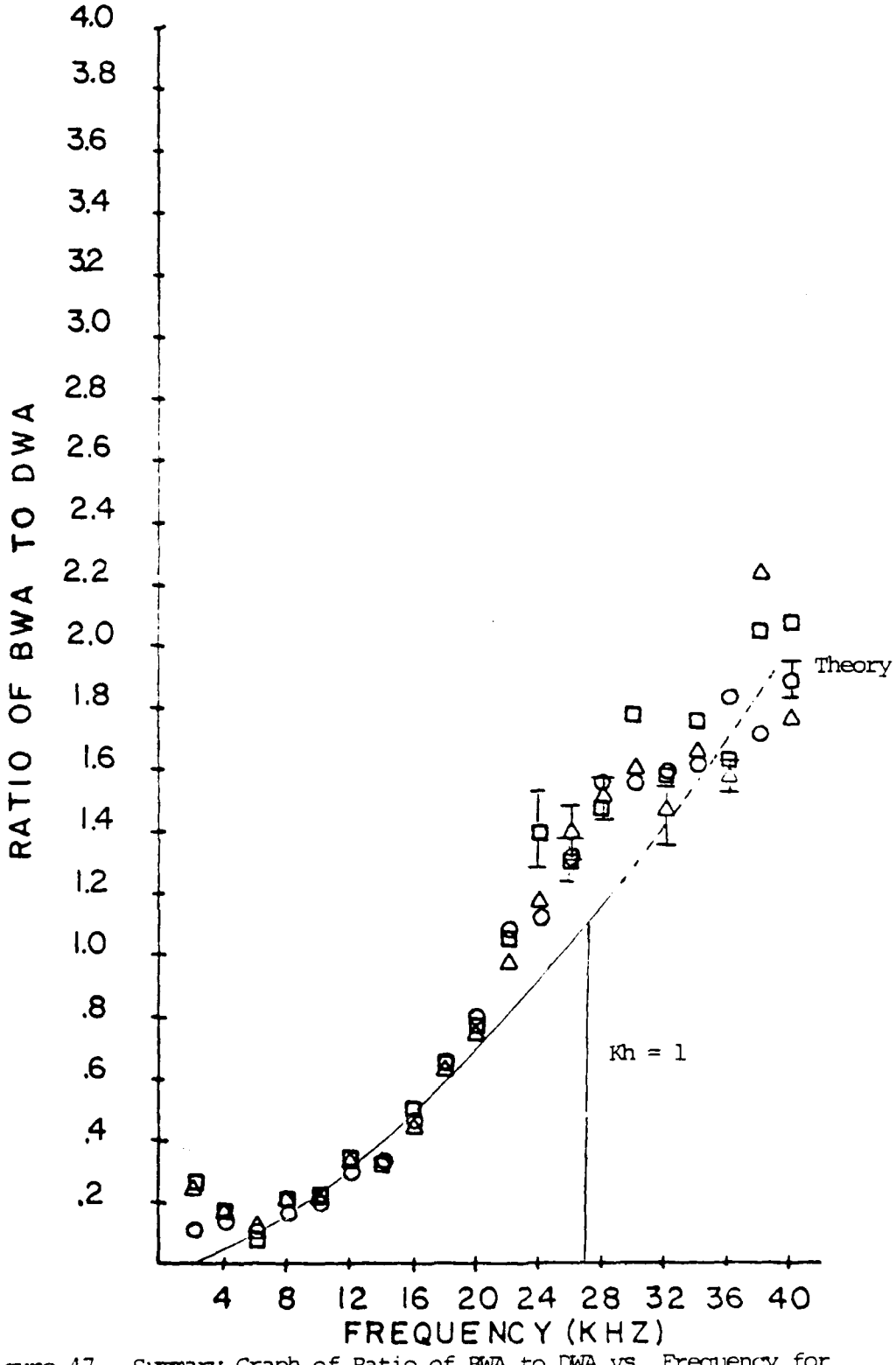

Figure 47. Summary Graph of Ratio of BWA to DWA vs. Frequency for Rough to Smooth Surface Wedge; Range of Data Value Plots, O (R = 10 cm), Δ (R = 20 cm), and □ (R = 30 cm). Tolstoy Theory Line for Sound Propagation, R_0 = 20 cm, Z = 0.0 cm, over Rough Planar Surface.

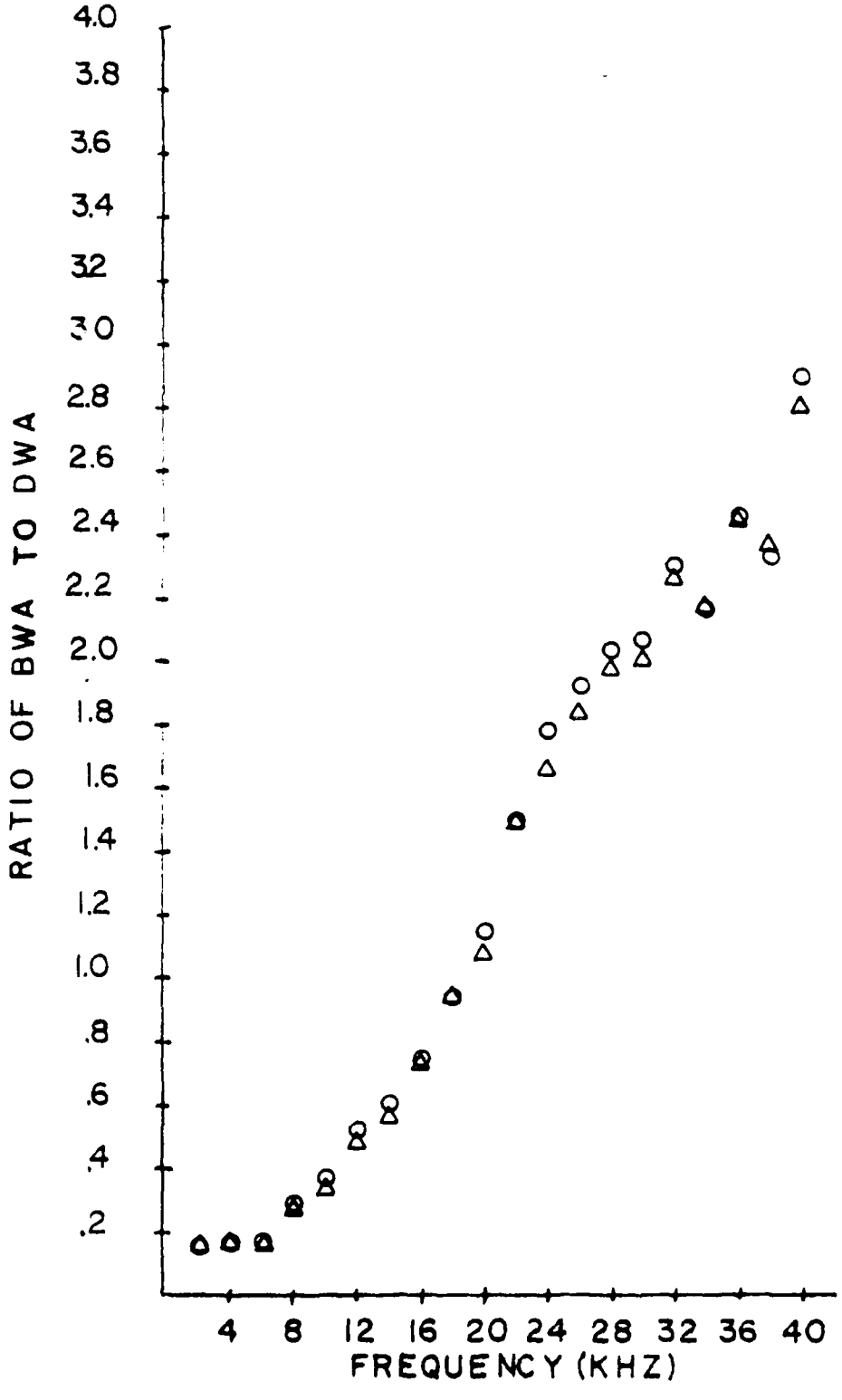

Figure 48. Ratio BWA to DWA vs. Frequency (R = 5 cm); R_0 = 20 cm, $Z = Z_0$ = 0.0 cm., 0 = Run I, and Δ = Run II.

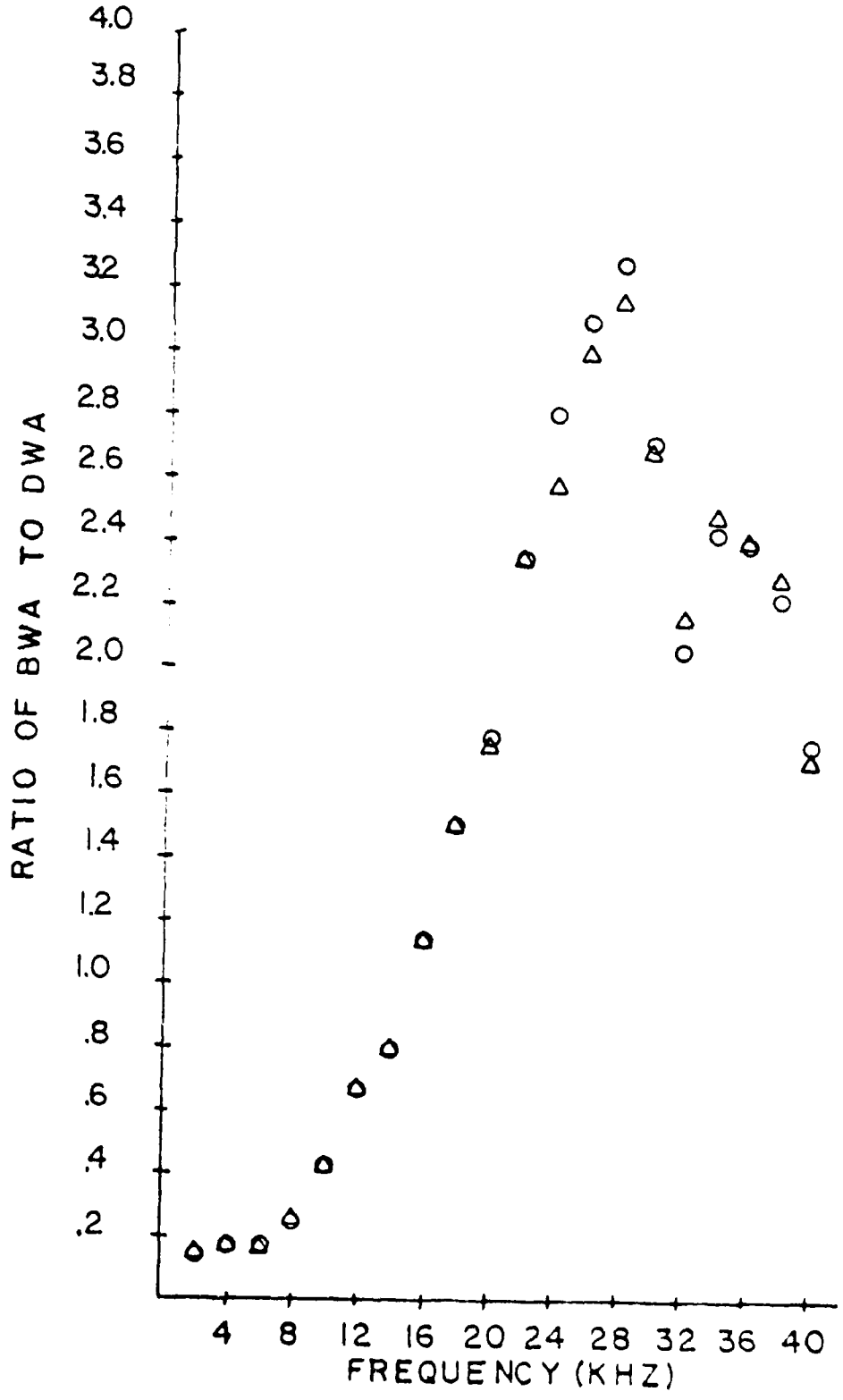

Figure 49. Ratio BWA to DWA vs. Frequency (R = 10 cm); R_0 = 20 cm, $Z = Z_0 = 0.0$ cm, O = Run I, and Δ = Run II.

AD-A098 048 NAVAL POSTGRADUATE SCHOOL MONTEREY CA F/G 20/1
THE PROPAGATION OF A SCATTERED ACOUSTIC BOUNDARY WAVE OVER A RO--ETC(U)
DEC 80 S J HOLLIS

UNCLASSIFIED NL

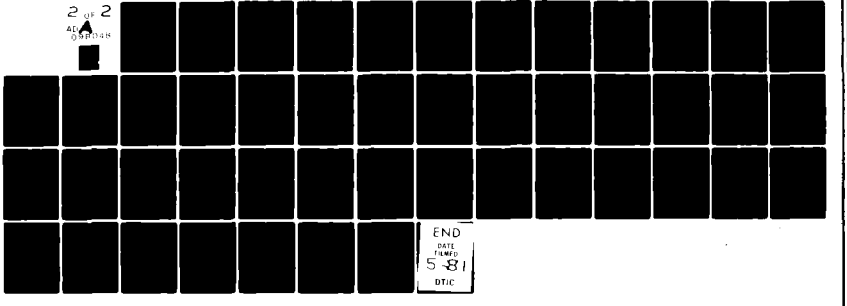

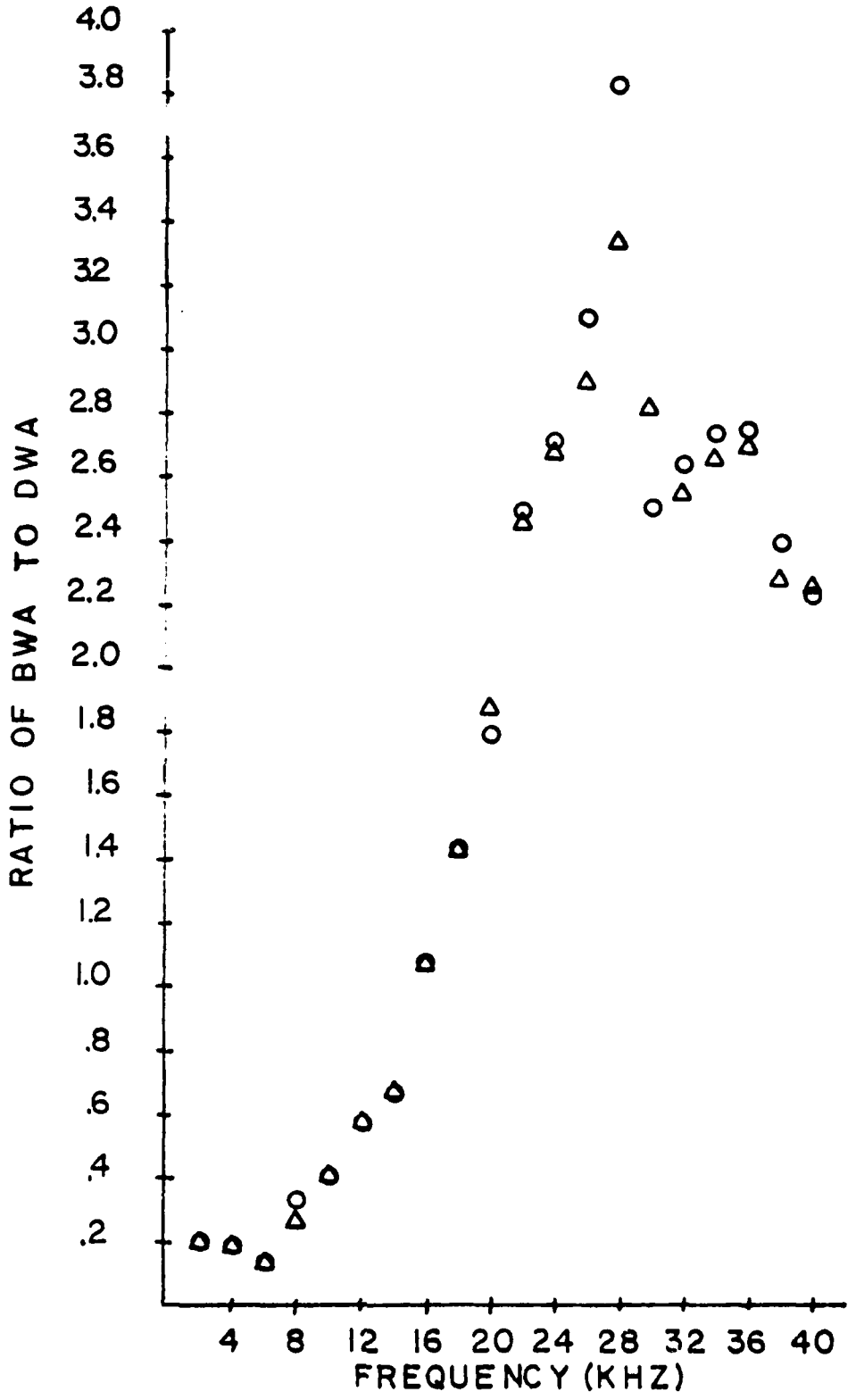

Figure 50. Ratio BWA to DWA vs. Frequency (R = 15 cm); R_0 = 20 cm, $Z = Z_0 = 0.0$ cm, O = Run I, and Δ = Run II.

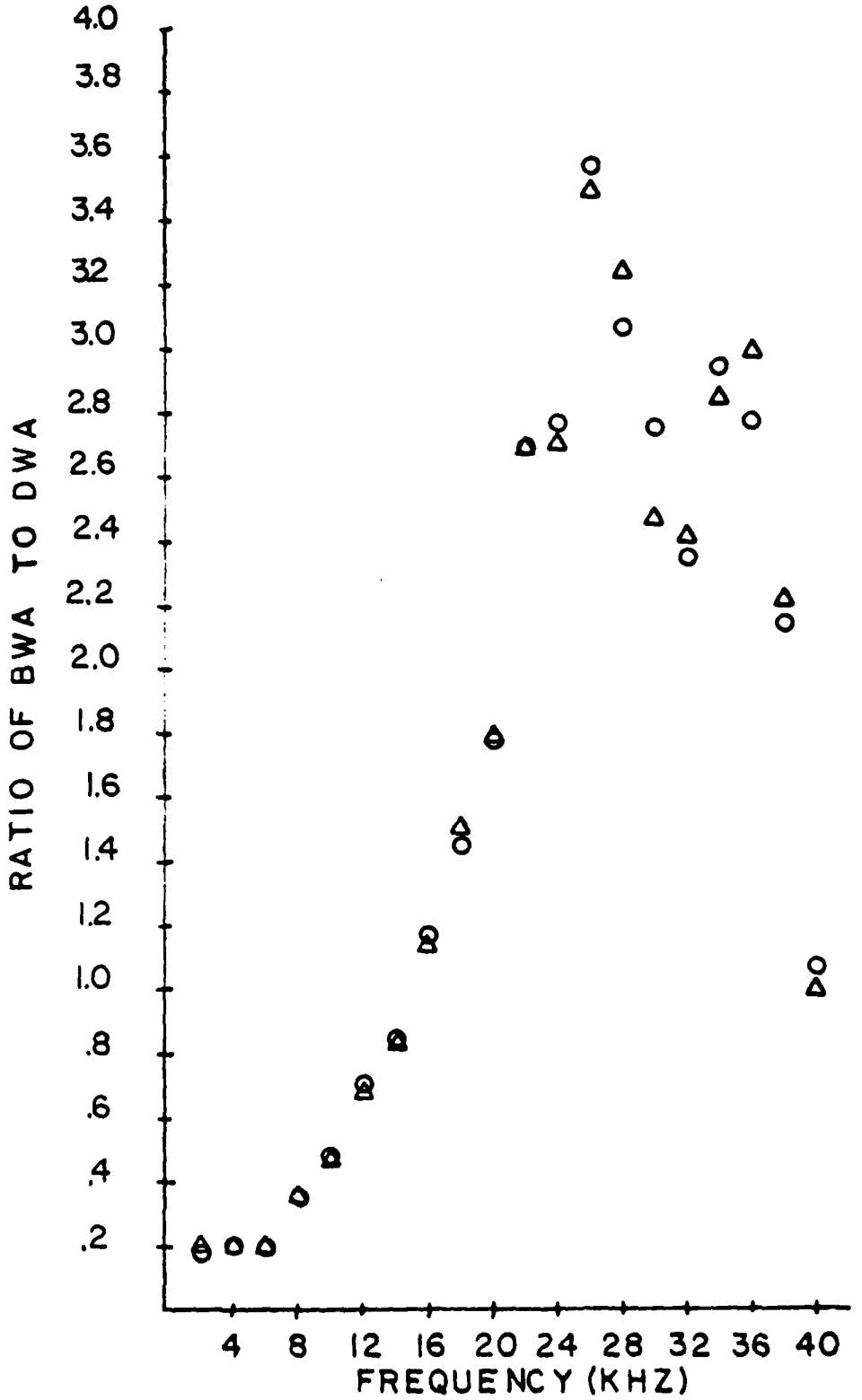

Figure 51. Ratio BWA to DWA vs. Frequency (R = 20 cm); R_0 = 20 cm, $Z = Z_0$ = 0.0 cm, O = Run I, and Δ = Run II.

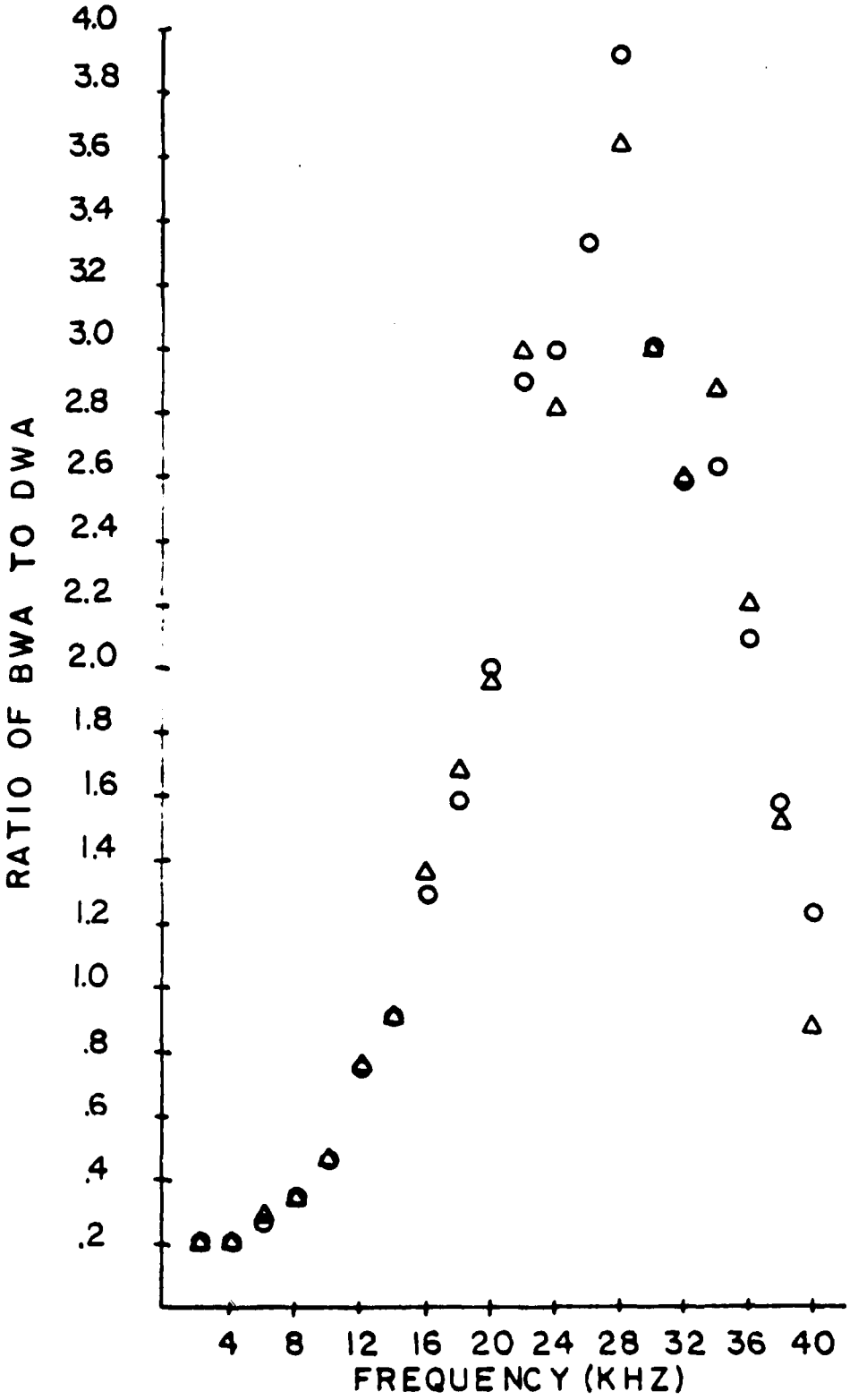

Figure 52. Ratio BWA to DWA vs. Frequency (R = 25 cm); R_0 = 20 cm, $Z = Z_0$ = 0.0 cm, O = Run I, and Δ = Run II.

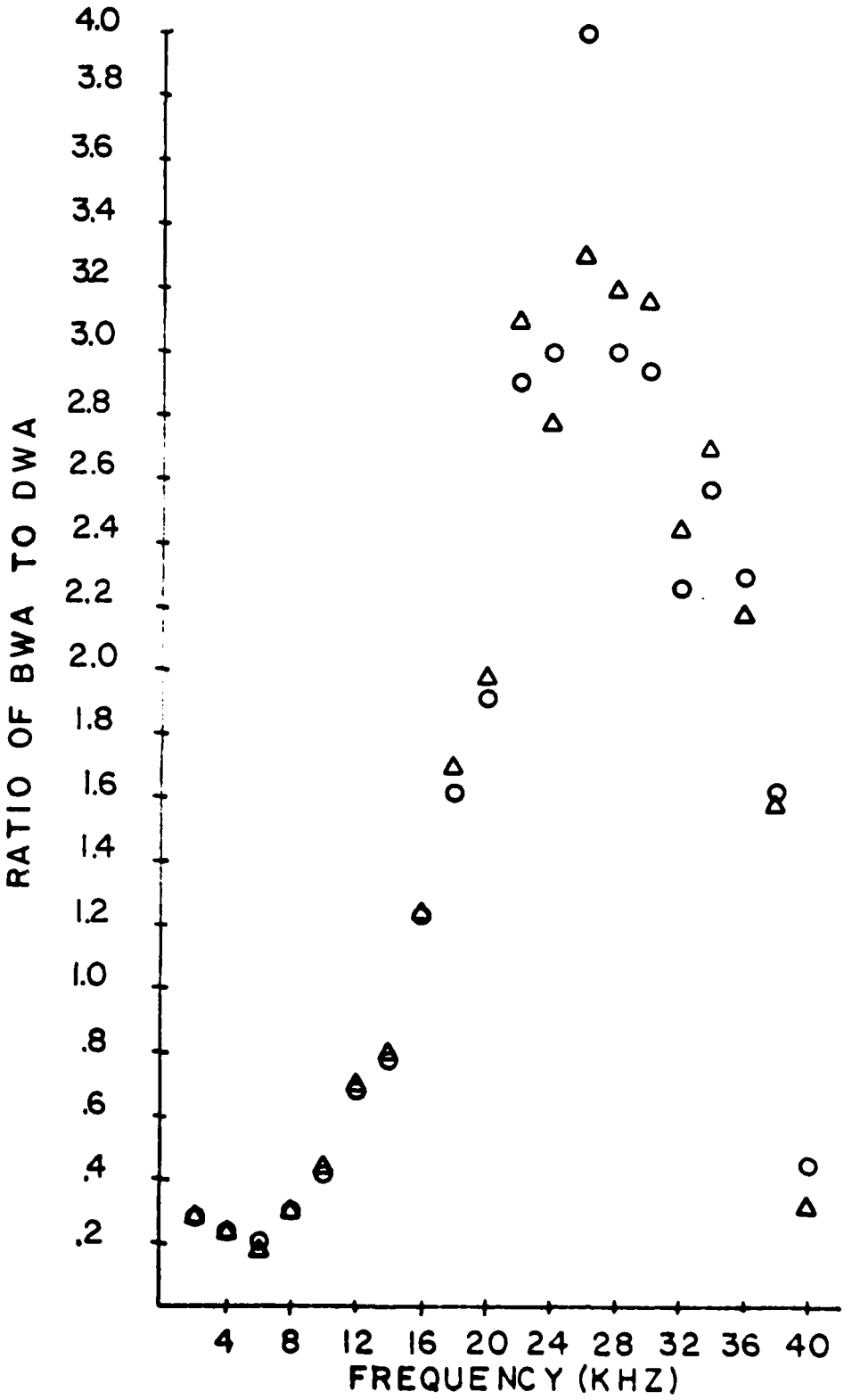

Figure 53. Ratio BWA to DWA vs. Frequency (R = 30 cm); R_0 = 20 cm, $Z = Z_0$ = 0.0 cm, O = Run I, and Δ = Run II.

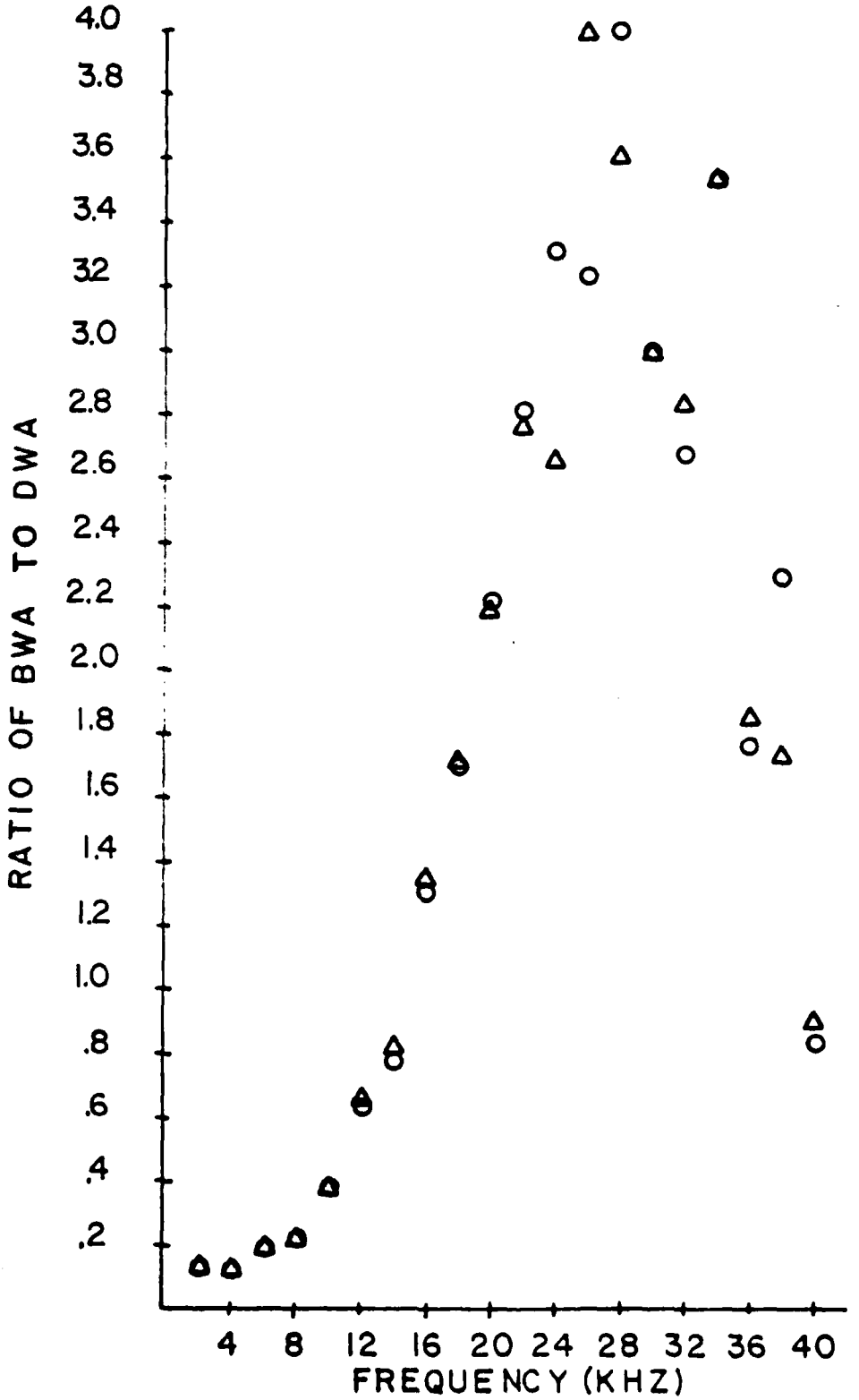

Figure 54. Ratio BWA to DWA vs. Frequency (R = 35 cm); R_0 = 20 cm, Z = Z_0 = 0.0 cm, O = Run I, and Δ^0 = Run II.

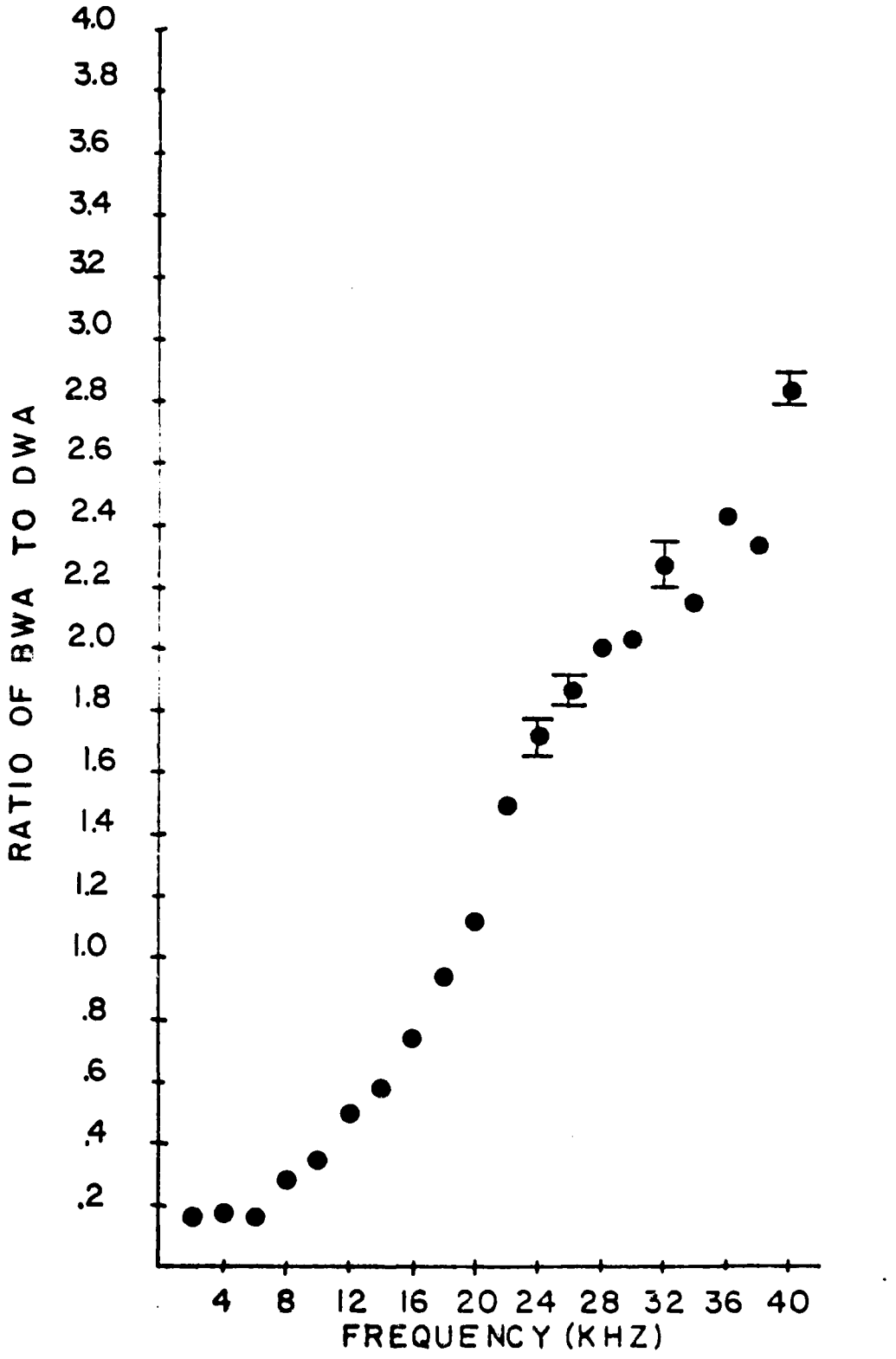

Figure 55. Range of Data Values for Ratio of BWA to DWA vs. Frequency (R = 5 cm); R_0 = 20 cm, Z = Z_0 = 0.0 cm, and 0 = Range of Four Data Values.

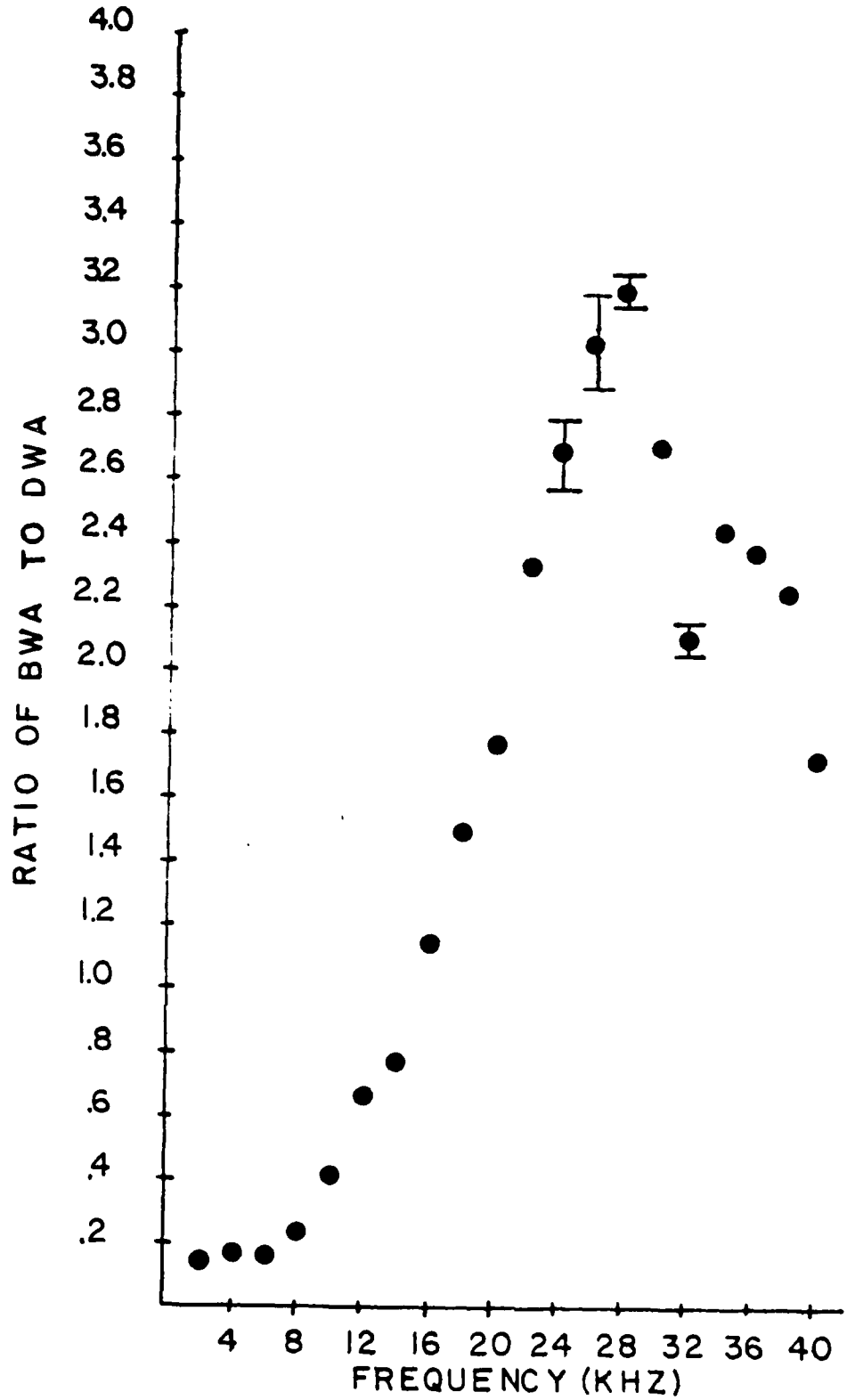

Figure 56. Range of Data Values for Ratio of BWA to DWA vs. Frequency (R = 10 cm); R_0 = 20 cm, Z = Z_0 = 0.0 cm, and 0 = Range of Four Data Values.

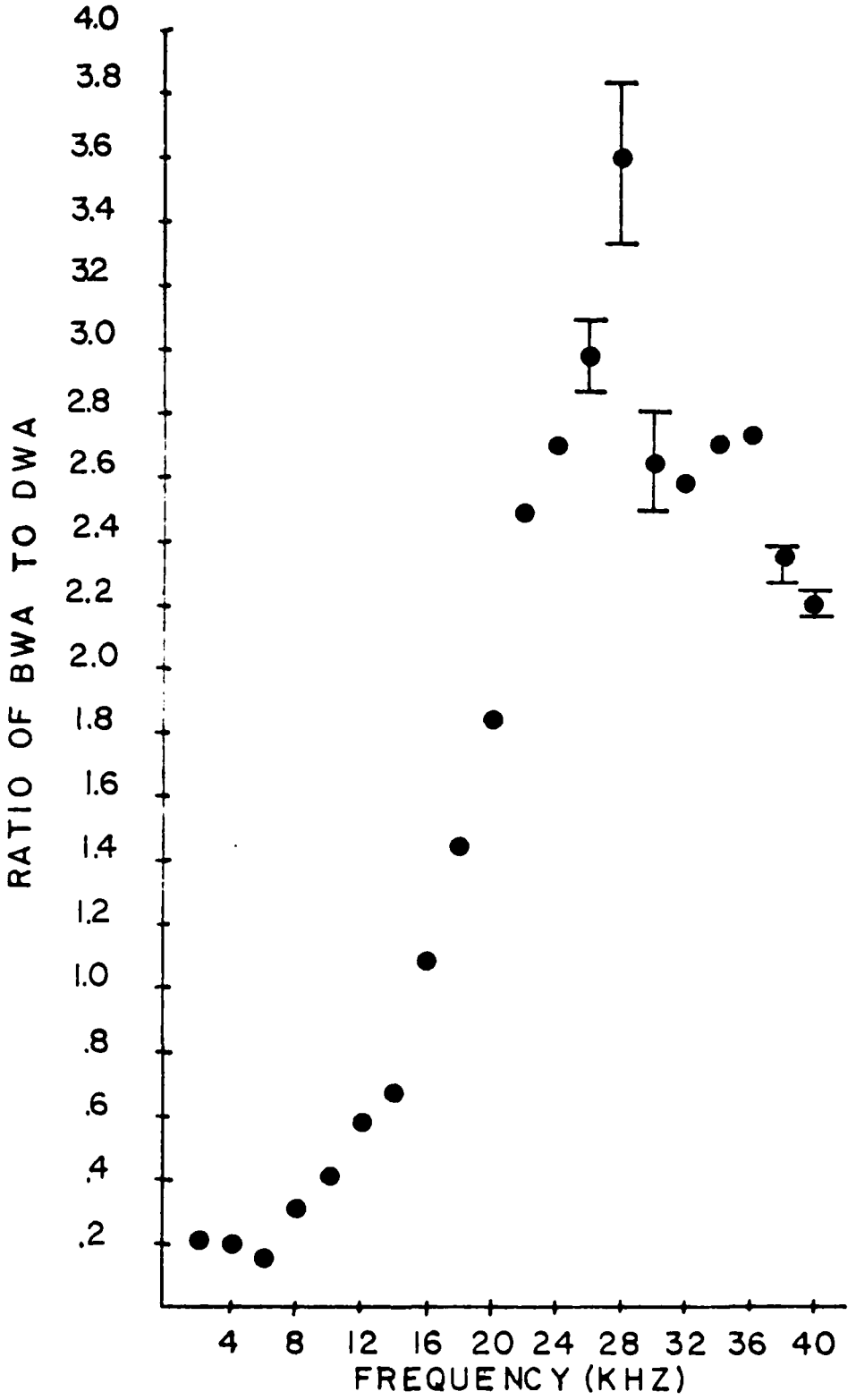

Figure 57. Range of Data Values for Ratio of BWA to DWA vs. Frequency (R = 15 cm); R_0 = 20 cm, Z = Z_0 = 0.0 cm, and 0 = Range of Four Data Values.

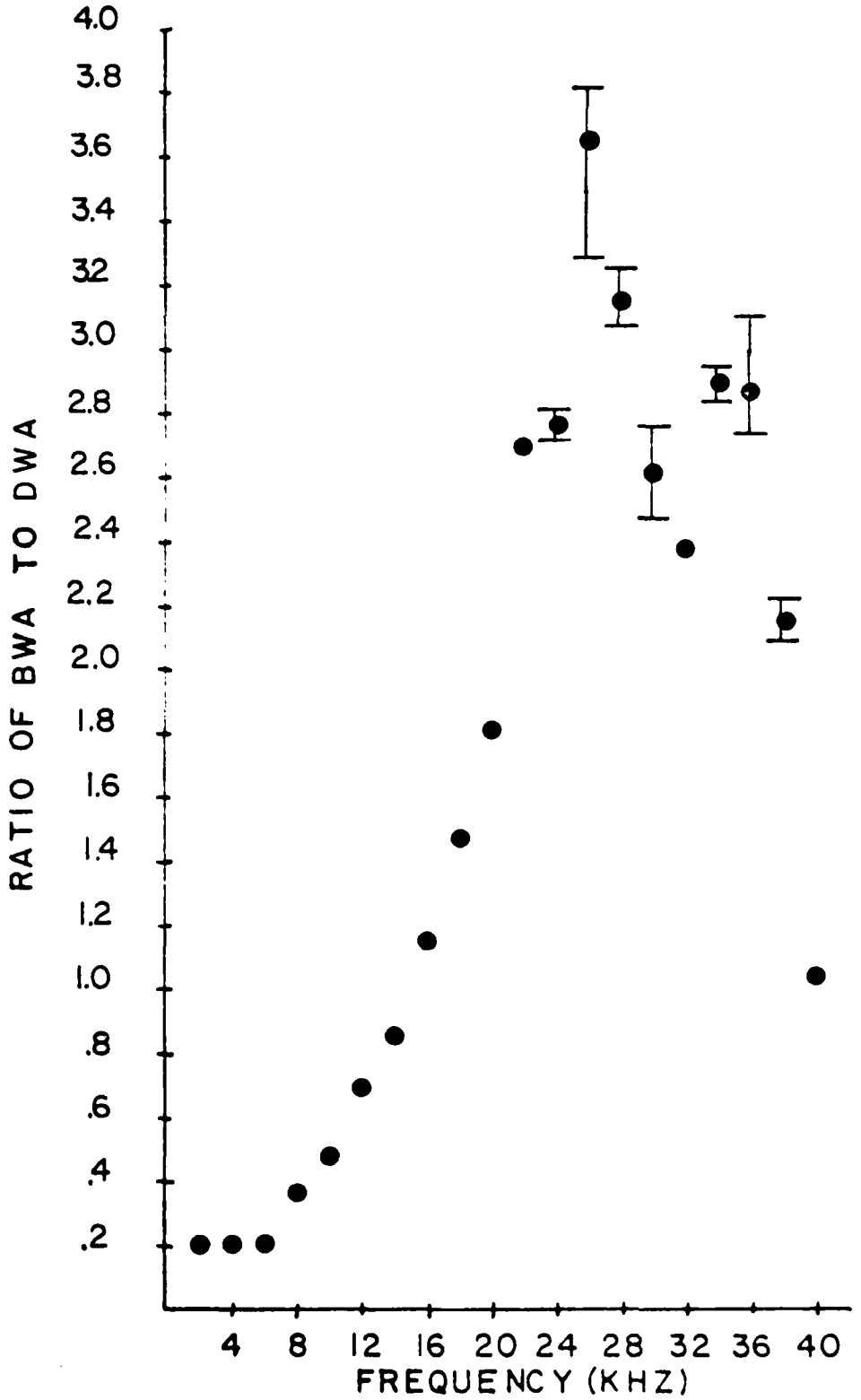

Figure 58. Range of Data Values for Ratio of BWA to DWA vs. Frequency (R = 20 cm); R_0 = 20 cm, Z = Z_0 = 0.0 cm, and 0 = Range of Four Data Values.

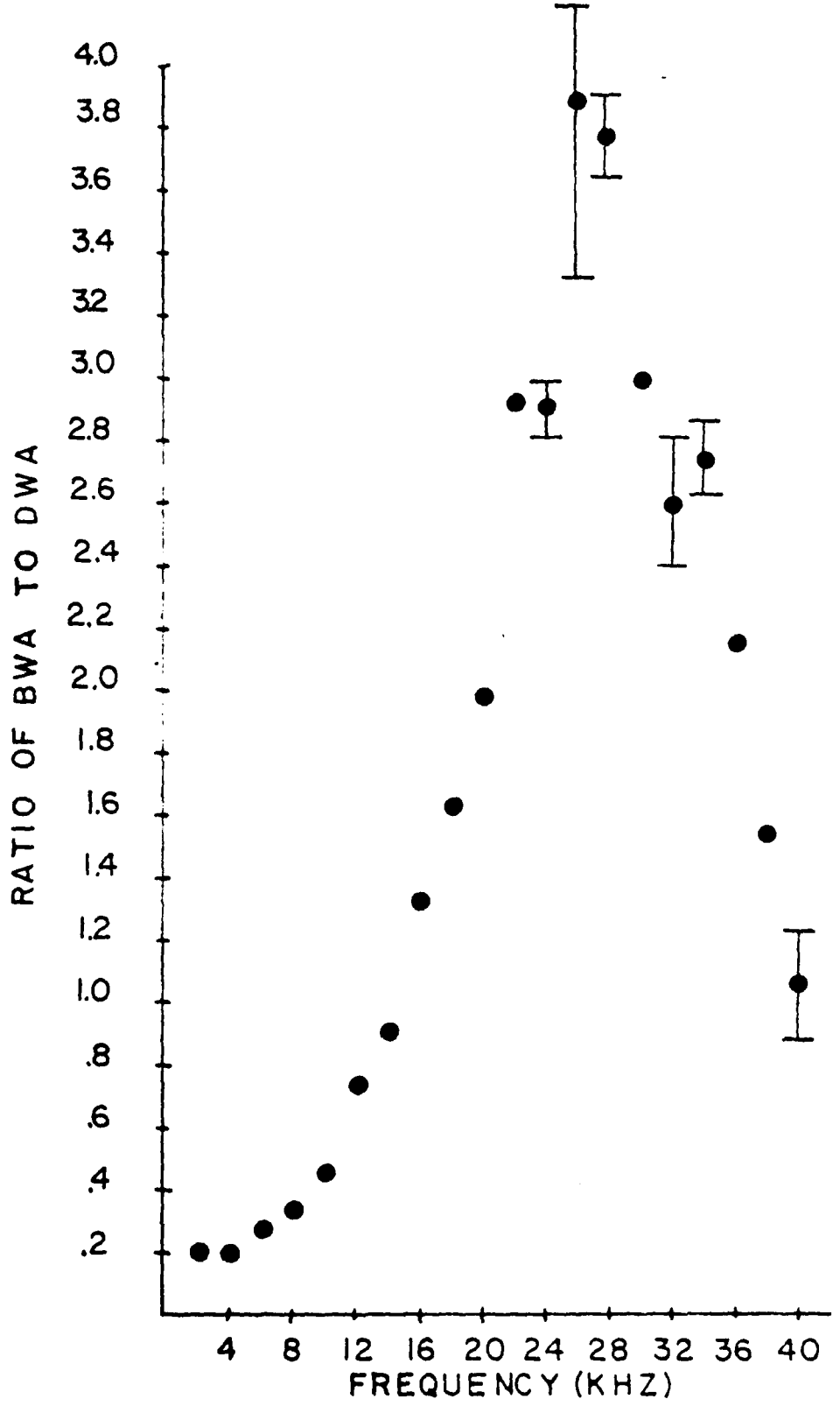

Figure 59. Range of Data Values for Ratio of BWA to DWA vs. Frequency (R = 25 cm); R_0 = 20 cm, Z = Z_0 = 0.0 cm, and 0 = Range of Four Data Values.

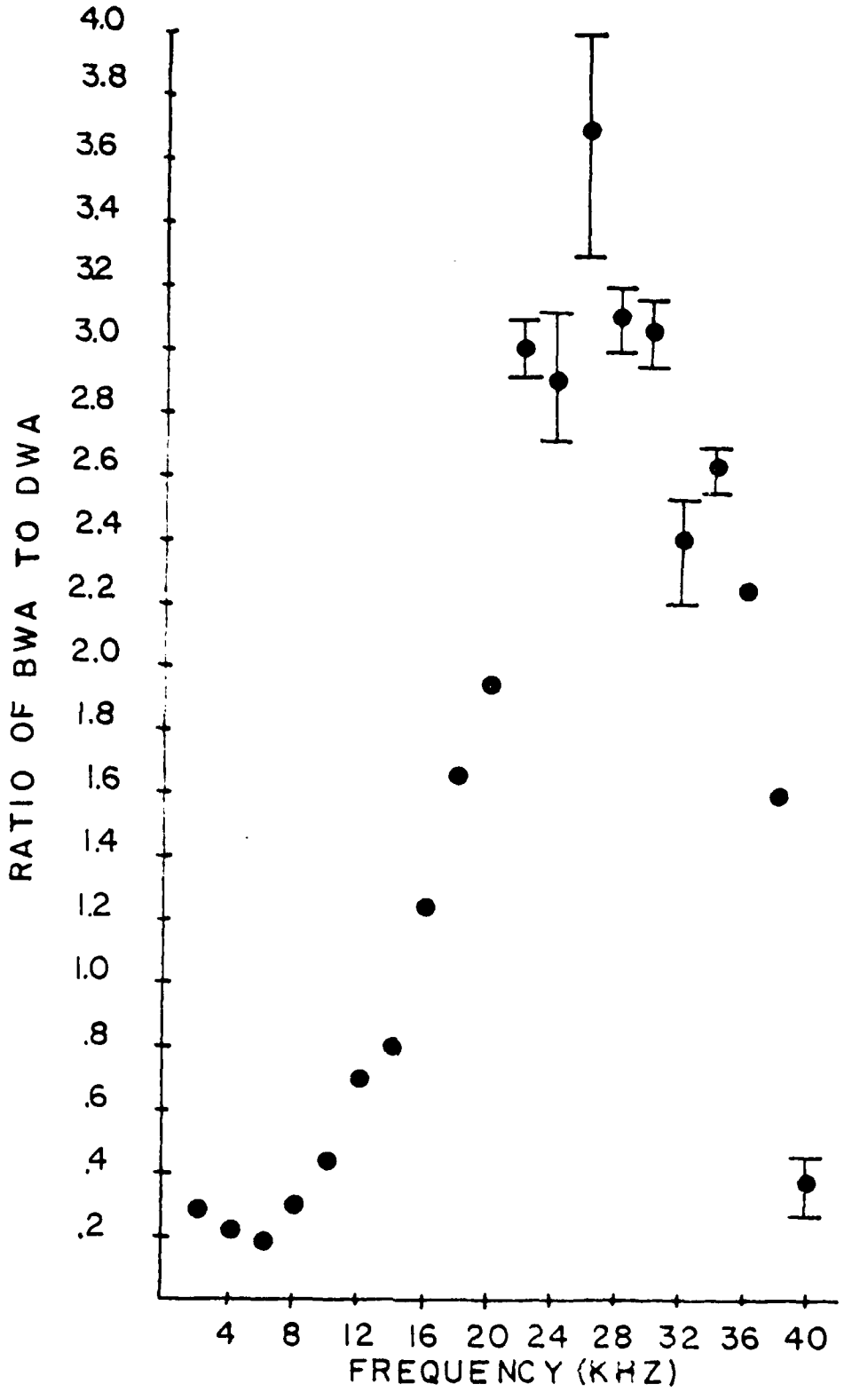

Figure 60. Range of Data Values for Ratio of BWA to DWA vs. Frequency (R = 30 cm); R_0 = 20 cm, Z = Z_0 = 0.0 cm, and 0 = Range of Four Data Values.

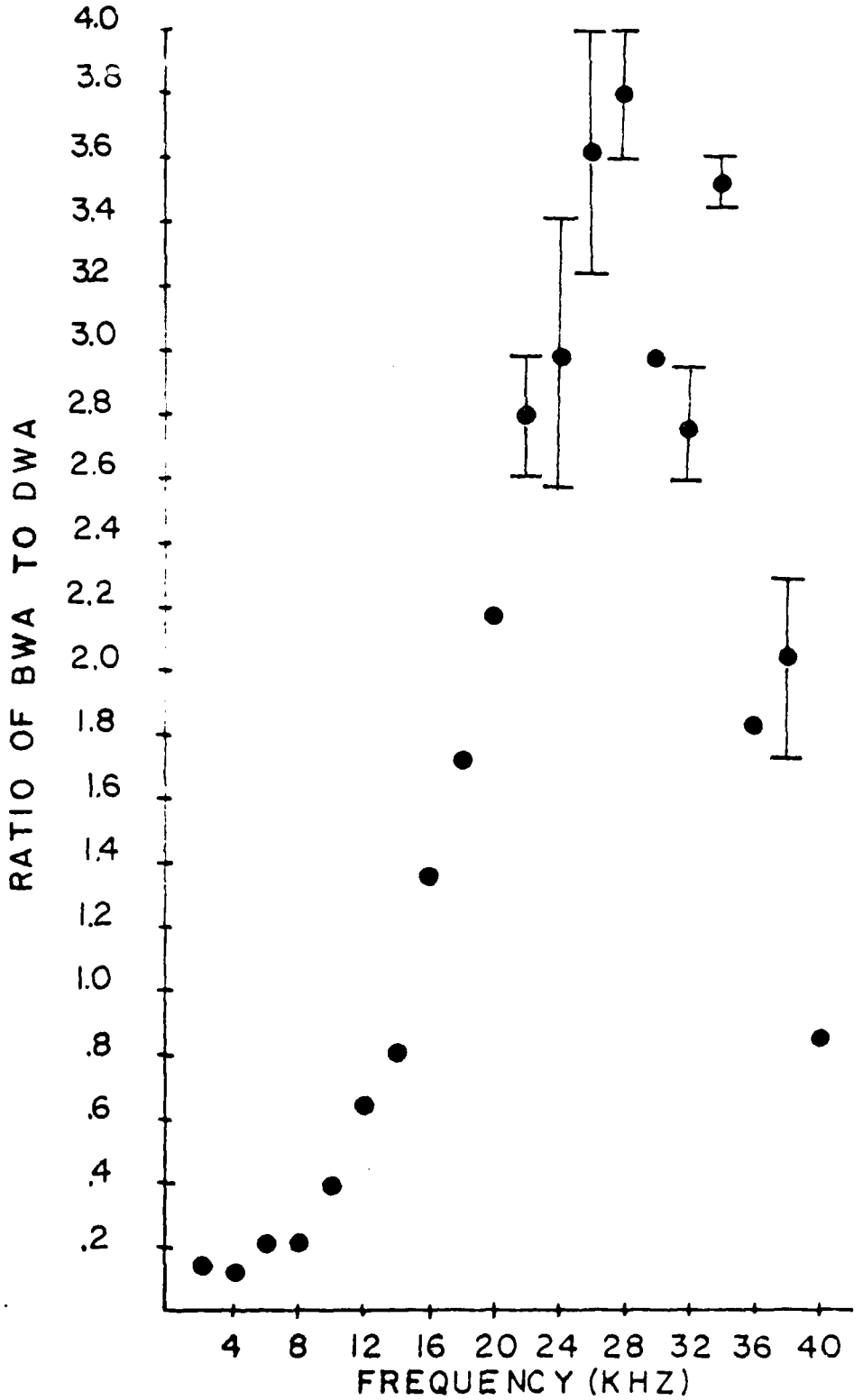

Figure 61. Range of Data Values for Ratio of BWA to DWA vs. Frequency (R = 35 cm); R_0 = 20 cm, Z = Z_0 = 0.0 cm, and 0 = Range of Four Data Values.

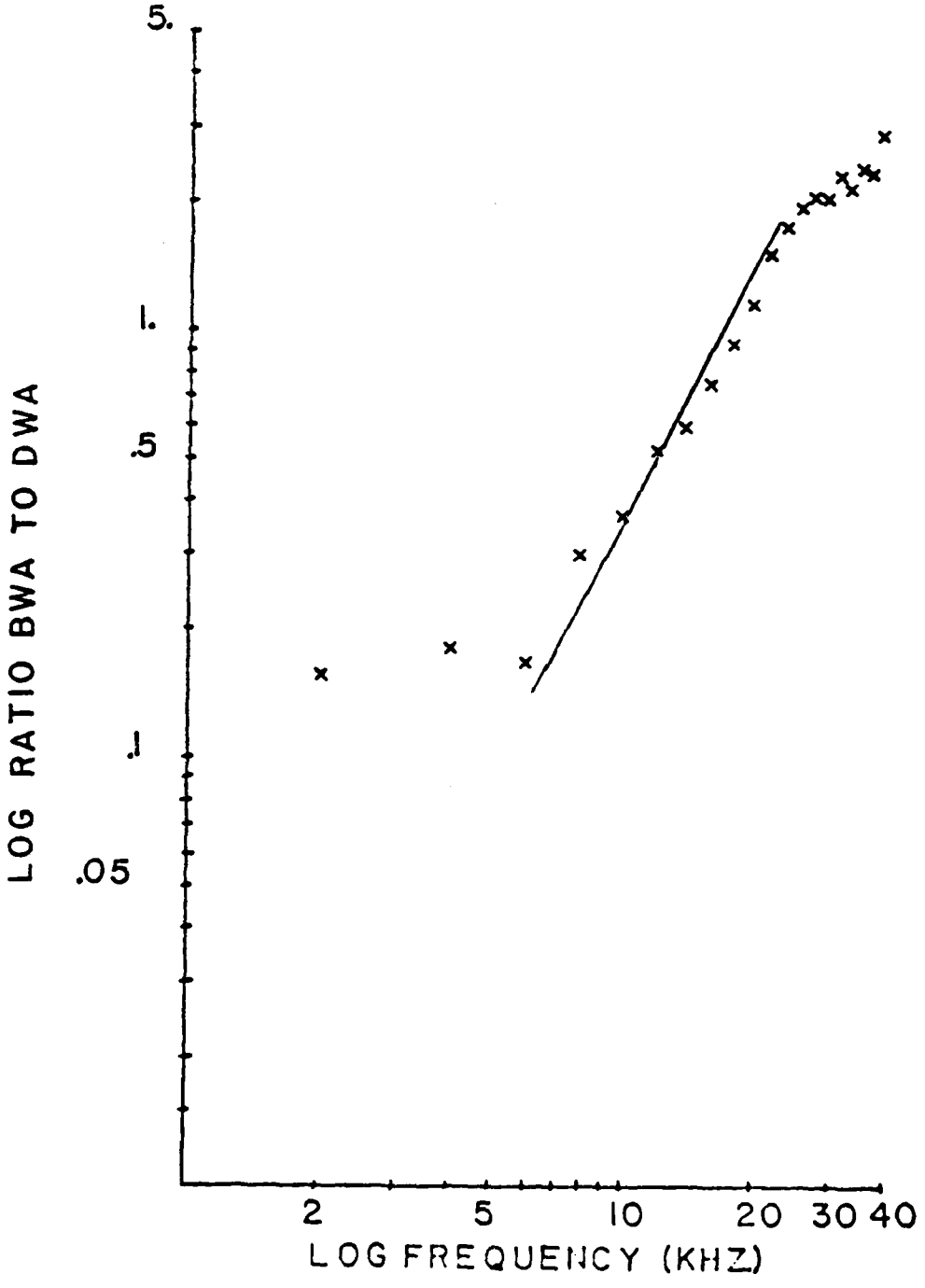

Figure 62. Log Ratio BWA to DWA vs. Log Frequency (R = 5 cm); R_0 = 20 cm, Z = Z_0 = 0.0 cm, x = Run I, and — = Slope (2.0) (see Table V).

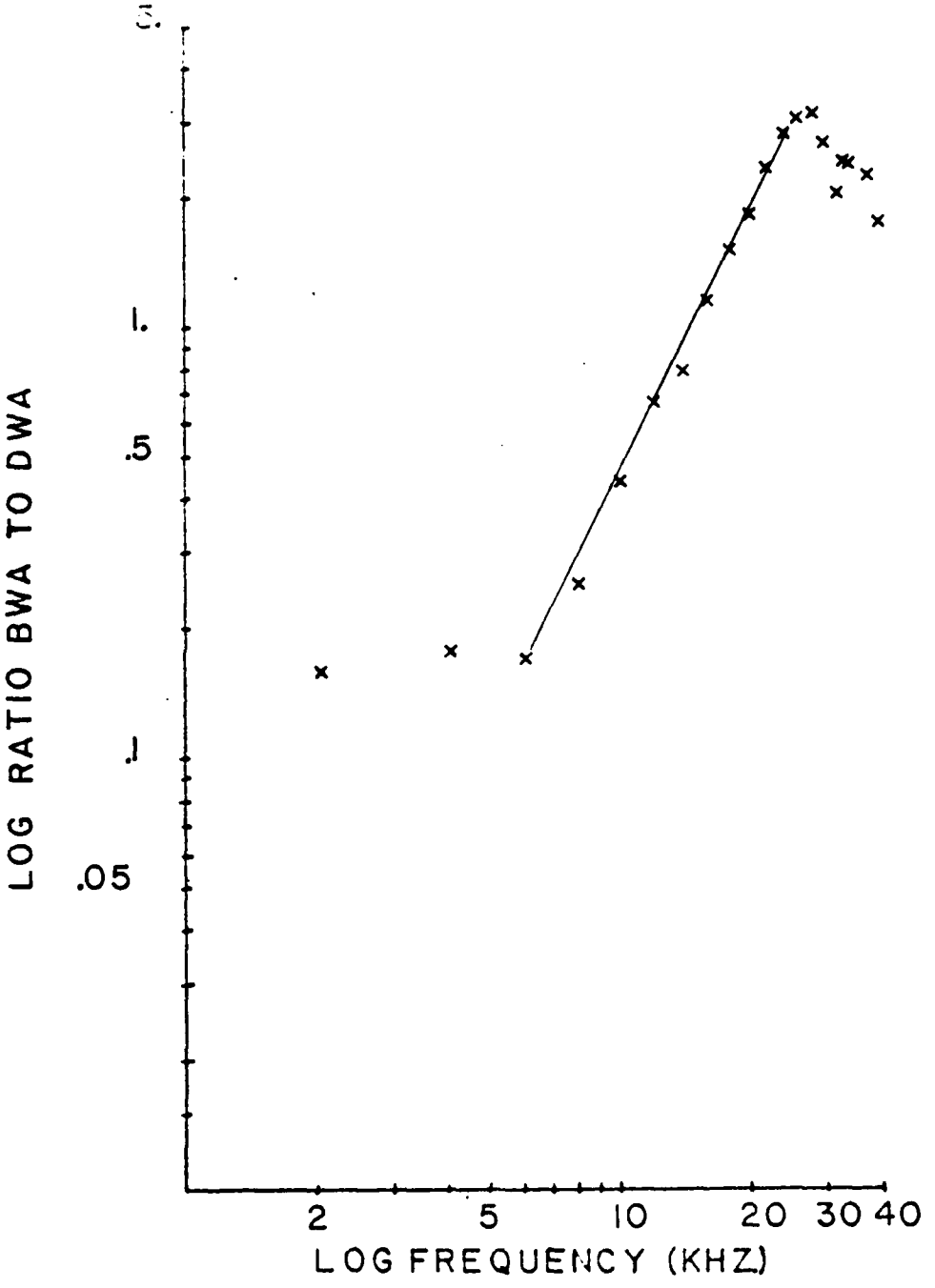

Figure 63. Log Ratio BWA to DWA vs. Log Frequency (R = 10 cm); R_0 = 20 cm, Z = Z_0 = 0.0 cm, x = Run I, and — = Slope (2.0) (see Table V).

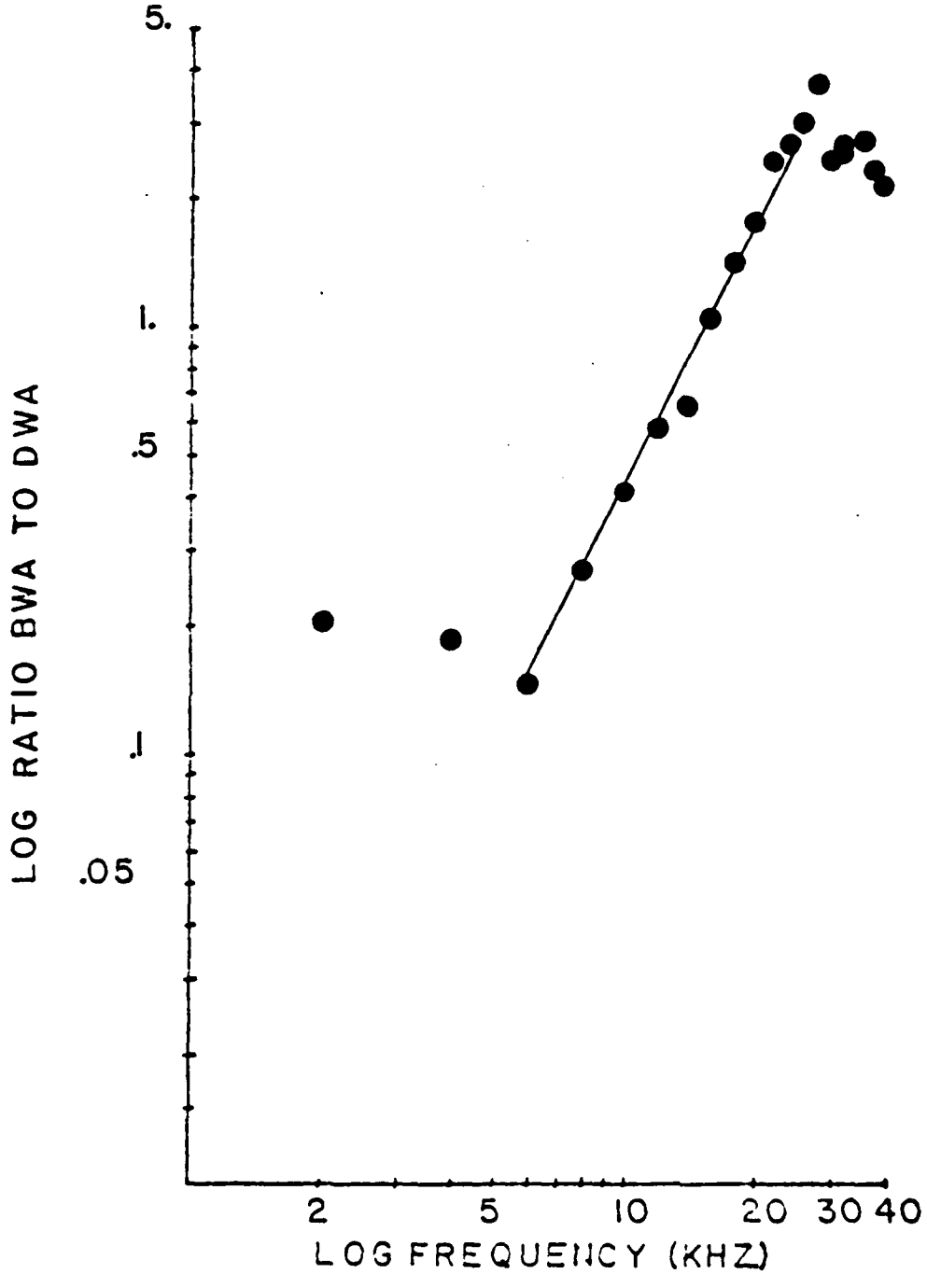

Figure 64. Log Ratio BWA to DWA vs. Log Frequency (R = 15 cm); R_0 = 20 cm, Z = Z_0 = 0.0 cm, 0 = Run I, and — = Slope (2.0) (see Table V).

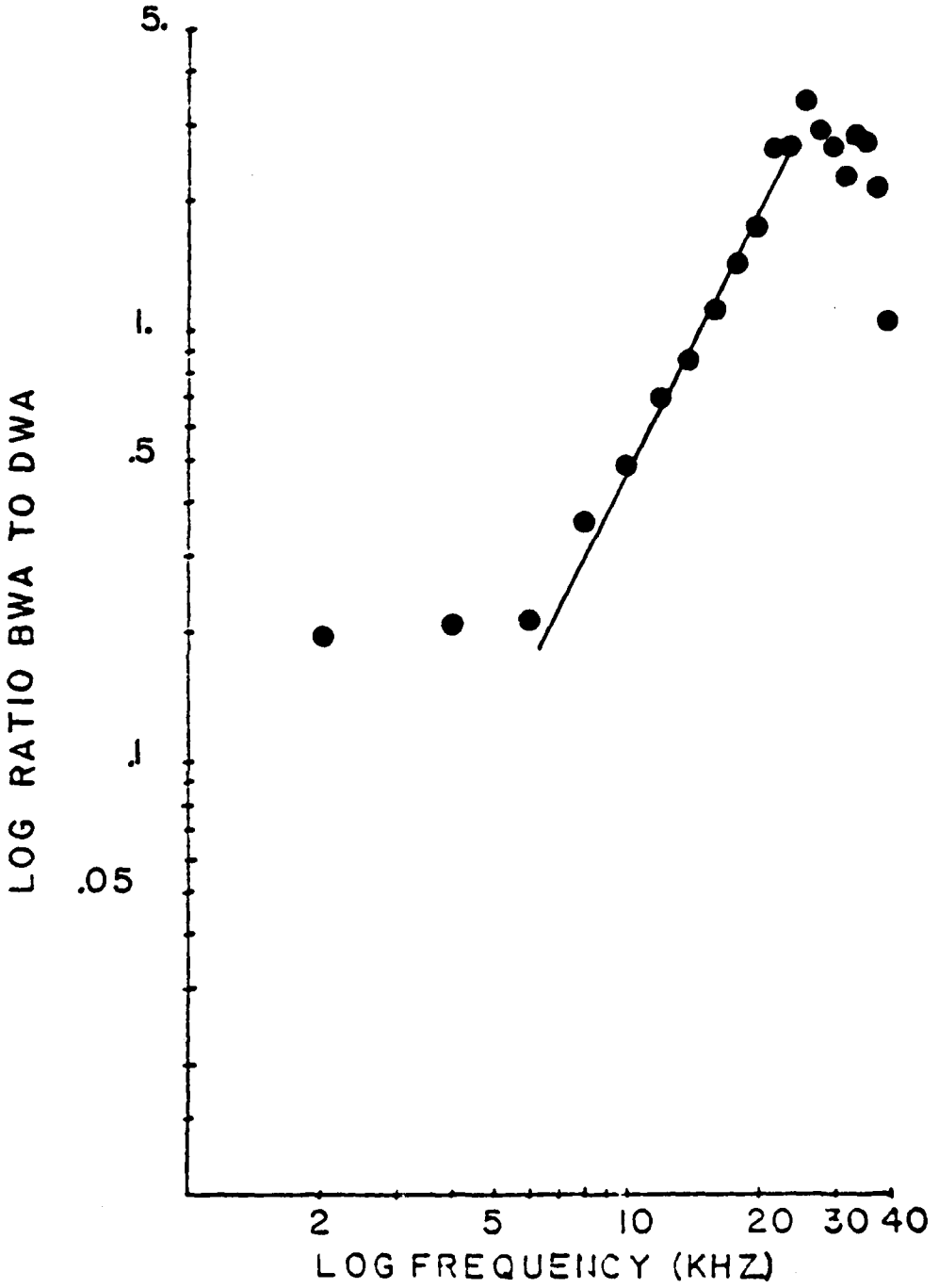

Figure 65. Log Ratio BWA to DWA vs. Log Frequency ($R = 20$ cm); $R_0 = 20$ cm, $Z = Z_0 = 0.0$ cm, 0 = Run I, and ^{0}— = slope (2.0) (see Table V).

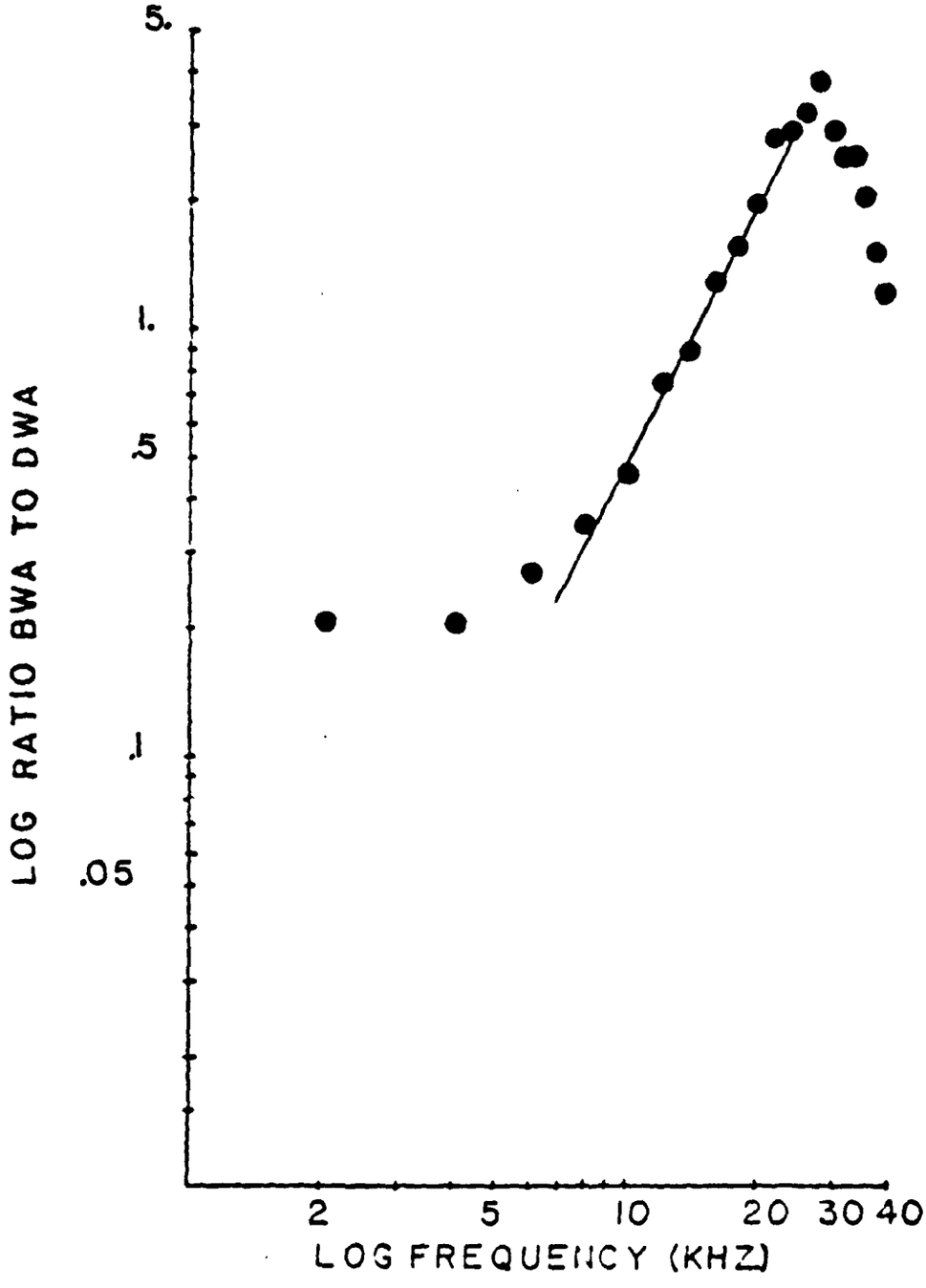

Figure 66. Log Ratio BWA to DWA vs. Log Frequency (R = 25 cm); R_0 = 20 cm, Z = Z_0 = 0.0 cm, 0 = Run I, and — = Slope (2.0) (see Table V).

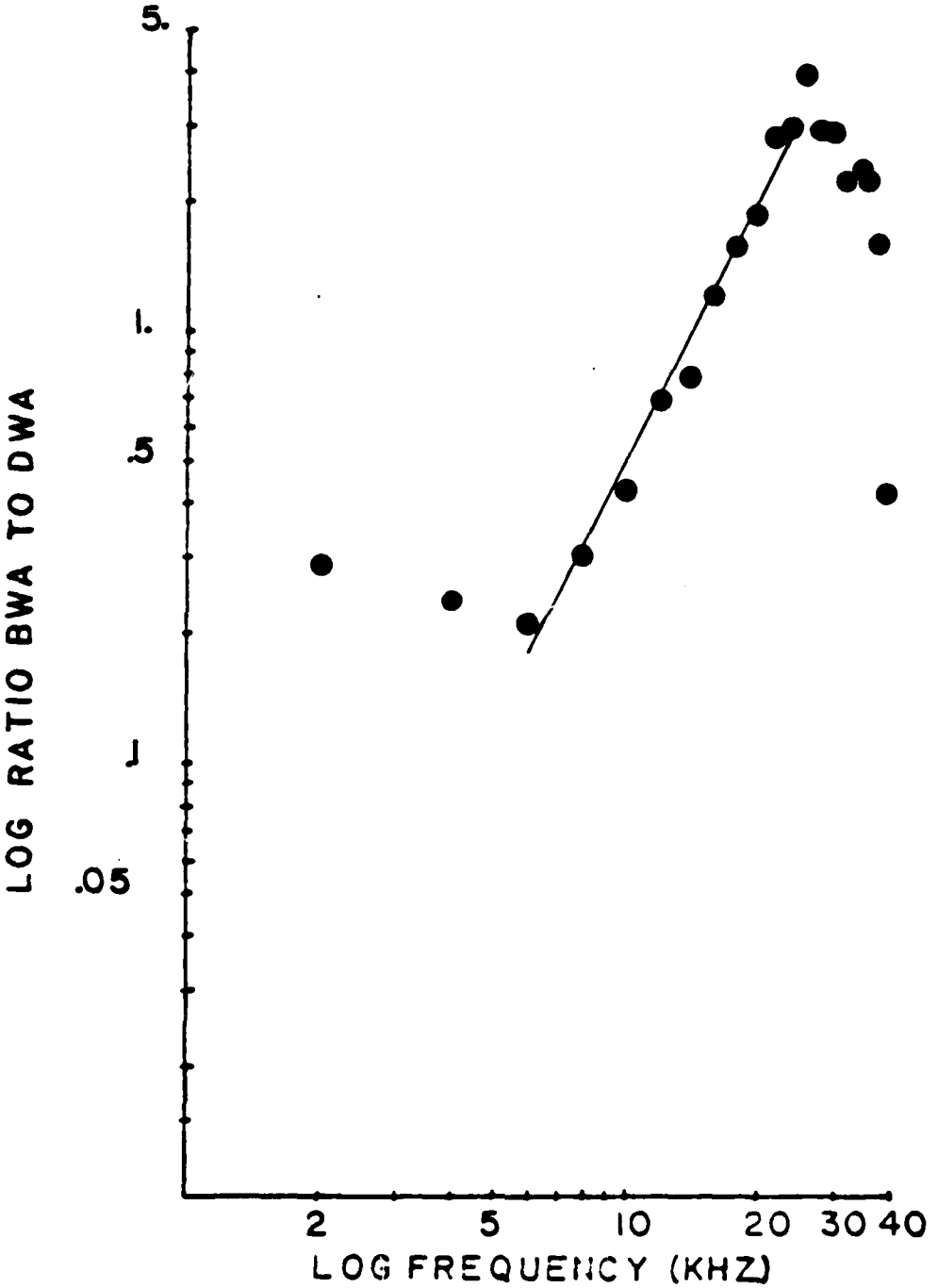

Figure 67. Log Ratio BWA to DWA vs. Log Frequency (R = 30 cm); R_0 = 20 cm, Z = Z_0 = 0.0 cm, 0 = Run I, and — = Slope (2.0) (see Table V).

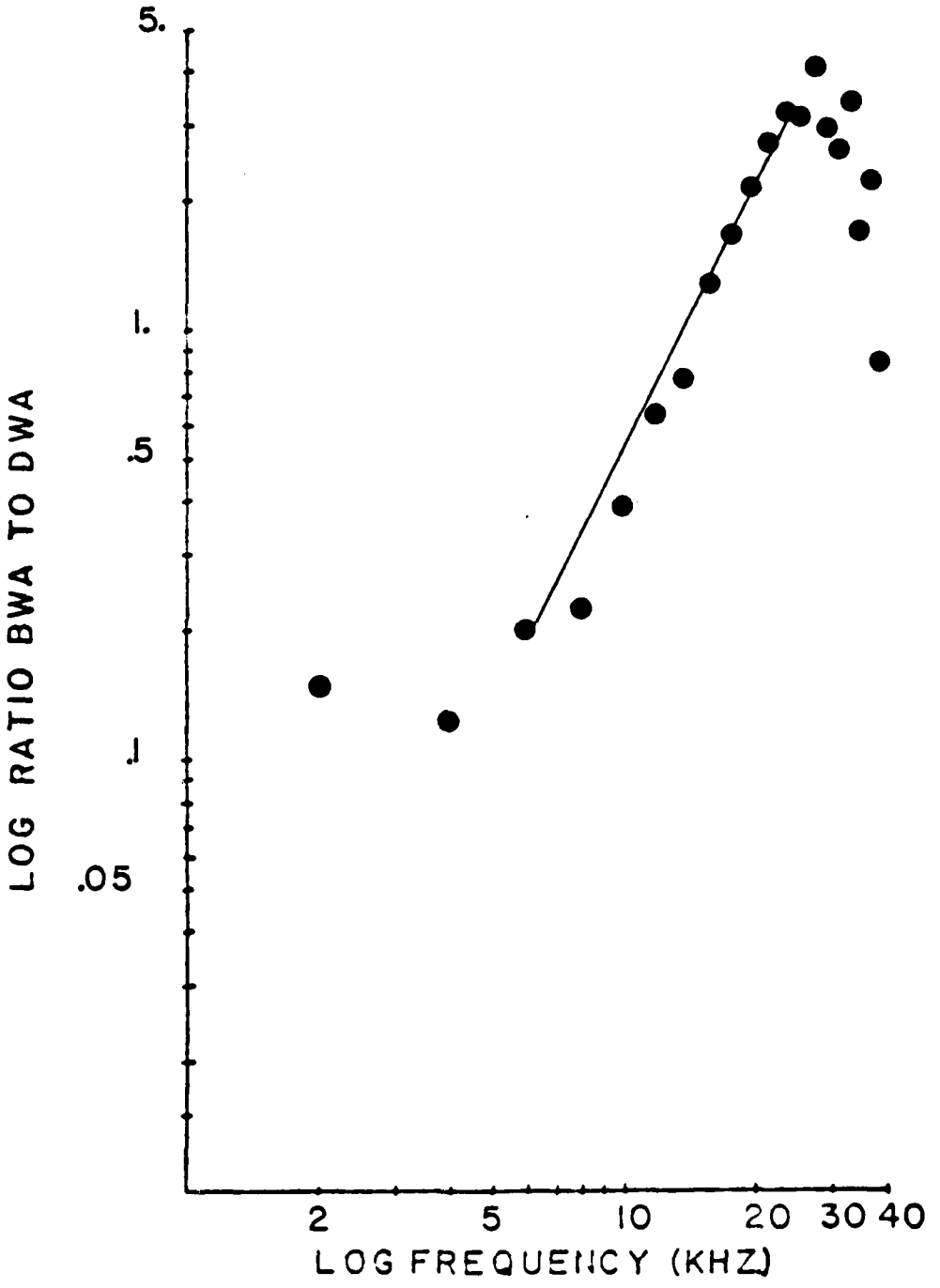

Figure 68. Log Ratio BWA to DWA vs. Log Frequency (R = 35 cm); R_0 = 20 cm, Z = Z_0 = 0.0 cm, 0 = Run I, and — = Slope (2.0) (see Table V).

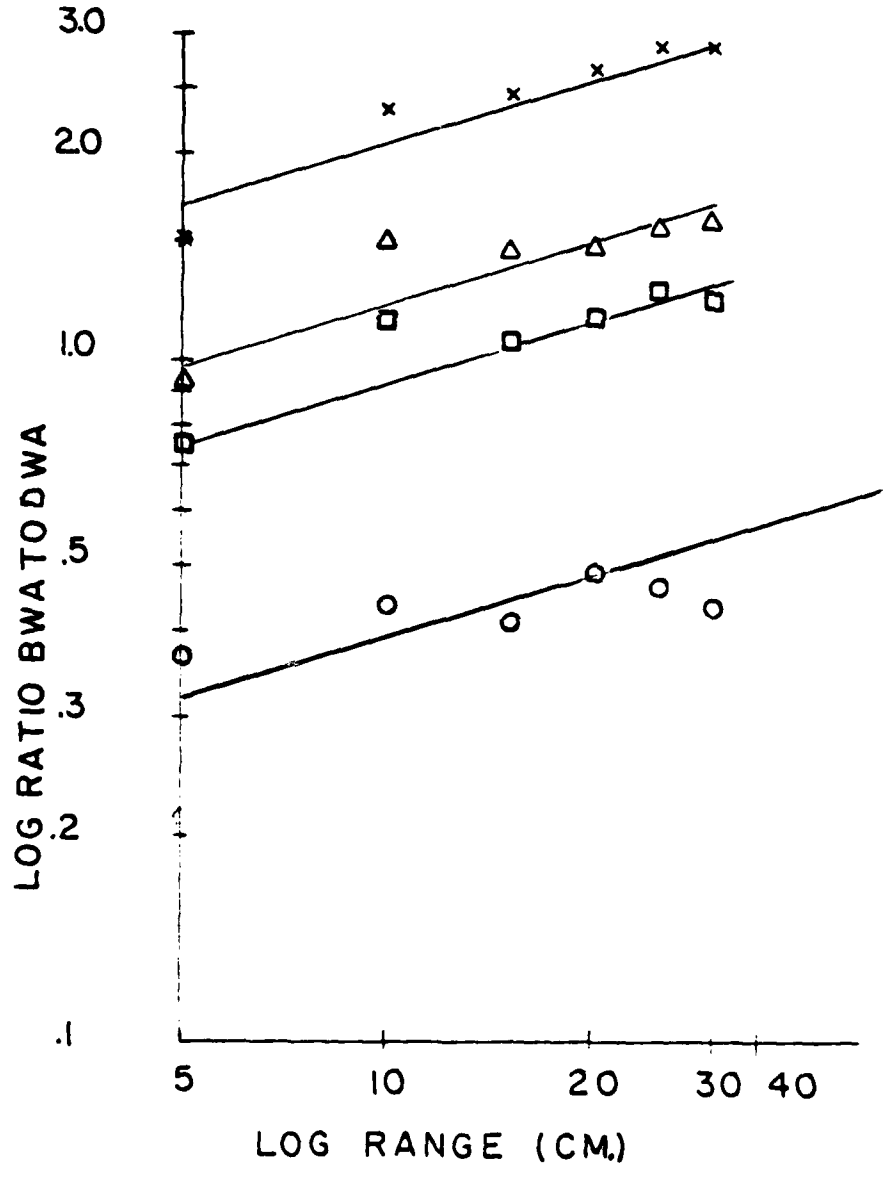

Figure 69. Log Ratio BWA to DWA vs. Log Range; R_0 = 20 cm, Z = Z_0 = 0.0 cm, 0 = 10 kHz, □ = 16 kHz, Δ = 18 kHz, x = 22 kHz, and — = Slope (0.3) (see Table VI).

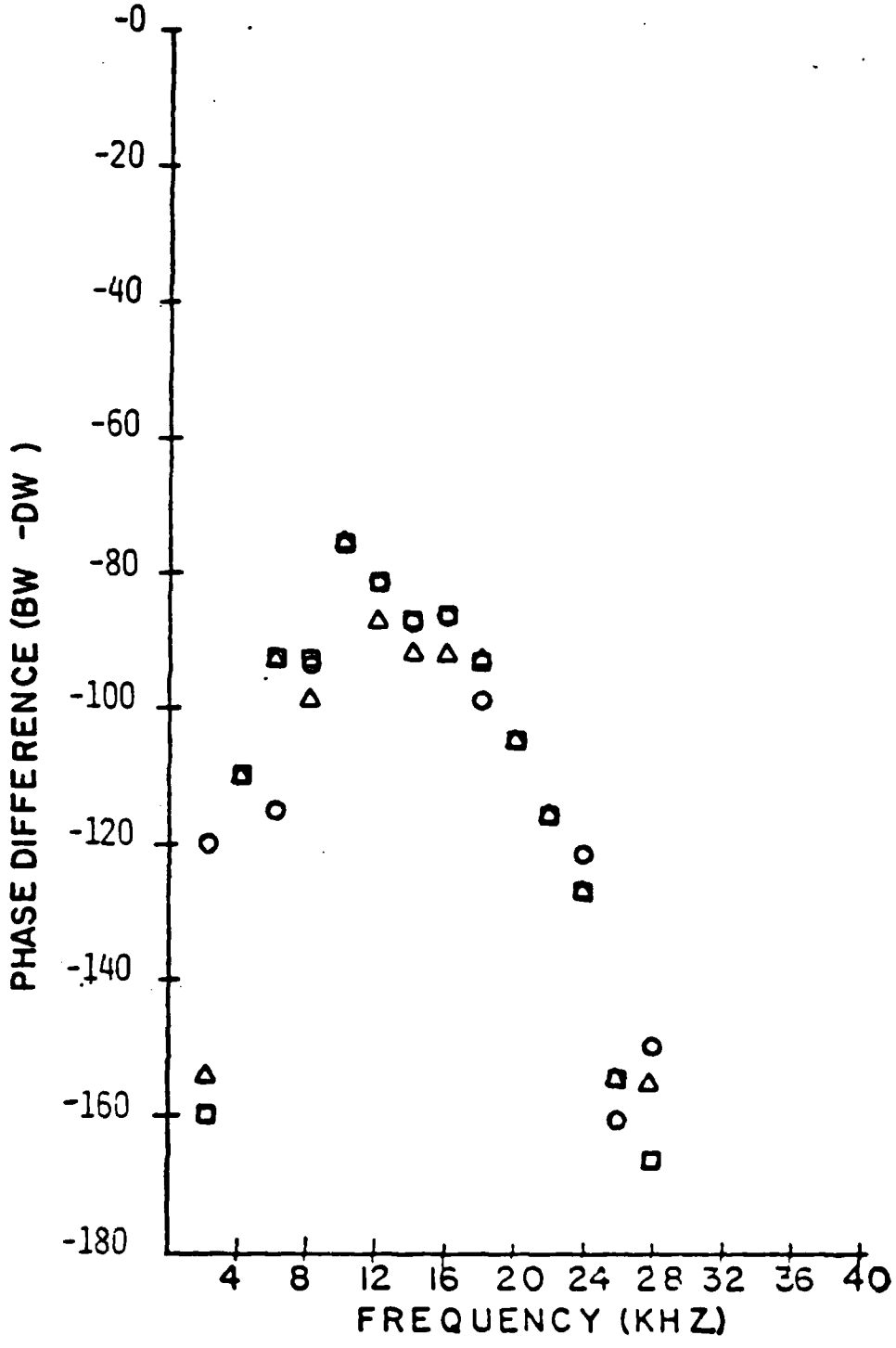

Figure 70. Phase Difference (BW-DW) vs. Frequency; R_0 = 20 cm, Z = Z_0 = 0.0 cm, 0 (R = 10 cm), Δ (R = 20 cm), and □ (R = 30 cm).

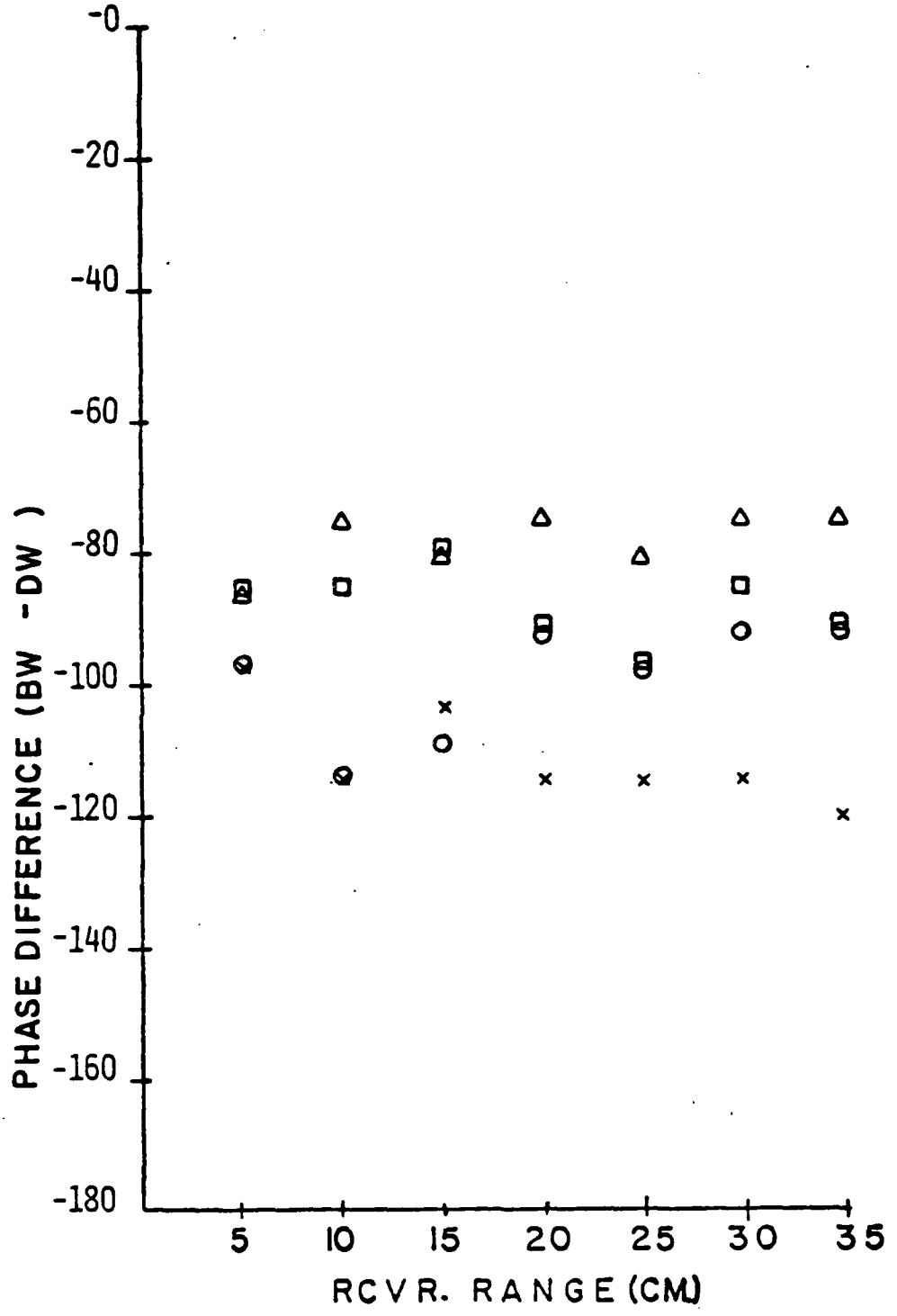

Figure 71. Phase Difference (BW-DW) vs. Range; R_0 = 20 cm, $Z = Z_0$ = 0.0 cm, 0 = 6 kHz, Δ = 10 kHz, □ = 16 kHz, and x^0 = 22 kHz.

10 kHz, reaches a minimum at 10 kHz, and increases through 24 kHz. The phase difference again only varies slightly with range from frequencies 8 to 24 kHz.

D. GENERATION OF A BOUNDARY WAVE BY A PHASED LINE SOURCE

The third task was run last to facilitate the wedge configuration. This phase required that the front side of the wedge be smooth and the back side be rough. This would enable the measurement of the growth of the boundary wave beyond the crest generated by the diffracting volume wave at the crest. The wedge configuration was readied by simply scraping off the shot from the source side of the previously used wedge. The procedure followed for taking data remained the same except only ranges, R, at 5, 20, 30, and 35 cm. were used. The data for two runs are plotted for each distance in Figures 72-75. The range of data values for the four possible combinations are plotted in Figures 76-79. The range of data values again is very small. In comparison with the theoretical growth with frequency of the boundary wave over a rough planar surface due to a point source, the amplitude ratio was observed to be growing more rapidly for the phased line source at the crest (see Figure 73). Figures 80-83 show the log amplitude plotted against the log frequency. An average frequency dependence of 1.99 was calculated using linear regression for the range from 16 to 24 kHz (see Table V). Figure 84 shows the plot of log amplitude versus log range.

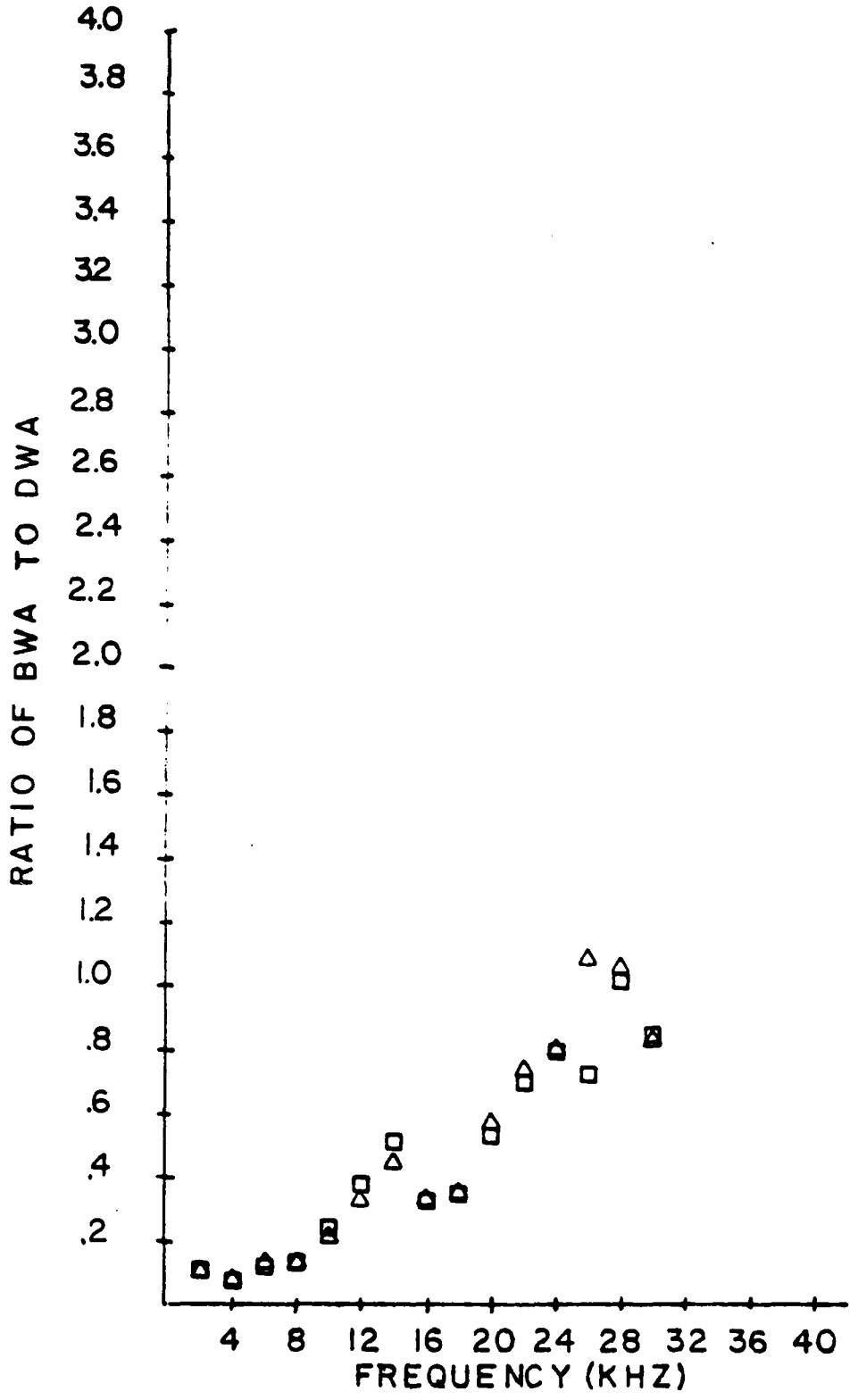

Figure 72. Ratio of BWA to DWA vs. Frequency (R = 5 cm); R_0 = 20 cm, $Z = Z_0 = 0.0$ cm, □ = Run I, and Δ^0 = Run II.

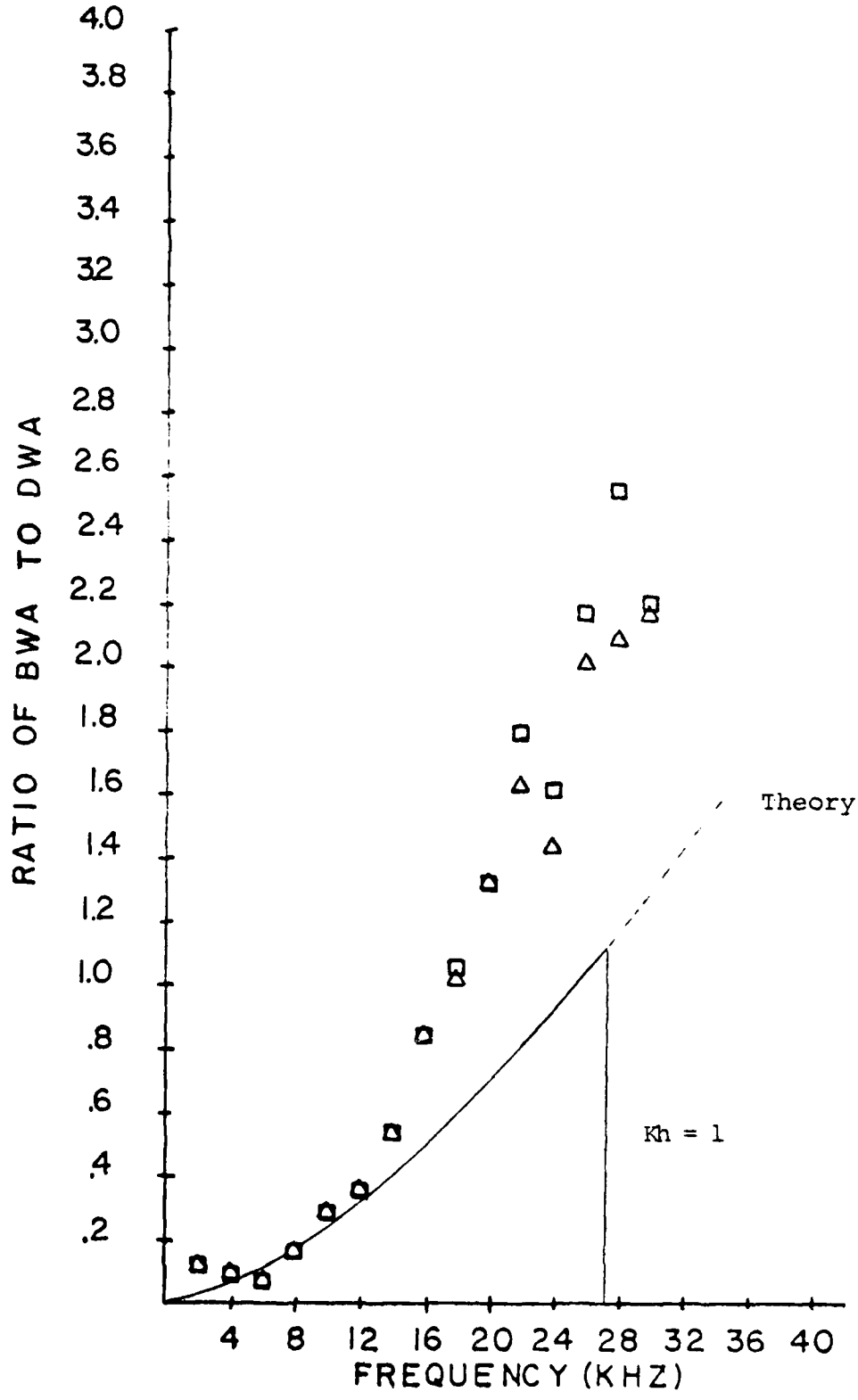

Figure 73. Ratio of BWA to DWA vs. Frequency (R = 20 cm); R_0 = 20 cm, $Z = Z_0 = 0.0$ cm, □ = Run I, and Δ = Run II. Tolstoy Theory for Sound Propagation at a Range of 20 cm, over a Rough Planar Surface.

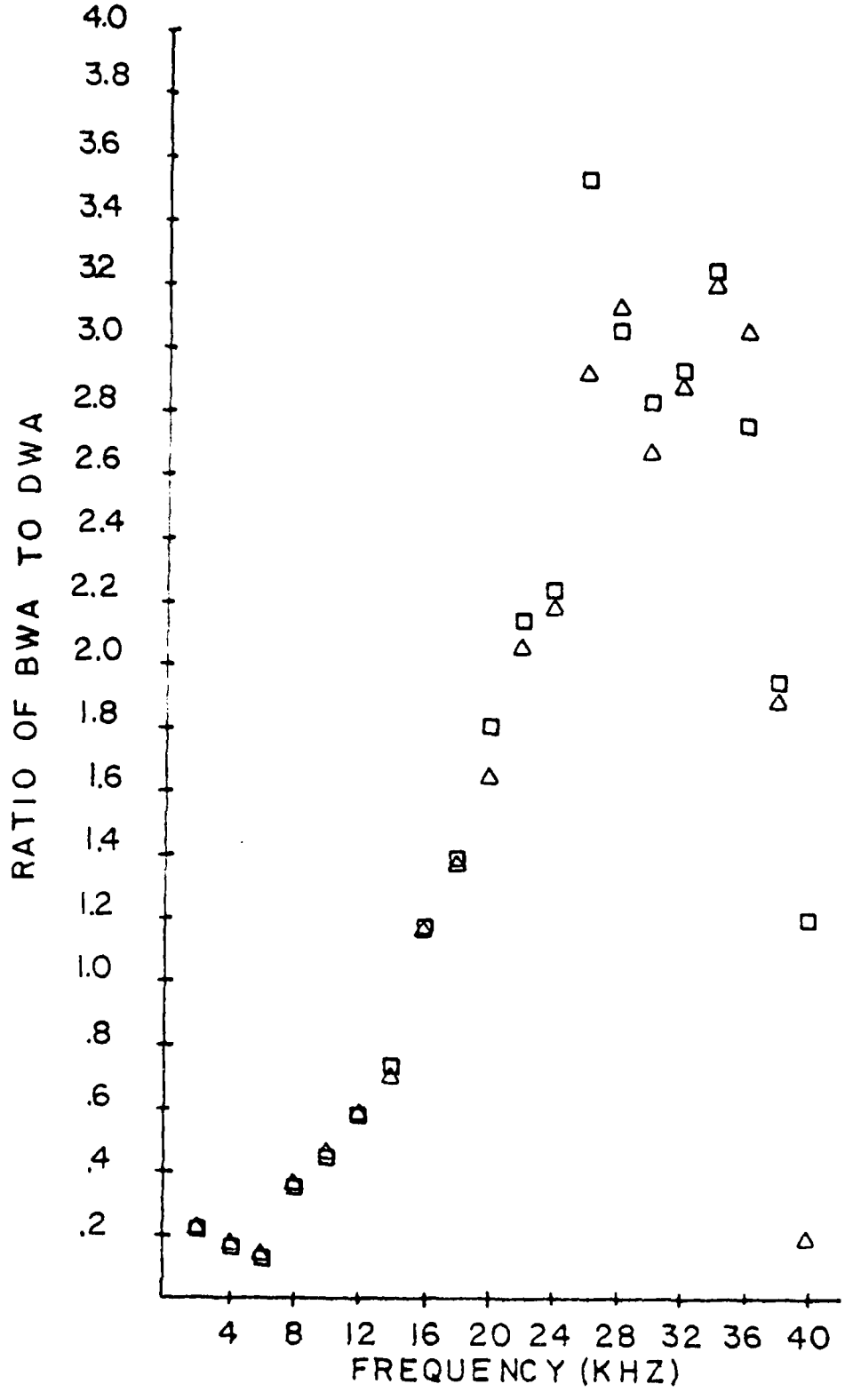

Figure 74. Ratio of BWA to DWA vs. Frequency (R = 30 cm); R_0 = 20 cm, Z = Z_0 = 0.0 cm, □ = Run I, and Δ^0 = Run II.

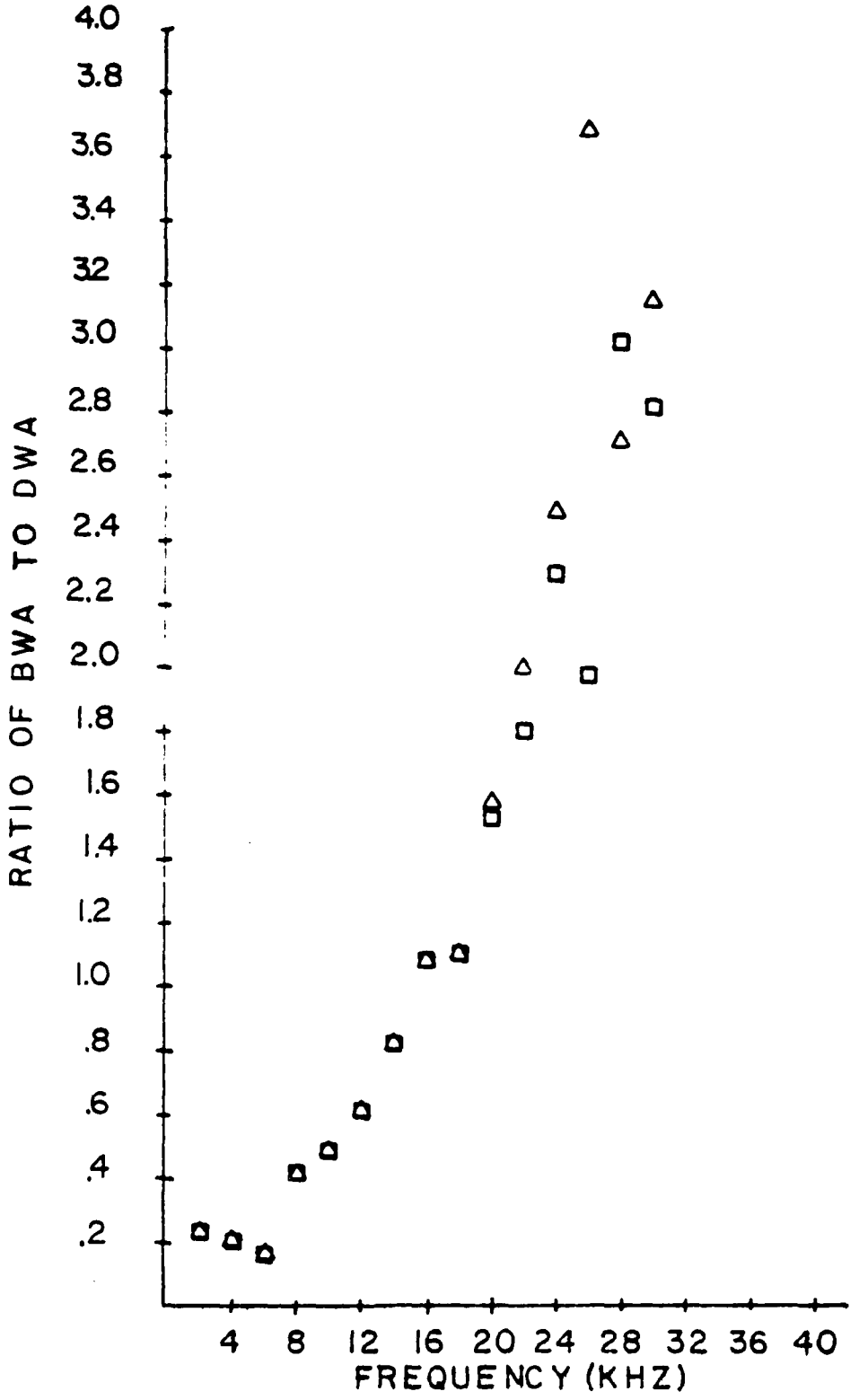

Figure 75. Ratio of BWA to DWA vs. Frequency (R = 35 cm); R_0 = 20 cm, Z = Z_0 = 0.0 cm, □ = Run I, and Δ^0 = Run II.

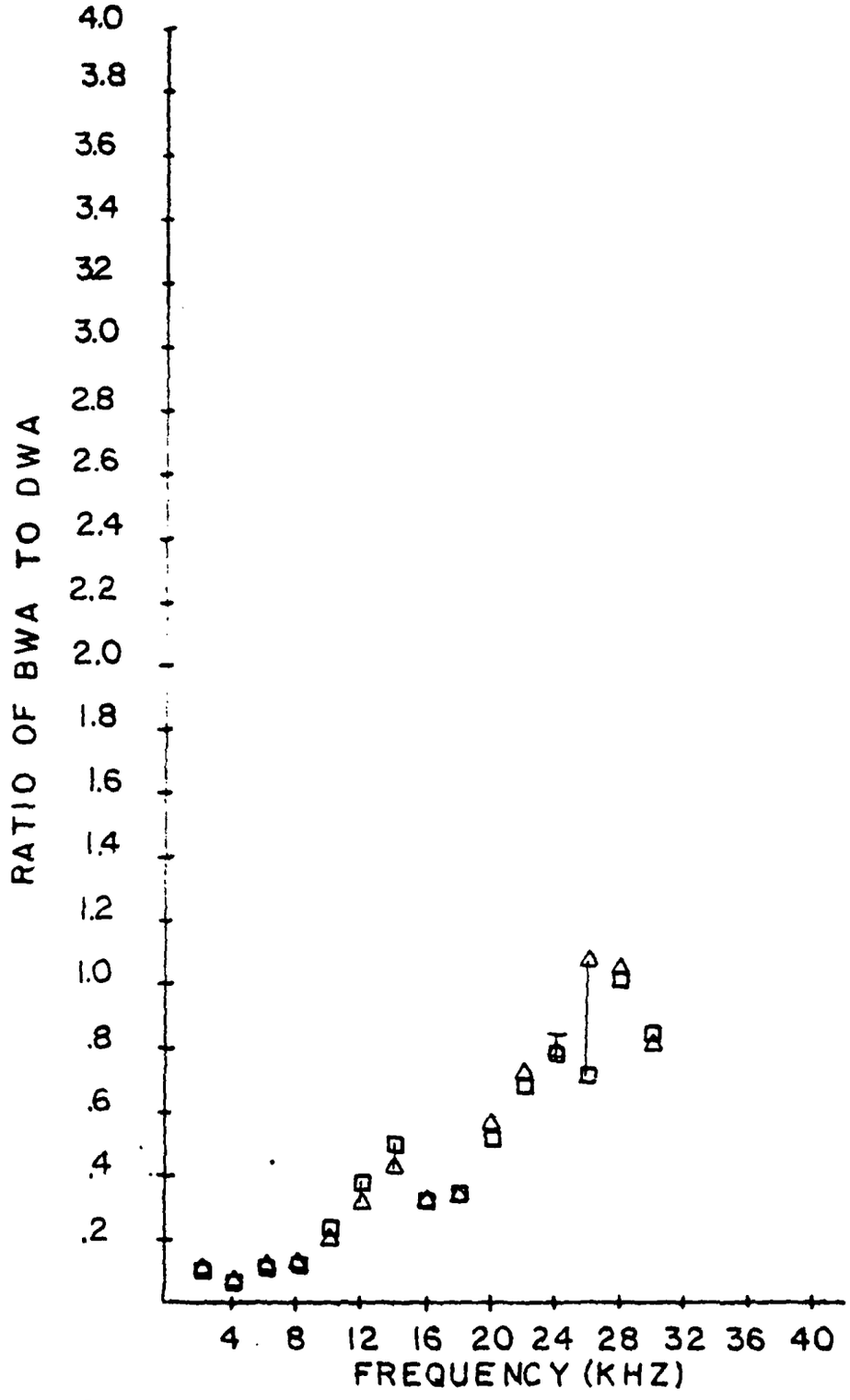

Figure 76. Range of Data Values for Ratio BWA to DWA vs. Frequency (R = 5 cm); Range of Four Data Values.

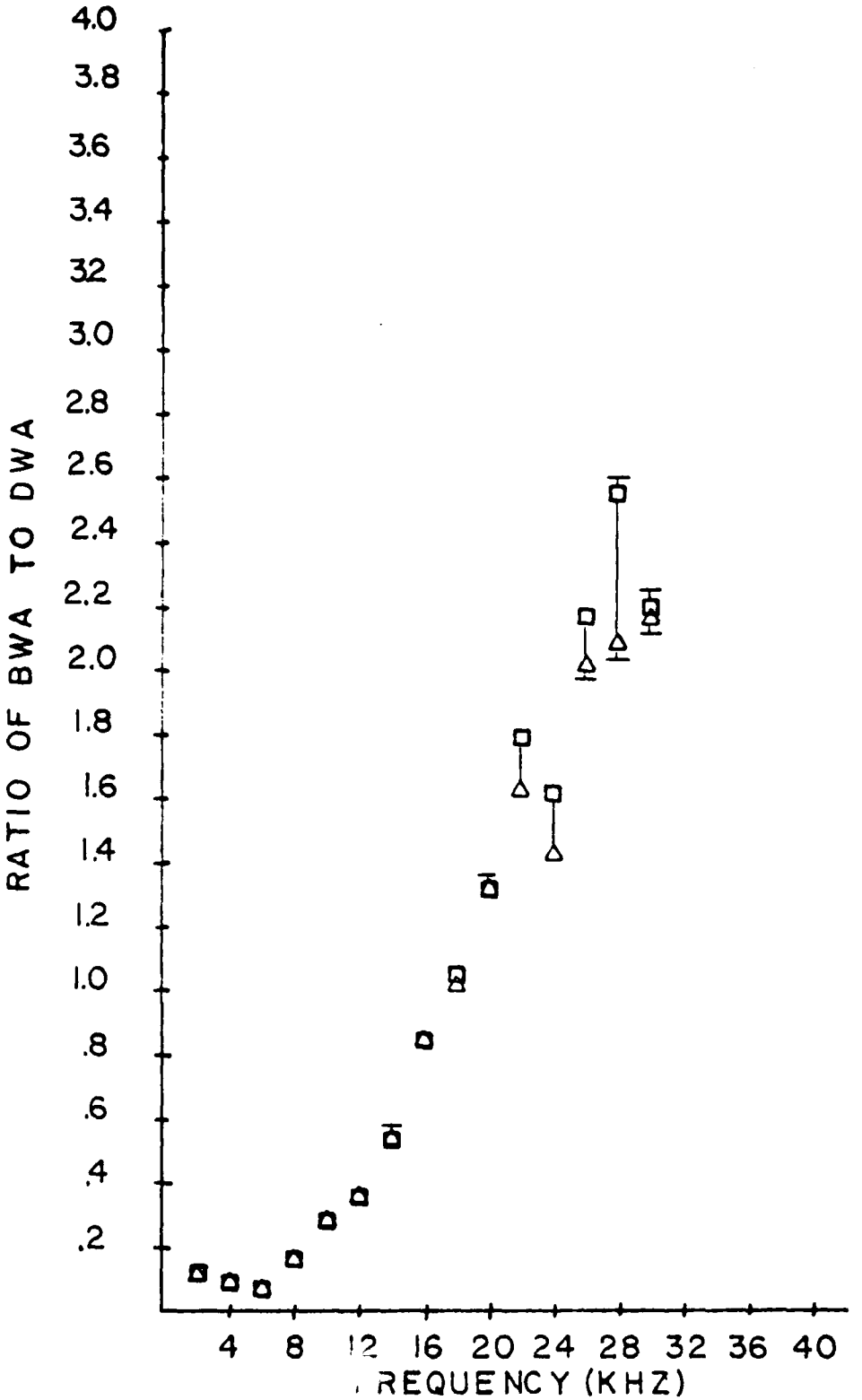

Figure 77. Range of Data Values for Ratio BWA to DWA vs. Frequency (R = 20 cm); R_0 = 20 cm, Z = Z_0 = 0.0 cm, Range of Four Data Values.

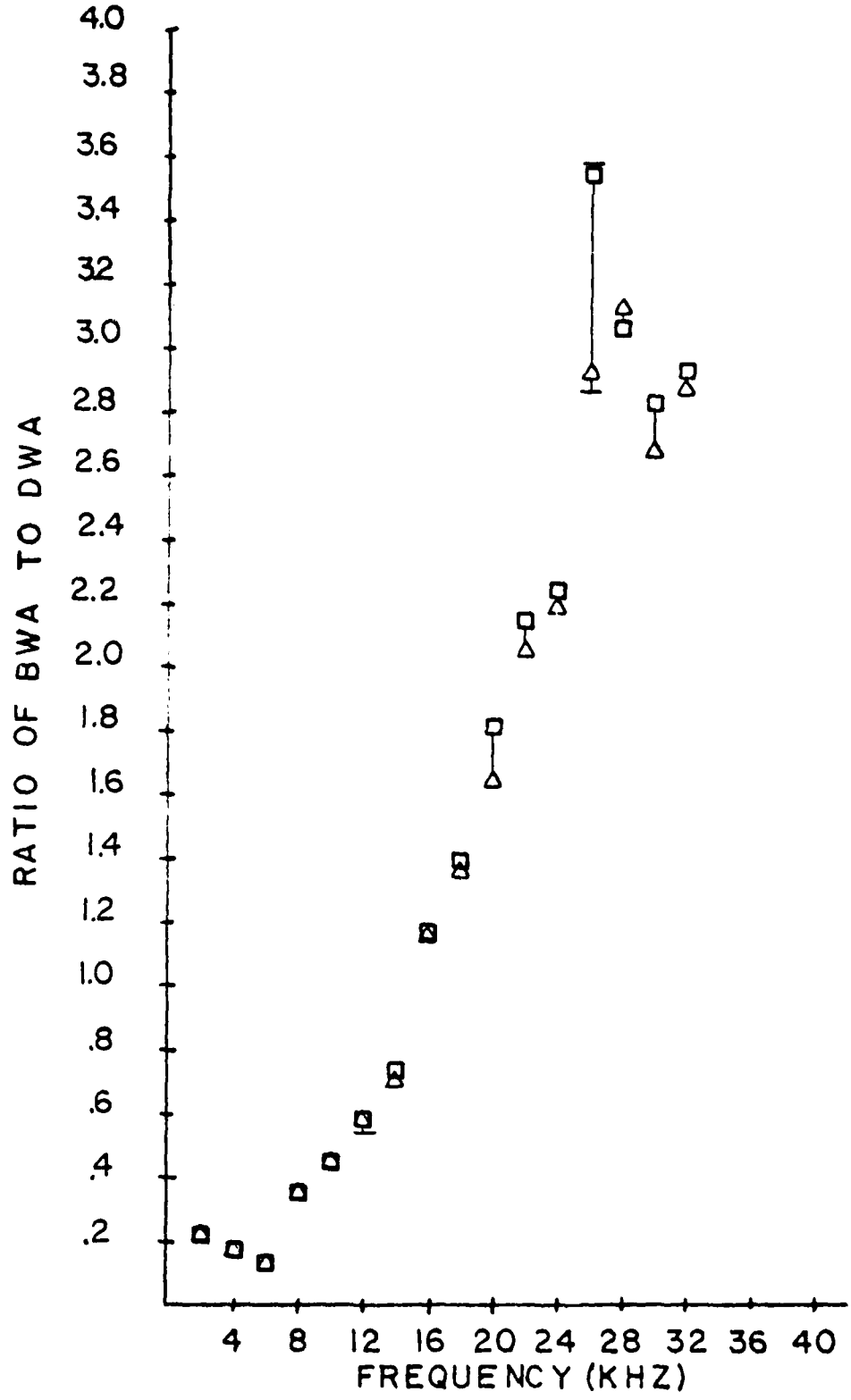

Figure 78. Range of Data Values for Ratio BWA to DWA vs. Frequency (R = 30 cm); R_0 = 20 cm, Z = Z_0 = 0.0 cm, Range of Four Data Values.

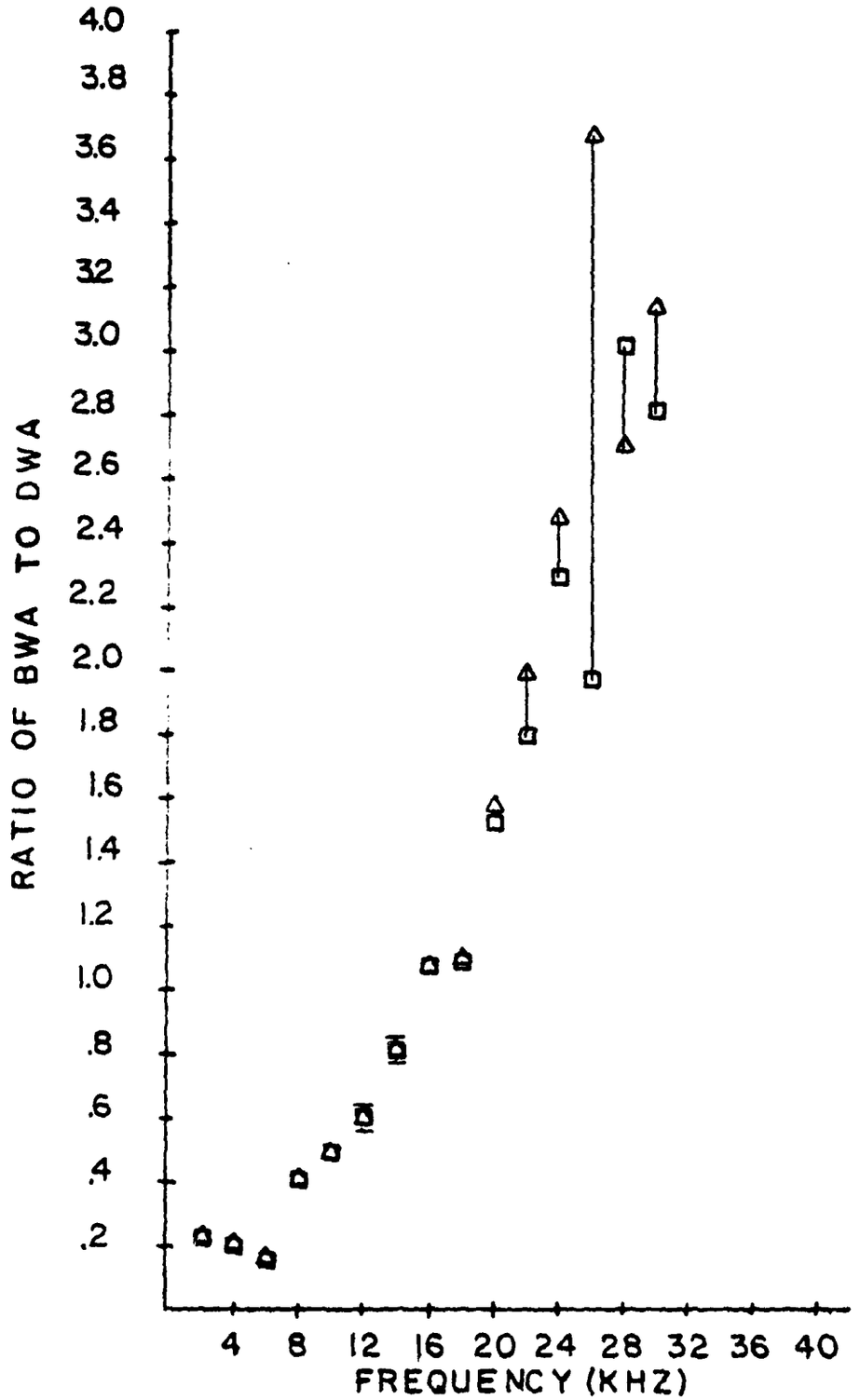

Figure 79. Range of Data Values for Ratio BWA to DWA vs. Frequency (R = 35 cm); Range of Four Data Values.

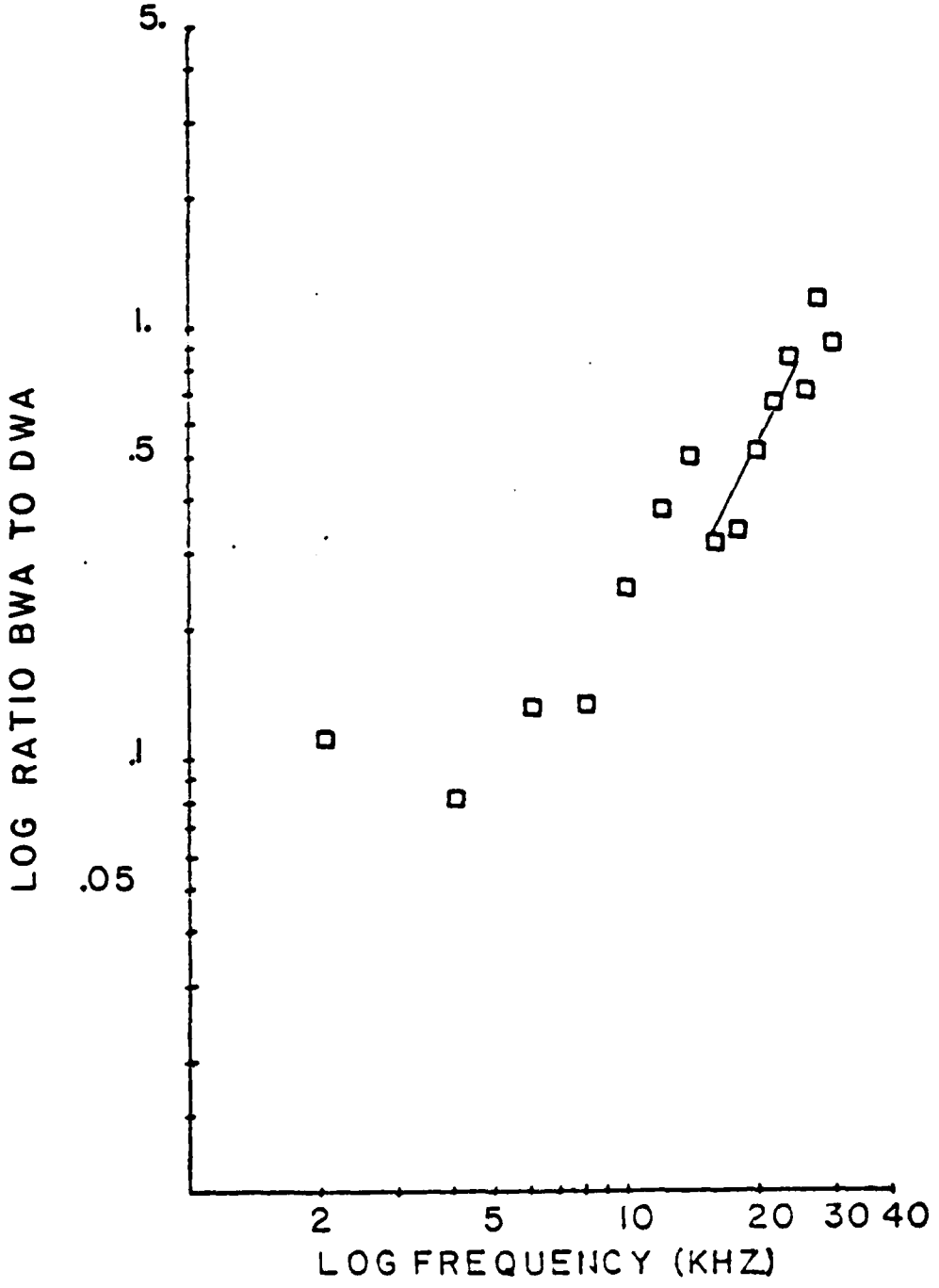

Figure 80. Log Ratio BWA to DWA vs. Log Frequency (R = 5 cm); R_0 = 20 cm, Z = Z_0 = 0.0 cm, □ = Run I, and — = Slope (2.0) (see Table V).

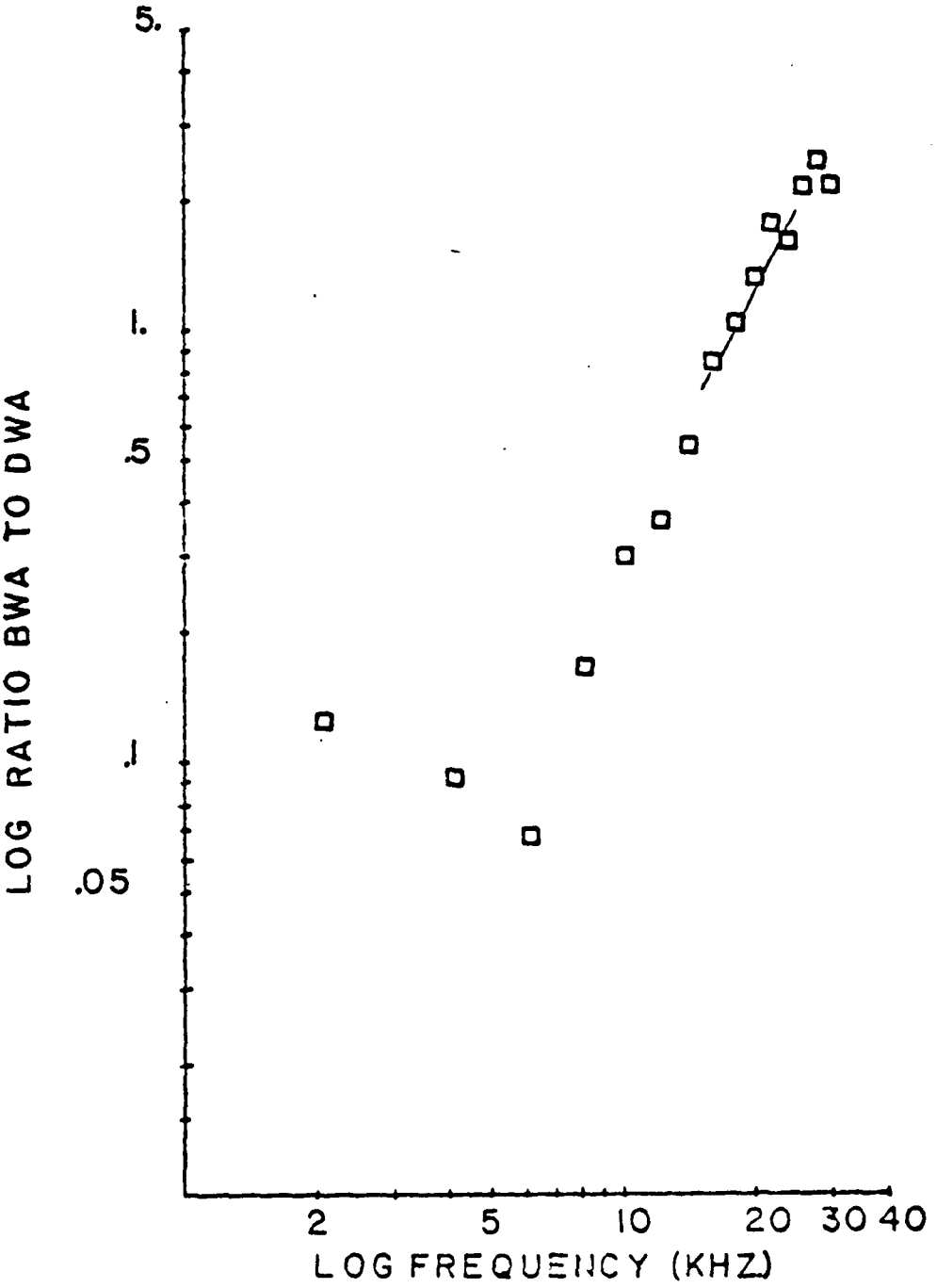

Figure 81. Log Ratio BWA to DWA vs. Log Frequency (R = 20 cm); R_0 = 20 cm, Z = Z_0 = 0.0 cm, □ = Run I, and — = Slope (2.0) (see Table V).

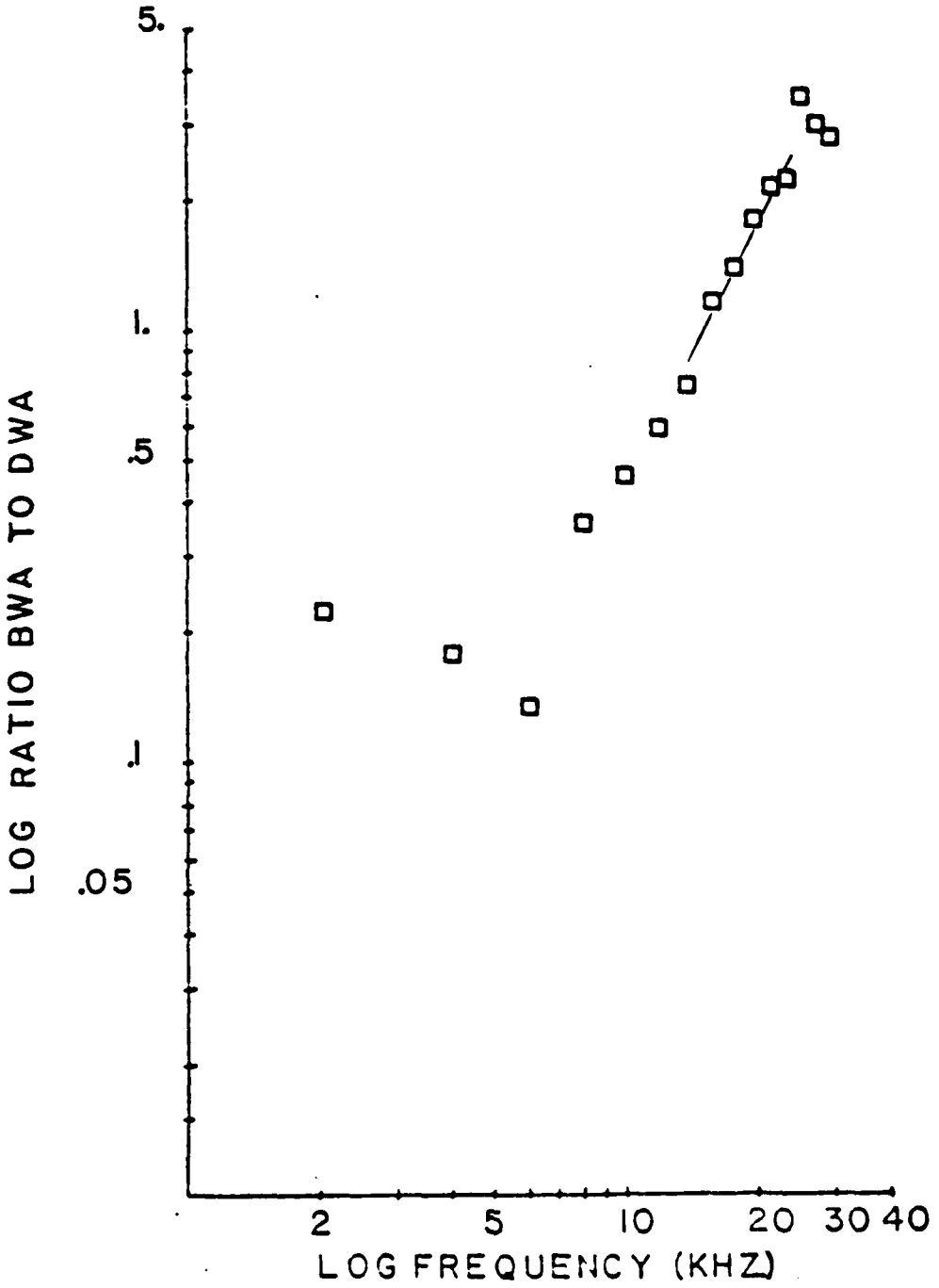

Figure 82. Log Ratio BWA to DWA vs. Log Frequency (R = 30 cm); R_0 = 20 cm, Z = Z_0 = 0.0 cm, □ = Run I, and — = Slope (2.0) (see Table 9).

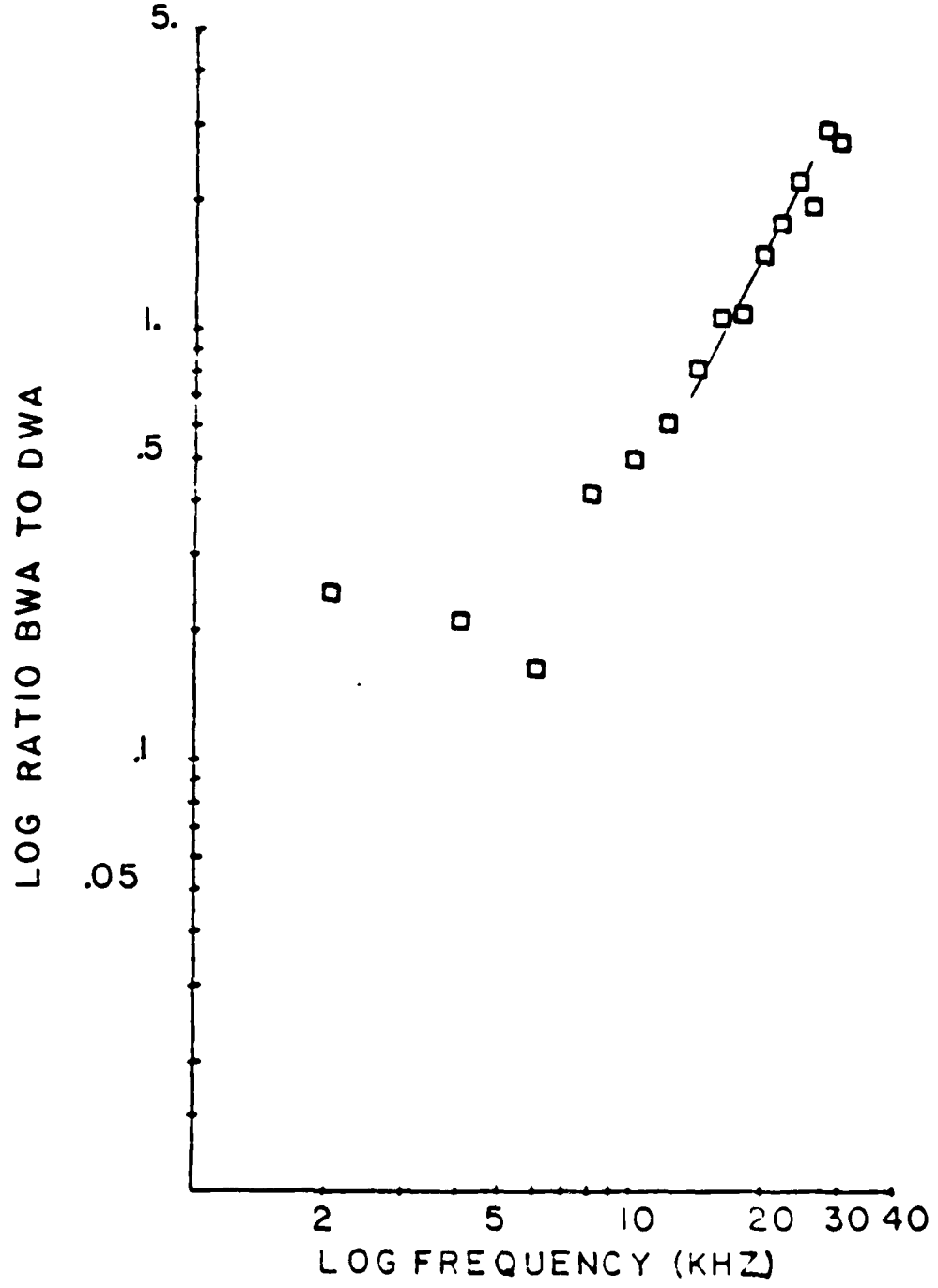

Figure 83. Log Ratio BWA to DWA vs. Log Frequency (R = 35 cm); R_0 = 20 cm, Z = Z_0 = 0.0 cm, □ = Run I, and — = Slope (2.0) (see Table V).

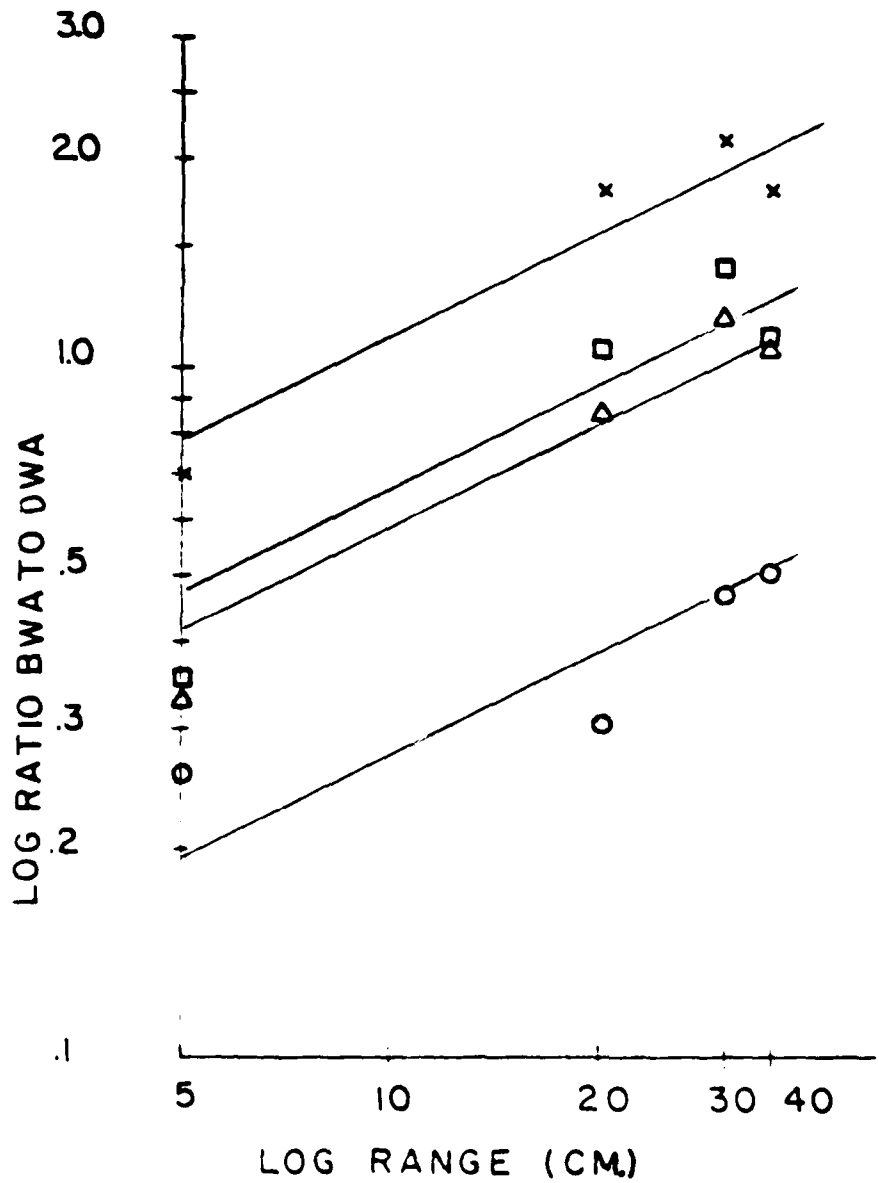

Figure 84. Log Ratio BWA to DWA vs. Log Range; R_0 = 20 cm, $Z = Z_0$ = 0.0 cm, 0 = 10 kHz, Δ = 16 kHz, x = 22 kHz, □ = 18 kHz, and — = Slope (0.5) (see Table VI).

Again using linear regression, an average range dependence of .48 was calculated for a frequency range of 10 to 24 kHz (see Table VI).

E. SEMI-EMPIRICAL DEVELOPMENT

In this experiment three different aspects of the boundary wave were observed, first the initial generation by near grazing incidence at a plane surface, second the diffraction over the crest, and subsequently the continued growth as the wave propagated over the other side. To develop a semi-empirical formula to predict the amplitude ratio of the boundary wave to the diffracted wave, the approach taken was to combine the Tolstoy theory of boundary wave generation over a rough plane surface and the Biot-Tolstoy theory for diffraction over an infinite smooth plane rigid wedge.

The amplitude of the boundary wave generated at grazing incidence by a source and receiver at zero height from Tolstoy theory is

$$|P_{BWA}| = \varepsilon(2\pi R)^{-1/2} k^{3/2} . \qquad (14)$$

Therefore if we assume the boundary wave grows in the same manner from source at range R_0 to crest to receiver at range R from crest

$$P_{BWA} = \varepsilon[2\pi(R + R_0)]^{-1/2} k^{3/2} \qquad (15)$$

However, assuming cylindrical divergence from the crest

$$|P_{BWA}| = \varepsilon[2\pi(R + R_0)]^{-1/2} \, k^{3/2} \, (\frac{R_{ref}}{R})^{1/2} \qquad (16)$$

where R_{ref} is the effective source range of the diverging wave measured from the crest. The Biot-Tolstoy theory for diffraction has been simplified for high frequencies by Medwin [Ref. 4].

$$|P_{DWA}| = \beta/f^{1/2} \, \sqrt{2}(4\pi\theta_w)(2\tau_0 \, R_0 \, R)^{1/2} \qquad (17)$$

where

$$\tau_0 = \frac{R + R_0}{C} \, . \qquad (18)$$

The ratio therefore is

$$|\frac{P_{BWA}}{P_{DWA}}| = \frac{4 \, \varepsilon \, k^2 \, \theta_w \, R_0^{1/2} \, R_{ref}^{1/2}}{\beta} \, . \qquad (19)$$

All the values have been experimentally measured except R_{ref} is unknown. R_{ref} is the point at which the boundary wave diverges cylindrically and should be the crest; however, since the boundary wave would be infinite at R = 0, a common reference point must be determined. Using the data from 8 to 24 kHz and R from 10 to 35 cm., a total of 54 values, the average value of R_{ref} was calculated to be 2.5×10^{-3} cm. In fact the reference point is essentially at the crest. The semi-empirical values are calculated for the amplitude

ratio of the boundary wave to diffracted wave from the formula using the above reference and are shown in Table IV. This semi-empirical theory is compared with the average data runs at 10, 20, and 30 cm in Figure 87. The agreement up to $Kh \leq 1$ is excellent.

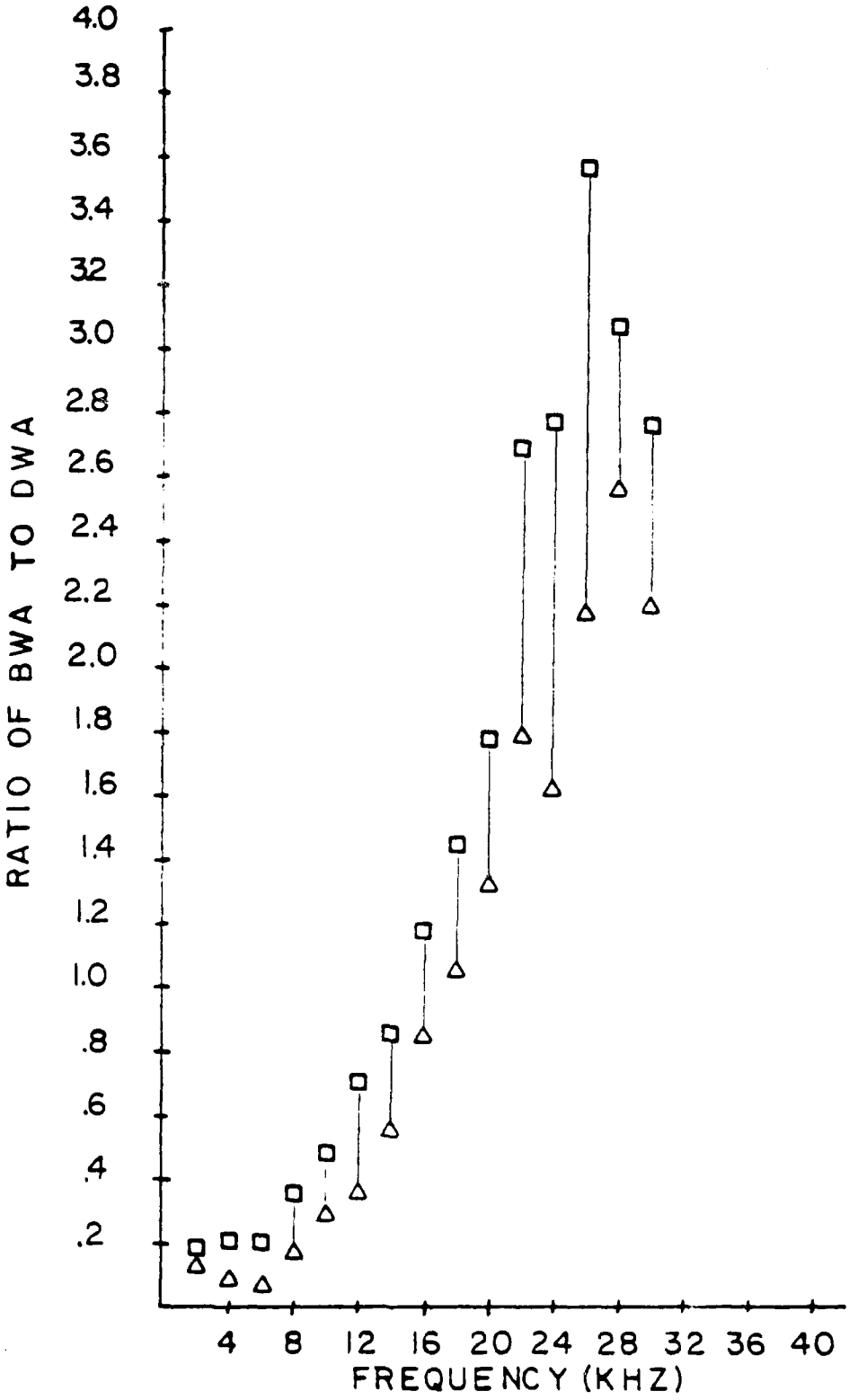

Figure 85. Effect of Boundary Wave Growth from Source to Crest (R = 20 cm); R_0 = 20 cm, Z = Z_0 = 0.0 cm, Δ = Smooth-Rough Wedge Run I, and □ = Rough Wedge Run I. The Effect is Shown by the Vertical Lines.

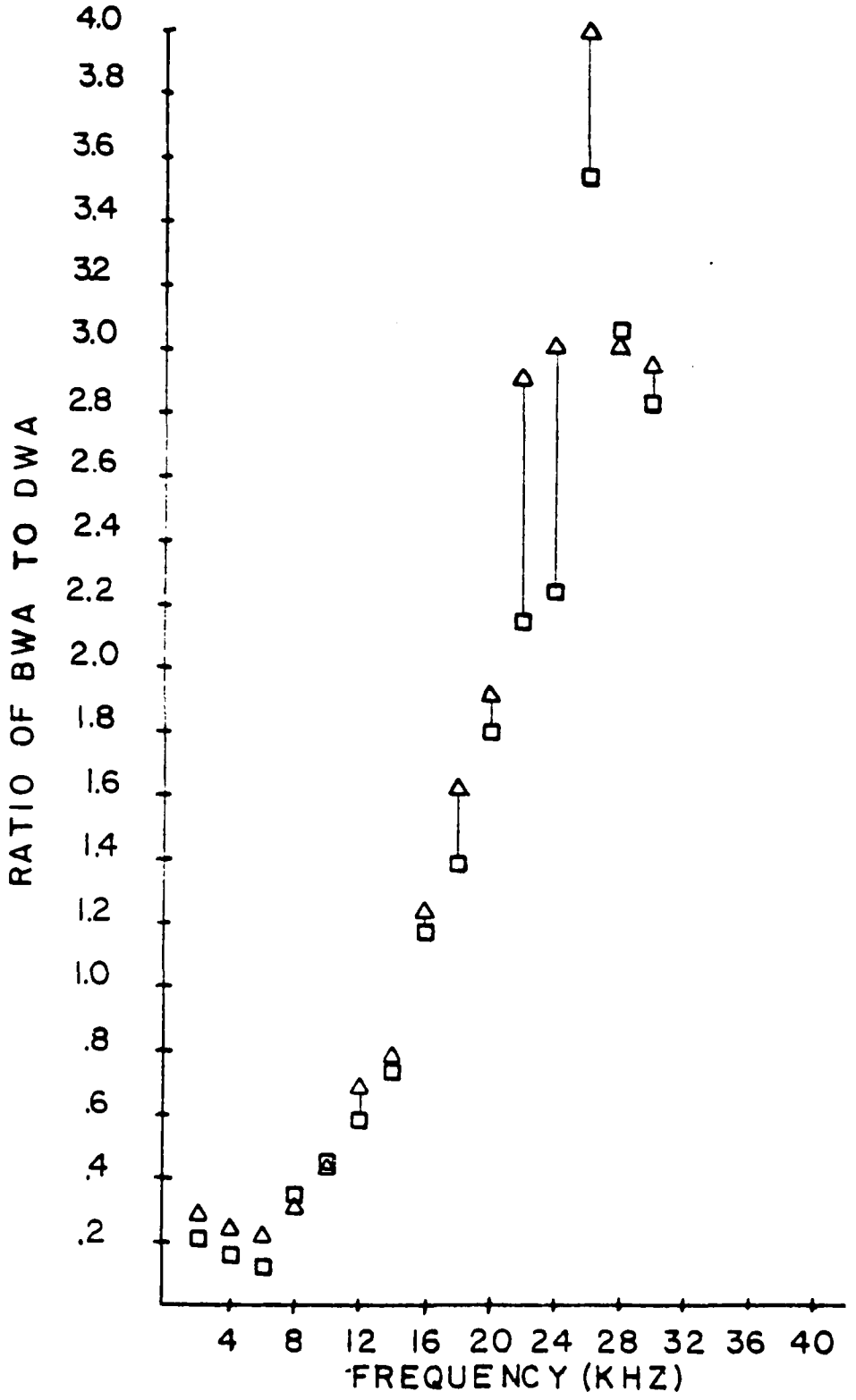

Figure 86. Effect of Boundary Wave Growth from Source to Crest (R = 30 cm); R_0 = 20 cm, Z = Z_0 = 0.0 cm, □ = Smooth-Rough Wedge Run I, and △ = Rough Wedge Run I. The Effect is Shown by the Vertical Lines.

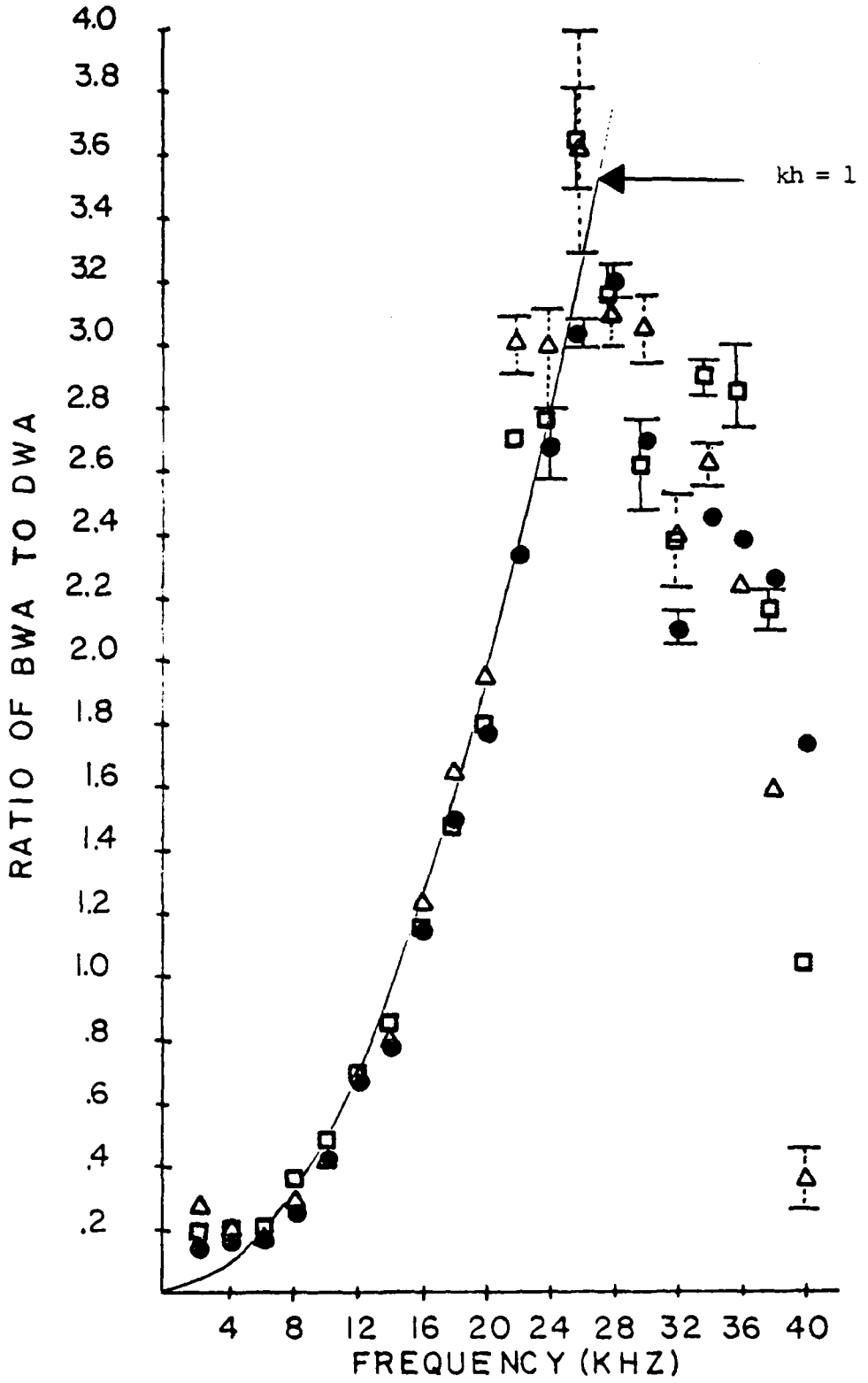

Figure 87. Comparison of Rough Wedge Data to Semi-Empirical Calculations; 0 (R = 10 cm), □ (R = 20 cm), and Δ (R = 30 cm). Range of Four Data Values for Each Distance are Shown.

VI. CONCLUSIONS

The experiment has studied the propagation over a rough wedge of an acoustic scattered boundary wave generated by low frequency radiation at near grazing incidence from a point source. Three important factors necessary for an understanding of this phenomenon are:

1. The boundary wave and the volume wave both diffract from the crest of the wedge and propagate over a smooth surface in an identical manner.

2. The increase with frequency of the amplitude ratio of the boundary wave to the geometrically spreading wave due to the phased line source created at the crest by the diffracting volume wave is more rapid than that from a point source over a rough plane surface.

3. The growth of the amplitude ratio of the boundary wave to the diffracted wave over a rough wedge has an average frequency dependence of $2.0 \pm .2$ and an average range dependence of $0.3 \pm .1$.

A semi-empirical approach combining the Tolstoy theory of boundary wave generation over a rough plane surface and the Biot-Tolstoy theory for diffraction over an infinite smooth plane rigid wedge has led to predicted values that are in excellent agreement with experimental results. The most significant aspect of this experiment from an application

point of view was the generation of a boundary wave over the surface whose experimentally measured amplitude for the maximum case was four times greater than the amplitude of the diffracting volume wave.

LIST OF REFERENCES

1. Tolstoy, I., "The Scattering of Spherical Pulses by Slightly Rough Surfaces", The Journal of the Acoustical Society of America, V. 66, p. 1135-1144, 1979.

2. Medwin, H., Bailie, J., Bremhorst, J., Savage, B. J., and Tolstoy, I., "The Scattered Acoustic Boundary Wave Generated by Grazing Incidence at a Slightly Rough Rigid Surface", The Journal of the Acoustical Society of America, V. 66, p. 1131-1134, 1979.

3. Biot, M. A., and Tolstoy, I., "Formulation of Wave Propagation in Infinite Media by Normal Coordinates with an Application to Diffraction", The Journal of the Acoustical Society of America, V. 29, p. 381-391, 1957.

4. Medwin, H., and Spaulding, R. P., "The Seamount as a Diffracting Body", Paper presented at Bottom-Interacting Ocean Acoustics Conference, SACLANTCEN, La Spazia, Italy, 11 June 1980.

5. Bailie, J. M., "Near Grazing Scattering by Slightly Rough Surfaces", M. S. Thesis, U. S. Naval Postgraduate School, Monterey, California, 1978.

6. Sessler, G. M. and West, J. E., "Electret Transducers: A Review", The Journal of the Acoustical Society of America, V. 53, p. 1589-1599, 1973.

7. Madsen, H. S., "Optimization of a Ridge Backplate for Electret Microphones", The Journal of the Acoustical Society of America, V. 53, p. 1616-1619, 1973.

8. Frederiksen, E., "Condenser Microphones Used As Sound Sources", Bruel and Kjaer Technical Review, No. 3, 1977.

INITIAL DISTRIBUTION LIST

		No. Copies
1.	Defense Technical Information Center Cameron Station Alexandria, Virginia 22314	2
2.	Library, Code 0142 Naval Postgraduate School Monterey, California 93940	2
3.	Department Chairman, Code 61 Department of Physics and Chemistry Naval Postgraduate School Monterey, California 93940	2
4.	Professor H. Medwin, Code 61Md Department of Physics and Chemistry Naval Postgraduate School Monterey, California 93940	6
5.	Lt. Stephen J. Hollis 1218 East Walnut Springfield, Missouri 65802	2
6.	Manager, Anti-Submarine Warfare Systems Project Office (ASW 13) Attn: CDR. J. Hagy Department of the Navy Washington, D.C. 20362	1
7.	Office of Naval Research Arlington, Virginia 22217 Attn: Code 480 Attn: Dr. M. McKisic (Code 486) Attn: Code 460 Attn: Code 102-05	 3 1 1 1
8.	Naval Electronics System Command Code 320 Attn: CDR P. Girard Washington, D.C. 20360	1
9.	Dr. I. Tolstoy Knockvennie Castle Douglas, KIRKS Scotland, United Kingdom	1

No. Copies

10. CDR Edward J. Mahon, Code 33 — 1
Curricular Officer
Weapons Engineering and ASW Programs
Naval Postgraduate School
Monterey, CA 93940